UCRL-53294-82
Distribution Category UC-70

Spent Fuel Test—Climax: Technical Measurements Interim Report, Fiscal Year 82

W. C. Patrick, L. B. Ballou, T. R. Butkovich,

R. C. Carlson, W. B. Durham, G. L. Hage,

E. L. Majer, D. N. Montan, R. A. Nyholm,

N. L. Rector, D. G. Wilder and J. L. Yow, Jr.

Manuscript date: February 1983

LAWRENCE LIVERMORE LABORATORY
University of California • Livermore, California • 94550

CONTENTS

Abstract 1

Chapter 1 Summary and Conclusions 1

1.1 Site Characterization and Geologic Investigations 2

1.2 Thermal Sources 3

1.3 Data Acquisition System 3

1.4 Near-Field and Intermediate-Field Temperature Measurements 4

1.5 Ventilation and Dew-Point Measurements 4

1.6 Radiation-Dose-to-Granite Measurements 5

1.7 Measurements of Radiation Dosage to Man 5

1.8 Rock Stress Measurements 5

1.9 Displacement Measurements 5

1.10 Acoustic Emission and Wave Propagation Measurements . . . 6

1.11 Data Management System 6

Chapter 2 Introduction 7

2.1 Objectives of the SFT-C 7

2.2 Areas of Research in FY 1982 9

2.3 Test Completion Plans 10

Chapter 3 Site Characterization and Geologic Investigations 11

3.1 Geology 11

3.2 Geologic Techniques 15

3.3 Radiation Effects Studies 15

3.4 Drilling Damage Assessment 17

Chapter 4 Thermal Sources 19

4.1 Pressurized Water Reactor Fuel Assemblies 20

4.2 Electrical Simulators 21

4.3 Guard Heaters 21

4.4 Facility Lights 22

Chapter 5 Data Acquisition System 22

5.1 System Configuration 23

5.2 Performance 23

Chapter 6 Near-Field Heat Transfer Measurements 29

6.1 Measurement System 29

6.2 Revised Calculations 30

6.3 Comparison of Data with Calculational Results 33

Chapter 7 Intermediate-Field and Far-Field Heat Transfer Measurements 37

7.1 Revised Calculations 37

7.2 Comparison of Data with Calculational Results 37

Chapter 8 Ventilation System Measurements 43

8.1 Instrumentation Reliability 43

8.2 Ventilation Measurements 45

Chapter 9 Radiation Measurements 49

9.1 Radiation Dose to Granite. 49

9.2 Reliability and Availability of RAM/CAM System 51

9.3 Summary of Radiation Levels Encountered During Handling and Storage Phases 51

Chapter 10 Rock Stress Measurements 55

10.1 Instrument Reliability 55

Chapter 11 Displacement Measurements 56

11.1 Instrument Reliability and Modifications 57

11.2 Effects of Boundary Conditions on Thermomechanical Calculations 65

11.3 Comparison of Measured and Calculated Displacements . . . 72

Chapter 12 Acoustic Emission and Wave Propagation Monitoring 88

12.1 Introduction 88

12.2 AE Monitoring 89

12.3 Wave Propagation Results 93

12.4 Discussion and Interpretation 97

12.5 Conclusions 100

Chapter 13 Data Management System 101

13.1 Current Processing Technique and Modifications 101

13.2 Quantity and Quality of Data Received to Date 108

Acknowledgments 115

References 116

SPENT FUEL TEST--CLIMAX: TECHNICAL MEASUREMENTS
INTERIM REPORT, FISCAL YEAR 1982

ABSTRACT

Tne Spent Fuel Test--Climax (SFT-C) is located 420 m below surface in the Climax stock granite on the Nevada Test Site. The test is being conducted for the U.S. Department of Energy (DOE) under the technical direction of the Lawrence Livermore National Laboratory (LLNL). Eleven canisters of spent nuclear reactor fuel were emplaced, and six electrical simulators were energized April-May 1980, thus initiating a test with a planned 3- to 5-year fuel storage phase.

The SFT-C operational objective of demonstrating the feasibility of packaging, transporting, storing, and retrieving highly radioactive fuel assemblies in a safe and reliable manner has been met. Three exchanges of spent fuel between the SFT-C and a surface storage facility furthered this demonstration.

Technical objectives of the test led to development of a technical measurements program, which is the subject of this and two previous interim reports. Geotechnical, seismological, and test status data have been recorded on a continuing basis for the first 2-1/2 years of the test on more than 900 channels. Data continue to be acquired from the test. Some data are now available for analysis and are presented here. Highlights of activities this year include analysis of fracture data obtained during site characterization, laboratory studies of radiation effects and drilling damage in Climax granite, improved calculations of near-field heat transfer and thermomechanical response, a ventilation effects study, and further development of the data acquisition and management systems.

CHAPTER 1
SUMMARY AND CONCLUSIONS

The Spent Fuel Test-Climax (SFT-C) is being conducted under the technical direction of the Lawrence Livermore National Laboratory for the U.S.

Department of Energy. As part of the Nevada Nuclear Waste Storage Investigations, it is managed by the Nevada Operations Office of the DOE.

The SFT-C is located 420 m below surface in the Climax granite stock where facilities were constructed between June 1978 (when funding for the test was initiated) and April 18, 1980 (when spent-fuel emplacement began). Spent-fuel emplacement between April 18 and May 28, 1980, and spent-fuel exchanges in January and October 1981 and August 1982 met the operational objective of the test: demonstration of safe and reliable packaging, transport, short-term storage, and retrieval of spent nuclear reactor fuel.

The technical measurements program is aimed at acquiring data about the ultimate qualification of granite as a repository medium, as well as the design and prediction of the response of such a repository in granite. Numerous technical objectives were established at the initiation of the test, as presented in the test Technical Concept (Ramspott et al., 1979). Our activities continue to focus on these stated aims.

Data have been recorded continuously on more than 900 channels during the first 2-1/2 years of the test. This period corresponds to spent-fuel ages of 2.5 to 5.0 years out of core (YOC). Most data are acquired through a central data acquisition system (DAS). Periodic displacement measurements and radiation dosimetry data are acquired manually and processed independently of the DAS. Acoustic emissions data are also acquired independently.

This report is the third in a series of technical interim reports (Carlson et al., 1980, and Patrick et al., 1982). It summarizes the data acquired and presents some preliminary analyses and interpretations. For the sake of completeness, we also summarize key results published in topical reports throughout the fiscal year. Some important results that became available in FY 1983 while this report was in preparation are also included.

1.1 SITE CHARACTERIZATION AND GEOLOGIC INVESTIGATIONS

Site characterization and geologic investigations completed this year focused on analysis of core logging and fracture mapping data, initiation of a series of confirmatory radiation effects studies, and analysis of drilling-induced damage around the canister emplacement holes. The following are recent observations:

- The presence of alteration minerals and structural interrelationships between joints indicates that six discrete joint sets are present in the stock. Relative ages of these sets were determined.
- The use of a distinctive low-angle joint set as a reference orientation permitted orientation of the other joint sets observed in the core.
- The damage induced in the rock by hammer-drilling the 0.61-m-diam canister emplacement holes is limited to an annular ring less than 30 mm thick around the hole.

1.2 THERMAL SOURCES

Thermal sources are monitored during the test to ascertain their input for use in thermal and thermomechanical calculations of SFT-C response. Results to date show that:

- Total thermal input to the SFT-C has been 923.4 MW•h during the first 2.5 years of the test.
- The input energy partition is 26.4% from the spent fuel, 14.9% from the electrical simulators, 56.0% from the peripheral guard heaters, and 2.7% from the facility lights.
- Electrical sources of heat, associated controllers, and instrumentation continue to display a high degree of reliability. A set of loop controllers with power-sensing feedback was installed on the electrical simulators to limit the variations associated with line voltage fluctuations.

1.3 DATA ACQUISITION SYSTEM

The data acquisition system continues to function with a high degree of accuracy and reliability. System statistics show that:

- System availability has averaged about 96% (Functionally Disabled Index is 4.13%).
- The accuracy of dc voltage measurements has been maintained within a ±4-μV envelope.
- The accuracy of 4-wire resistance measurements has not been within the anticipated ±0.0092-Ω envelope because of digital voltmeter (DVM) failures which occurred, and were repaired this year.

1.4 NEAR-FIELD AND INTERMEDIATE-FIELD TEMPERATURE MEASUREMENTS

A revised set of calculations was made using a spent-fuel decay curve with slightly lower power at fuel ages greater than 3.0 YOC and different emittances for emplacement-hole components. Comparisons of data and calculations show:

- Agreement at the midplane of the thermal sources is excellent, considerably improved from previous calculations. We conclude from this high level of agreement between calculated and measured temperatures that the rock is relatively homogeneous and continuous with respect to heat flow.
- At the top and bottom of the thermal sources, differences of 5°C or more are observed at the canisters and liners. Some aspects of heat transfer are still being imperfectly modeled. Additional models of convective and radiative heat transfer mechanisms are being considered.
- Agreement throughout the 10 000-m^3 instrumented test volume is good, with the measured temperatures, in general, being slightly cooler than calculated. The slightly cooler temperatures are believed to result from the actual spent-fuel decay power being different from the decay power used in the calculations. Post-test calorimetry of a fuel assembly is expected to confirm this supposition.

1.5 VENTILATION AND DEW-POINT MEASUREMENTS

Ventilation and dew-point measurements document the heat removed from the SFT-C by the ventilation system. To date we have seen that:

- All associated measurements systems have functioned reliably.
- Total heat removal from the SFT-C was about 125 MW•h 2-1/2 years into the test. Of this, 75% was removed as sensible heat and 25% as latent heat of vaporization. Our ability to calculate this heat removal is limited, as noted in the previous Interim Report. Additional models of this aspect of heat flow are being considered.
- About 20 tonnes of water are removed from the facility each year in the ventilation airstream.

1.6 RADIATION-DOSE-TO-GRANITE MEASUREMENTS

Radiation-dose-to-granite measurements with the lithium fluoride dosimeters continued. These measurements are made at the emplacement hole wall and at distances of 200 and 360 mm into the rock. Elevated temperature calibration data were obtained to compensate for the effects of simultaneous heating and irradiation on the response of the dosimeters. In addition, short-term dose measurements were obtained using calcium fluoride and magnesium borate TLDs to investigate the effects of post-irradiation annealing over extended times. In general, data and calculations of radiation-dose-to-granite agree within about ±25%.

1.7 MEASUREMENTS OF RADIATION DOSAGE TO MAN

Measurements of radiation dosage to man indicate that no whole-body dose above background was received during spent-fuel handling and storage operations. Very low finger doses were recorded on technicians responsible for thermocouple installation on the emplaced canisters.

1.8 ROCK STRESS MEASUREMENTS

Analysis of failures of TRAD vibrating-wire stressmeters continued. The entire complement of 18 stressmeters has now been replaced with units having a new hermetically sealed design.

1.9 DISPLACEMENT MEASUREMENTS

Several advances in the measurement and calculation of displacements were made this year. Activities and findings include:

- Temperature compensation instrumentation, including thermocouples and 4-wire resistance measurement devices, was added to the displacement monitors.
- Laboratory measurements of the coefficient of thermal expansion of superinvar indicated an average CTE of about $-33.2 \times 10^{-8}/°C$ over the temperature range of interest.

- Two superinvar connecting rods used in the near-field borehole extensometers failed. Metallurgical analyses indicated stress corrosion cracking.
- A limited number of displacement transducers experienced failures this year; these are units which replaced previously failed potentiometers.
- The SFT-C stress and displacement calculations were repeated using a range of mesh sizes and boundary conditions to study these effects and to confirm the adequacy of calculations which are compared with data.
- Overall agreement between measured and calculated displacements continued to be good. It appears at this time that the thermomechanical response of the SFT-C facility is being accurately calculated by the thermoelastic continuum model. This is in marked contrast with the high level of disagreement between measured and calculated responses to excavation of the facility. Some divergence is developing between the calculated and tape extensometer-measured displacements as a function of time.

1.10 ACOUSTIC EMISSION AND WAVE PROPAGATION MEASUREMENTS

Monitoring of acoustic emission (AE) and wave propagation characteristics continued this year. Observations include:

- Recorded AE activity was a few events per week except when significant perturbations to the thermal field (such as de-energizing a heater) occurred. These perturbations led to rapid, spacially localized increases in AE for brief time periods.
- Trends in shear-to-compression (S/P) wave ratios are stable or slightly increasing with time.

1.11 DATA MANAGEMENT SYSTEM

Activities this fiscal year have focussed on development of the program responsible for compensating the acquired data for temperature effects. Development of a data base of conversion and calibration parameters is nearing completion. Several trial operations of the program on subsets of acquired

data (up to a million words) have been made in order to debug and verify operation of the program. We anticipate having a fully operational version of the code available during the next fiscal year.

CHAPTER 2
INTRODUCTION

The National Waste Terminal Storage (NWTS) Program of the DOE sponsors research and development activities aimed at providing reliable long-term isolation of commercial nuclear reactor wastes in geologic repositories in a variety of host media. This large, multidisciplinary program plans the creation of an operational repository in the 1990s. There will be few opportunities early in the program for field tests involving actual reactor waste.

One such opportunity is being exploited at the Nevada Test Site (NTS). Two existing facilities at NTS are in use to conduct a test of packaging, transport, storage, and retrieval of a limited number of actual spent-reactor-fuel assemblies.

The first of these, the engine maintenance, assembly, and disassembly (E-MAD) facility in southwestern NTS (originally developed for the nuclear rocket program), has the capability to encapsulate spent-fuel assemblies in canisters suitable for geologic storage. All of the remote-handling equipment and interim storage facilities needed to support a geologic storage test were established there in connection with DOE's Commercial Waste and Spent Fuel Packaging Program.

The second facility (consisting of underground construction originally built in the 1960s for weapons effects testing) provides access to an intrusive granitic rock mass (the Climax stock) at a depth comparable to that being considered for geologic storage. This site (located in northeastern NTS about 80 km [50 mi] from the E-MAD facility) required relatively little rehabilitation to accommodate the SFT-C.

2.1 OBJECTIVES OF THE SFT-C

The overall objective of the SFT-C is to evaluate the feasibility of safe and reliable short-term storage of spent reactor fuel assemblies at a

plausible repository depth in a typical granitic rock, and to retrieve the fuel afterwards (Ramspott et al., 1979). An additional objective of the original concept was to evaluate the difference--if any--between the effects of an actual radioactive waste source and an electrical simulator.

Furthermore, since the test involves the largest scale heating of a hard rock medium to date for a test of this type, we have the opportunity to collect technical data addressing two subjects: the ultimate qualification of granite as a medium for deep geologic disposal of high-level reactor waste, and the design of future repositories in granite, or other hard rock, and the prediction of their response to reactor-waste exposure. The following scientific objectives are being pursued to address these two subjects:

- Documentation of displacements and stress changes in the rock comprising the pillars between the central and side drifts due to the mechanical disturbance of mining the central drift.
- Comparison of that response to the results of existing computational modeling to assess the validity of those models in terms of mechanical effects alone.
- Documentation of the temperature and radiation dose in the close-in heated zone to infer both the total power level of the spent-fuel assemblies and the proportion of that power transported out of the canisters by nuclear radiation, as opposed to thermal processes.
- Documentation of displacement and stress effects in the intermediate heated zone due to the thermal disturbance of the fuel and heaters.
- Comparison of measured thermomechanical responses with computational modeling to assess the validity of those thermomechanical models.
- Documentation of the amount of heat removed by ventilation.
- Documentation of the thermal field (both close-in and intermediate) and comparison with calculational models.
- Documentation of the relative effect of existing fractures on rock response by duplication of all mechanical measurements in regions which are either fractured or relatively unfractured, and by direct instrumentation of selected, prominent geologic fractures.
- Evaluation of displacement and stress instrumentation under simulated repository conditions.

2.2 AREAS OF RESEARCH IN FY 1982

Research continued this year toward meeting the stated test objectives. Investigations were carried out in seven general areas.

Site characterization field activities were previously completed. This year we focussed on analyzing the fracture data obtained from core borings and field mapping.

Laboratory studies included further investigation of the effects of gamma irradiation on the mechanical properties of Climax granite. Dose-rate and thermal annealing effects are under study. We also studied the extent of damage induced during hammer-drilling the canister emplacement holes. This work precedes post-test analyses of the effects of heat and heat plus radiation on the borehole walls.

Measurement of near-field and intermediate-field temperatures supported heat transfer studies. Additional calculations were performed to improve the agreement with field data. A ventilation effects test examined heat removal from the facility at four ventilation rates.

Additional radiation dose-to-granite measurements were made and were compared with calculated results. Dose-to-man monitoring also continued.

The principal accomplishment in rock stress measurements was the replacement of nine failed vibrating-wire stressmeters. Most of these had failed previously but were not removed until all units of each of the three sets had failed. The improved, hermetically sealed units described in last year's report were installed (Patrick et al., 1982).

Displacement monitoring continued with the five types of extensometers in use at the SFT-C. To facilitate analysis and comparison with calculated displacements, thermal expansion effects were compensated for in selected data from rod and tape extensometers and the Whittemore gauge.

Acoustic emission monitoring continued this fiscal year. Several interesting AE events were recorded during periods of reduced thermal input to the rock.

In addition to these seven areas of investigation, we maintained the test environment, maintained and operated facilities for data acquisition, and continued development of a system for processing and archiving the acquired data.

The results of these activities are summarized in Chapter 1 and detailed in Chapters 3 through 13.

2.3 TEST COMPLETION PLANS

Plans were developed and published this year which describe activities leading to the orderly completion of the SFT-C (Ballou et al., 1982). The plan details the work elements which will result in the test being completed by mid-FY 1985 with all test objectives being achieved. These work elements are outlined below.

- Spent fuel retrieval will take place in March-April 1983 and will be controlled by existing technical operation procedures. The retrieved fuel assemblies will be placed in lag storage at the Westinghouse E-MAD facility. Electrical simulators will also be removed and stored at the E-MAD facility.
- Removal of storage hole liners will progress in parallel with fuel retrieval. Removal of the liners is necessary to allow post-test coring at the canister emplacement holes.
- Geological characterization will provide in situ stress and modulus data at elevated temperatures.
- Geological sampling will provide specimens for examination of thermal and combined thermal/ionizing radiation effects on the granite.
- Metallurgical sampling and testing will provide important data on corrosion and other damage produced by the test environment on the various metallic components of the test.
- Thermal and thermomechanical response of the SFT-C will continue to be monitored for six months following spent fuel retrieval. Resulting data will aid in validating computer codes and models and will provide important data related to the responses of a repository during conditions of cooling.
- Instrument calibration and evaluation are essential to confirming the validity of acquired test data. In situ and laboratory calibration of instrumentation (as appropriate) will be performed. In addition, vibrating-wire stressmeters will be overcored and

calibrated in a biaxial cell in the laboratory to establish gauge-specific calibration parameters.

- Facility decommissioning will result in mothballing in place or removing for further use (as appropriate) key equipment and systems in use on the test. This decommissioning will be completed by the end of FY 1984, thus completing field activities at the site.
- Preparation of final and topical reports on the project will be completed by mid-FY 1985. These reports will complete the documentation of test operations, results, and conclusions.

CHAPTER 3
SITE CHARACTERIZATION AND GEOLOGIC INVESTIGATIONS

3.1 GEOLOGY

The major effort this year has been to examine the field data that have been collected and to analyze the data in more detail than previously. Preliminary analysis of some of these data has been reported in previous interim reports. The results of the detailed analysis was reported in two topical reports during FY82. The results as presented in these reports (Wilder et al., 1983a, and Wilder et al., 1983b) are summarized in this section but will not be discussed in detail to avoid repetition. The reader is referred to the topical reports for more details.

The objectives of this year's more detailed analysis were to consider four site-specific issues and four basically generic issues. The site specific objectives were to gain a better understanding of:

- Structure of Climax stock.
- Rock mass responses.
- Input parameters for modelling.
- Instrumentation responses--specifically related to their siting and design.

The general or generic issues dealt with characterization criteria and the adequacy of various techniques or methods. Since the general issues are more appropriate in general repository discussions, the results will not be

summarized here. The findings are summarized in the report on the SFT-C structural geology (Wilder et al., 1982b).

The regional structure of the NTS and of the area surrounding the SFT-C has been reported in several earlier reports. Considering the implications of the regional structure on the SFT-C has led investigators to conclude that the general extensional stress condition interpreted elsewhere (Carr, 1974) is valid for the Climax area. This implies that features which are oriented northeasterly (perpendicular to the minimum in situ stress) have the potential for opening due to the relatively low compressional stress acting across them. The Boundary Fault which separates the Climax stock from adjoining alluvium is a capable fault based on Nuclear Regulatory Commission criteria having its last movement between 10 000 and 217 000 years before present. The similarity of orientation between the Boundary Fault, identified in the receiving room of the SFT-C (Patrick et al., 1982), and a fault identified in the area of the shaft station might indicate similar ages for the faults identified subsurface (Fig. 3-1), (Wilder et al., 1982b).

The joints and shears that were reported last year have been examined for trends and relative ages. It was found that six joint sets could be identified. These joint sets include the high and low angle sets but do not include the shears and faults reported earlier. The joint sets are summarized in Table 3-1. It was found that the low angle joint sets are the oldest and were formed during the cooling of the stock. These low angle joints, which were consistently healed and exhibited wall rock alteration, were formed before or during hydrothermal alteration phases during the late stages of stock formation. The chronology developed from detailed study of the joint and wall rock alteration is consistent with the structure observed wherein the low angle joints cause truncation of other joint sets. It is judged that these truncations indicate the inability of younger joints to propagate across the older or preexisting joints during formation. The lack of hydrothermal alteration in the higher angle joints also supports their formation after the hydrothermal activity had ceased. The northeast trending near-vertical joint set was judged to be the youngest set. The chronology of jointing developed indicates that most high angle joints formed before the current stress regime developed.

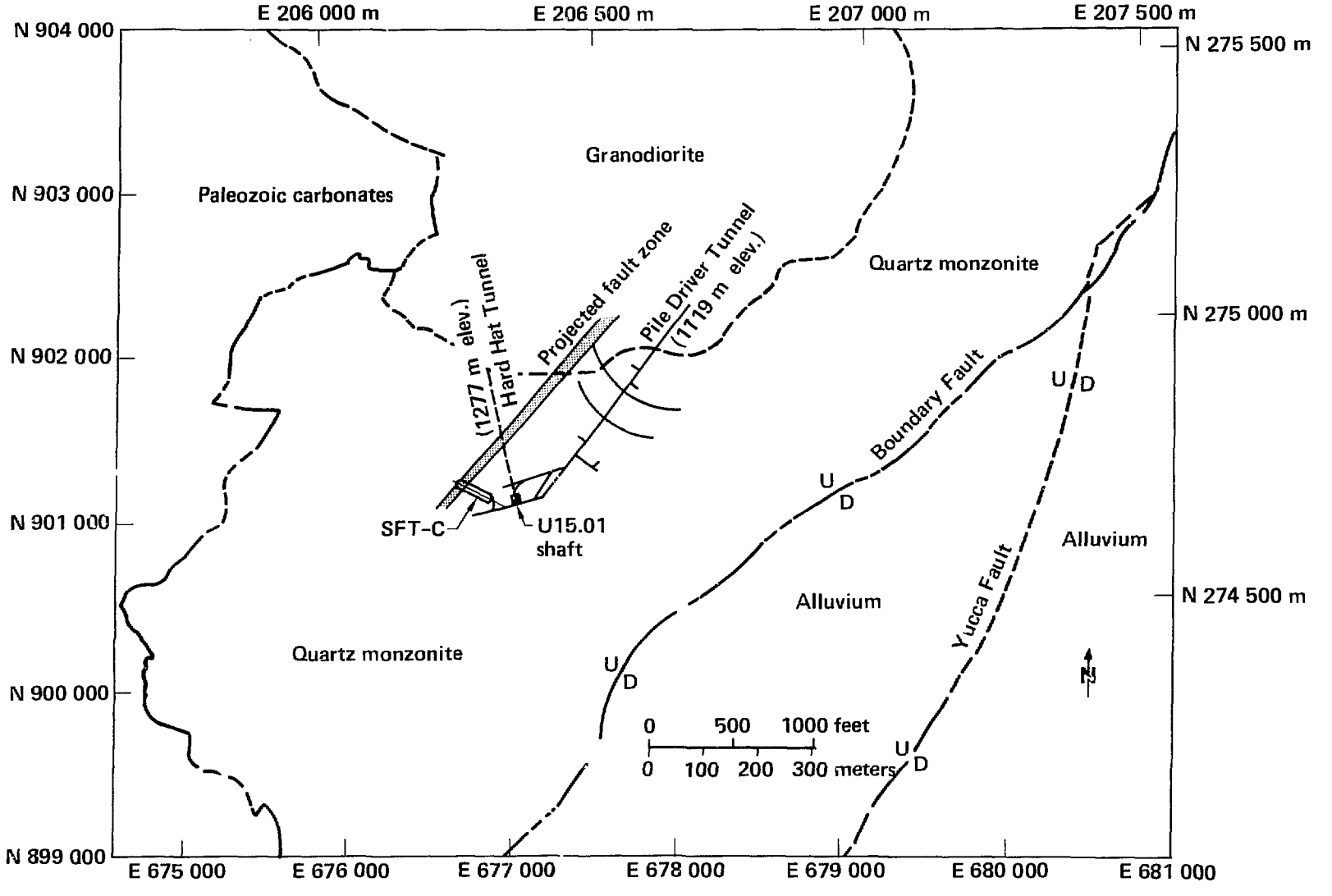

Figure 3-1. Geologic structure of Spent Fuel Test--Climax.

Table 3-1. Joint sets in Climax stock at SFT-C in relative chronological order.

Set	Orientation	Type of joint set
1	N59°E - 39°NW	Healed and hydrothermally altered
2	N44°W - 20°NE	Healed and hydrothermally altered
3	N24°W - near-vertical	Open with calcite and iron staining
4	N59°W - near-vertical	Open with calcite and some iron staining
5	N82°W - near-vertical	Open with some calcite
6	N48°E - 80°SE	Open with calcite, sericite, chlorite

Since the youngest set is the one that is trending northeast, it is subject to opening under the current northwesterly, extensional stress regime postulated for the Nevada Test Site in general and measured in the stock during in situ stress measurements. The orientation of the SFT-C is roughly perpendicular to these joints so that any joint opening caused by excavation-induced stress changes should have minimal impact on the facilities.

Studies of alteration within the Climax stock indicate that an overall deuteric alteration took place while the rock mass was between 365 and 450°C. The hydrothermal fluids involved in this alteration were in rough thermal equilibrium with the rock mass. Joints which formed or were preexisting at this time were altered similar to the general alteration of the rock mass.

A later stage of alteration occurred at temperatures between 330-430°C. Alteration mineralogy indicates that at this time the rock mass was cooler than the fluids in the joints indicating that a period of renewed hydrothermal activity took place after the stock had cooled below the 330°C temperature, but while the magma chamber was still hot. The younger or high angle joints likely formed in response to existing stress fields sometime after the renewed hydrothermal activity had ceased.

An analysis of the possible stress orientations existing at the time of formation of the joints was conducted. This analysis, although based on many assumptions, is judged to be consistent. The early stresses, indicated by the low angle joints that formed under extensional stresses from cooling, are

quite different from those associated with later joints. This was interpreted to reflect a cooling stage for the two earlier joint sets while the regional stress field was still perturbed within the stock. After cooling had progressed to an extent that the regional stress field could be imposed on the stock with little perturbation, the joints formed would reflect the regional stress orientations. Figure 3-2 shows the orientation of the least principal stress as interpreted from the joint analysis. This analysis assumes that the joint sets formed under extensional, rather than shear, conditions. As can be seen, there appears to be a smooth transition in the orientation of the least principal stress orientation from northeast to northwest. Because of the significant difference in orientation for the stresses of the first two joint sets, it seems unlikely that the second set formed after the stock had cooled significantly and stresses re-adjusted. This is consistent with mineralogical and structural relationships which indicate that the second joint formation and filling alteration were contemporaneous.

Statistical analyses of the data indicate that joint spacings are both dispersed and concentrated. This makes the analysis of joint spacing based only on core a very difficult-to-impossible task. Furthermore, analysis of the possible orientation biases using borehole information alone indicated that it would be impossible to completely describe the Climax joint sets from existing core only. The fracture data acquired during underground mapping were utilized in these analyses.

3.2 GEOLOGIC TECHNIQUES

Techniques for orienting core were also developed and evaluated this year. It was found that orienting core based on the average orientation of low angle joints was successful. This allows future core taken from this general area within the stock to be oriented without employing expensive orientation techniques which are commonly used elsewhere.

3.3 RADIATION EFFECTS STUDIES

Following the discovery of an apparent degrading effect of γ irradiation upon the mechanical strength of Climax Stock Quartz Monzonite (CSQM) (Durham 1982), additional laboratory work was undertaken to determine

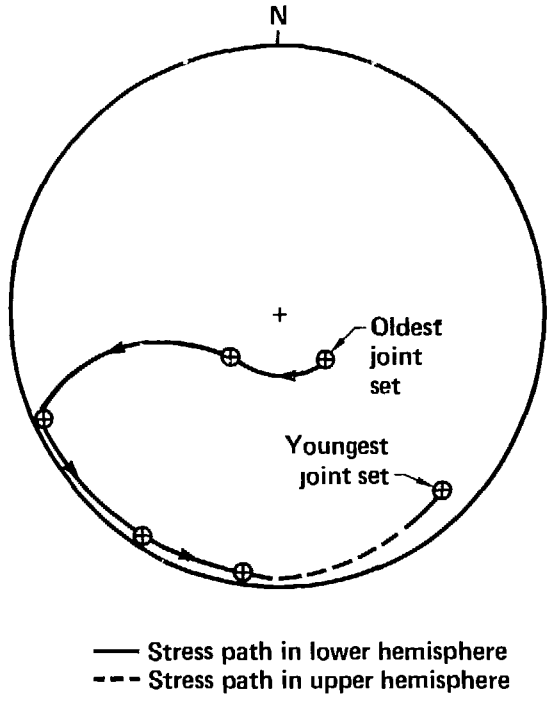

Figure 3-2. Orientation of least principal stress with time (assumes no rotation of Climax stock.

the veracity of the effect and some of its details. In the first study, reported in detail in last year's interim report (Patrick et al., 1982), a group of 14 cylindrical test samples of CSQM were γ-irradiated over a 9-day period to a total dose of 10.5 MGy (1.05×10^9 rad), roughly five times the total dose to rock at the SFT-C over the course of the test. The irradiated samples and a similar number of control samples were then loaded compressionally at a confining pressure of 1 atm until failure. The γ group showed a compressive strength roughly 20% below that of the control group.

In the second round of tests begun this year the effects of the following conditions are being researched: a decrease in dose rate by a factor of 6, irradiation followed by a week long anneal at 85°C, and irradiation followed by a week long anneal at 100°C. As in the earlier tests, unconfined compressive strength is the principal diagnostic property. The total dose to the irradiated samples is approximately the same as in the earlier tests, and a repeat of the earlier tests is built into the test matrix. Including control samples, there are 110 rock samples in the test matrix.

In addition to the second round of irradiation and mechanical testing, an observational examination of irradiated and unirradiated rock is underway to investigate the mechanism of weakening associated with γ irradiation. Based on the effects which irradiation was shown to have on the elastic constants and compressive strength, Durham (1982) inferred that irradiated samples under load begin forming microfractures at a lower "threshold" stress than do unirradiated samples. Microfractures in rock are conveniently imaged in the scanning electron microscope (SEM). A group of 10 samples, half of them γ-irradiated with the same nine day, 10.5-MGy dose, were loaded compressionally to 150-MPa differential stress and then unloaded to generate SEM samples. Polished SEM sections have been made from each of the samples, and crack counting (using the same techniques described in Section 3.4) is underway. Approximately 800 cracks have been photographed and measured in the 10 samples to this point (one third of the intended goal), and no significant difference in crack parameters (length, distribution, density) has yet emerged between the irradiated and unirradiated specimens. As was the case for the observations described in Section 3.4, the rock sections under study here are generally not highly populated with fractures, so that the data tend to be rather noisy. Therefore, no conclusion is being drawn in this portion of the study until substantially more cracks are counted.

3.4 DRILLING DAMAGE ASSESSMENT

In order to discriminate physical changes to rock induced by the waste storage canisters from damage induced by drilling the canister emplacement holes, Weed and Durham (1983) undertook an observational study of rock from the wall of an emplacement hole. Since the emplacement holes (610-mm diam) were hammer-drilled, a technique which requires that rock be broken up before it is removed, a possibility exists that fractures generated by hammer drilling extend into the wall rock around the hole. The importance of identifying drilling-induced damage is raised by the fact that the wall rock receives the most intense radiation and thermal energy from the canisters and will, therefore, be the focus of attention when the canisters are removed.

Weed and Durham examined rock from a section of 150-mm-diam core which intersected, along its length, the edge of canister emplacement hole CEH-18. This core was obtained prior to the introduction of thermal and radiation sources to the test area and thus serves as a "control" for future studies of

thermal and radiation effects. Several 25-mm-diam sections were cut from the 150-mm core parallel to the hole axis at varying distances from the wall of the canister hole. These sections were polished and their surfaces examined for fractures and microfractures in the SEM. Several hundred fractures were documented photographically and quantified with the help of image analyzing hardware. Plots were then made of crack density and average fracture length as a function of distance from the wall [illegible] of the results is shown in Fig. 3-3.

As a general statement, the rock in the 150-mm-diam core turned out not to contain a high density of fractures, so the noise level in the crack counting statistics was quite high. At most points in the core the densities and length distributions of fractures could not be distinguished from background levels observed in rock far from the canister wall. The only 25-mm-diam sections observed to contain abnormal fracture statistics were those which intersected the canister emplacement hole.

The conclusion of the study was therefore that the hammer drilling of the canister emplacement holes changed the physical nature of the rock only within a thin annulus less than 30 mm thick around the emplacement hole and that the physical change involved only a subtle increase in fracture density and length.

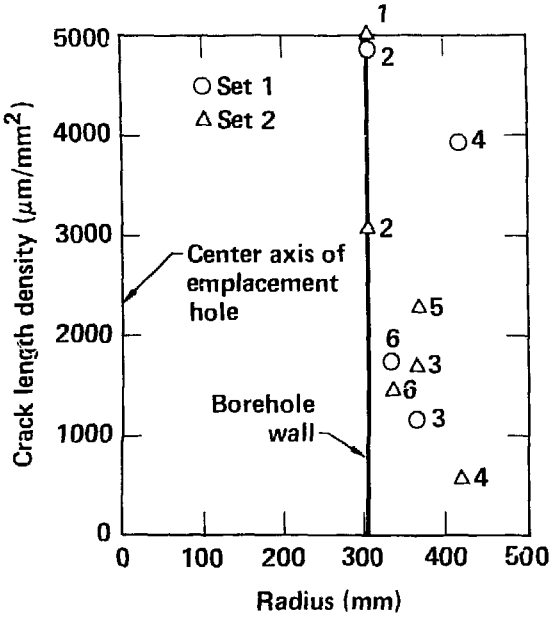

Figure 3-3. Example plot of crack length density vs radial distance from borehole wall; two independent sets of measurements were made (sets 1 and 2) on six specimens (numerals adjacent to data points indicate specimen numbers).

CHAPTER 4

THERMAL SOURCES

During the entire test period from 2.4 to 5.0 YOC, the total thermal energy input to the test array has been 923.4 MW•h, of which 360.6 MW•h was input during the past year. The total is the aggregate of four sources: decay heat of the 11 spent-fuel assemblies from a pressurized water reactor (PWR), 6 electrically heated simulators, 20 electrical guard heaters, and the facility lights. The partition of these loads is summarized in Table 4-1 and shown in Fig. 4-1.

Table 4-1. Cumulative energy input to SFT-C by source.

Source	Cumulative energy, MW•h	%
PWR fuel assemblies (11)	244.1	26.4
Electrical simulators (6)	137.3	14.9
Guard heaters (20)	516.6	56.0
Facility lights	25.4	2.7
TOTAL	923.4	100.0

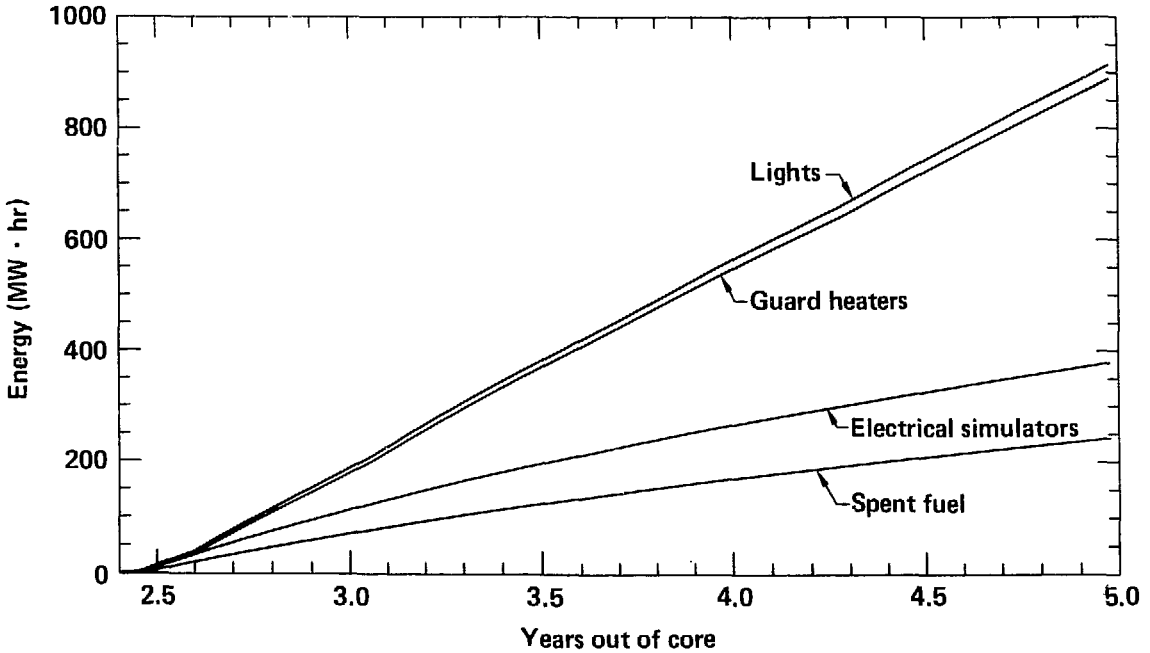

Figure 4-1. Cumulative thermal input by source.

4.1 PRESSURIZED WATER REACTOR FUEL ASSEMBLIES

The thermal characteristics are essentially unchanged from those reported previously. The power level of the assemblies has decayed from 870 to 680 W during the past year and the fraction of the total input has decreased from 30.0 to 26.4%. One additional fuel assembly exchange occurred during this year. Fuel assembly S/N D04 was removed from storage hole CEH 11 on August 16, 1982. Assembly S/N D18 was moved from CEH 16 to CEH 11 on that date. Assembly S/N D22 was placed in the array (CEH 16) on August 18. The D18 assembly was relocated to keep the power of the assemblies in the central portion of the array matched. The D22 assembly, which has not been in the array previously, is a somewhat lower burnup unit and hence has a lower power output. The calculated average spent-fuel decay power curve, adjusted for calorimeter results, is shown in Fig. 4-2.

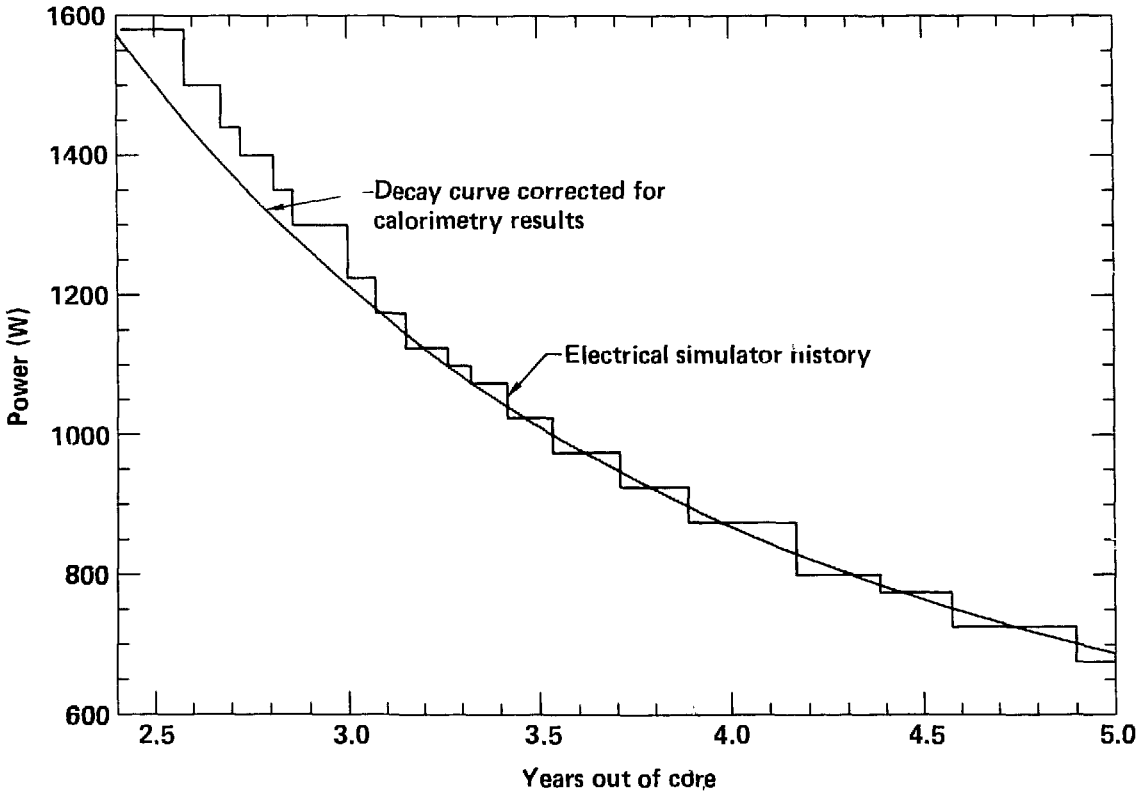

Figure 4-2. PWR fuel assembly and electrical simulator power history.

4.2 ELECTRICAL SIMULATORS

The electrical simulators, located in alternate holes on either end of the storage array, have continued to operate completely reliably during the past year. The simulator power history is shown in Fig. 4-2. As the power level of the simulators was reduced (to match the fuel-assembly decay), the sensitivity of the partial duty cycle controllers to variations in the line voltage became excessive. A set of loop controllers including a power sensing feedback was installed to reduce this effect. The improvement was substantial as is shown in Fig. 4-3.

4.3 GUARD HEATERS

The 20 guard heaters have continued to operate reliably during the past year. No heaters have failed or shown any evidence of erratic performance. The heater power level was increased from 1250 to 1400 W each on March 1, 1982. This level was subsequently reduced to 1350 W each on April 8th. At this point well over half (56%) of the total energy input to the test has come from the guard heaters.

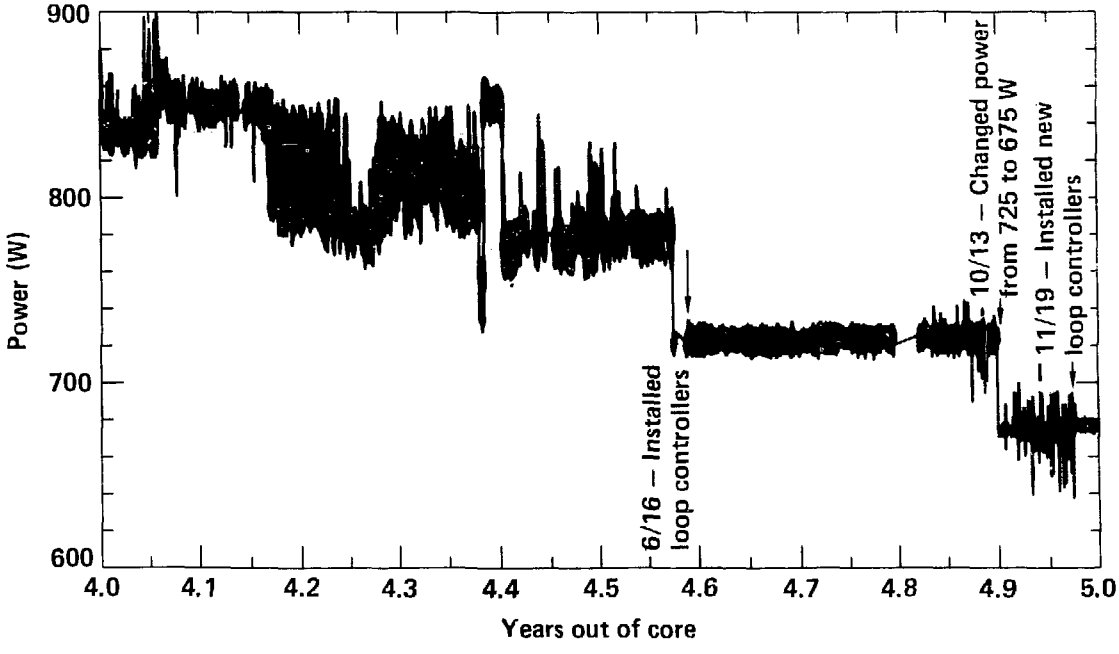

Figure 4-3. Electrical simulator power history showing effect of loop controller addition.

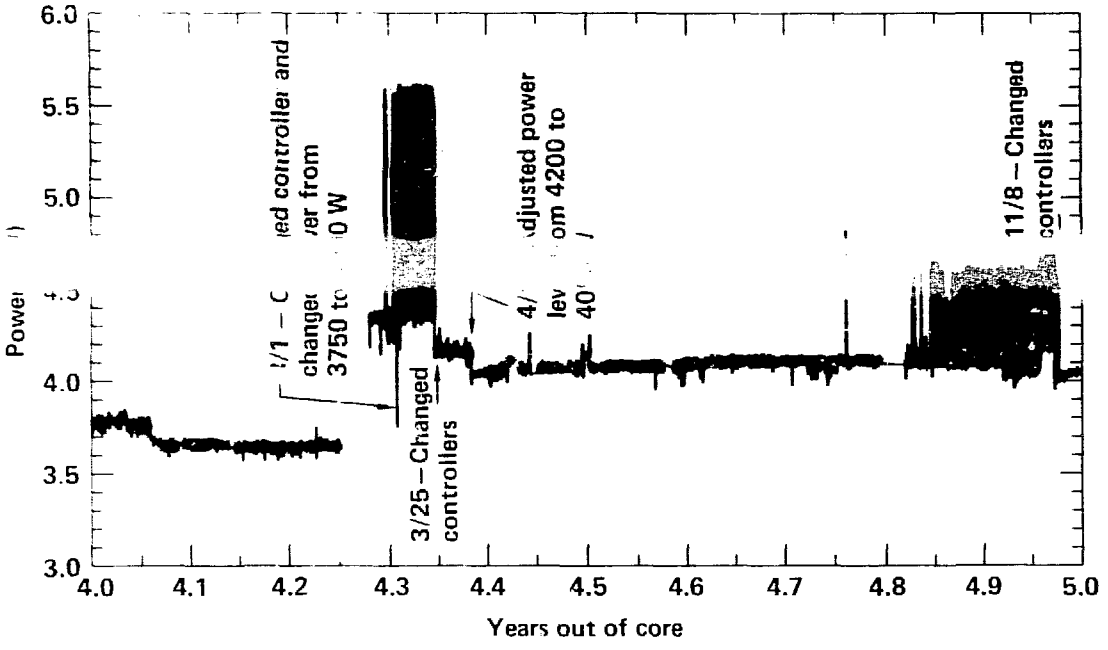

Figure 4-4. Guard heater power history for north heater drift group showing effect of controller malfunctions.

Problems were again encountered this year with one of the heater controllers (NHW003). This controller malfunctioned twice during the year. Once the problem was attributed to a faulty control board component. The second malfunction was more elusive but eventually localized to a heat-sensitive silicon-controlled rectifier. The effect of this erratic controller performance is shown in Fig. 4-4.

4.4 FACILITY LIGHTS

The facility lights were on a total of 400 h during the past year during some 230 tours, the fuel exchange operations, and routine instrumentation maintenance. The total fraction of the input energy is 2.7%.

CHAPTER 5

DATA ACQUISITION SYSTEM

The Spent Fuel Test--Climax Data Acquisition System (SFT-C DAS) has been specified and documented in Nyholm, Brough, and Rector (1982) and Nyholm

(1983). In addition, the DAS has been reported in the ongoing series of annual interim reports (Carlson et al., 1980, and Patrick et al., 1982). The purpose of this section is to further report upon the operation of the DAS, including herein those enhancements that have been made during the last year of operation.

The SFT-C DAS hardware configuration, as illustrated in Fig. 5-1, has been updated to reflect three recent changes. First, the node 100 HP-2648 user terminal now has a HP-2671 hardcopy device attached. Second, a TV system status monitor has been added to computer node 100. Finally, the custom-built modem switching network (MSN) has been modified to interface Bell Telephone Co. dial-up and/or leased telecommunications lines to the computers. Leased line service (type 3002, C2 conditioned) was installed in April 1982 to the CP-40 and LLNL remote terminal stations. This enhancement, circumventing the typically poor dial-up telephone service available at the experiment site, has made the remote-alarm and remote interactive communication capabilities of the DAS fully operational.

As noted in our last report (Patrick et al., 1982), the driver interface to the IRAD datalogger was thought to be responsible for a recurring operating system conflict which resulted in erratic outages of computer node 100. The problem was identified as suspected and as a result, custom driver DVL05 was replaced with "dumb terminal" driver DVB00. This replacement driver was obtained from the Massachusetts Institute of Technology and, since its installation on March 26, 1982, the DAS has operated without another related fault.

5.2 PERFORMANCE

5.2.1 Measurement Accuracy

In our last report, we stated that although the DAS is capable of making measurements over a broad range of scales, its scientific data most heavily depends on dc voltage readings in the millivolt range and on 4-wire resistance readings in the 125-Ω range. To assure long-term measurement accuracy, the digital voltmeters (DVMs) are recalibrated every 90 days and are operated at

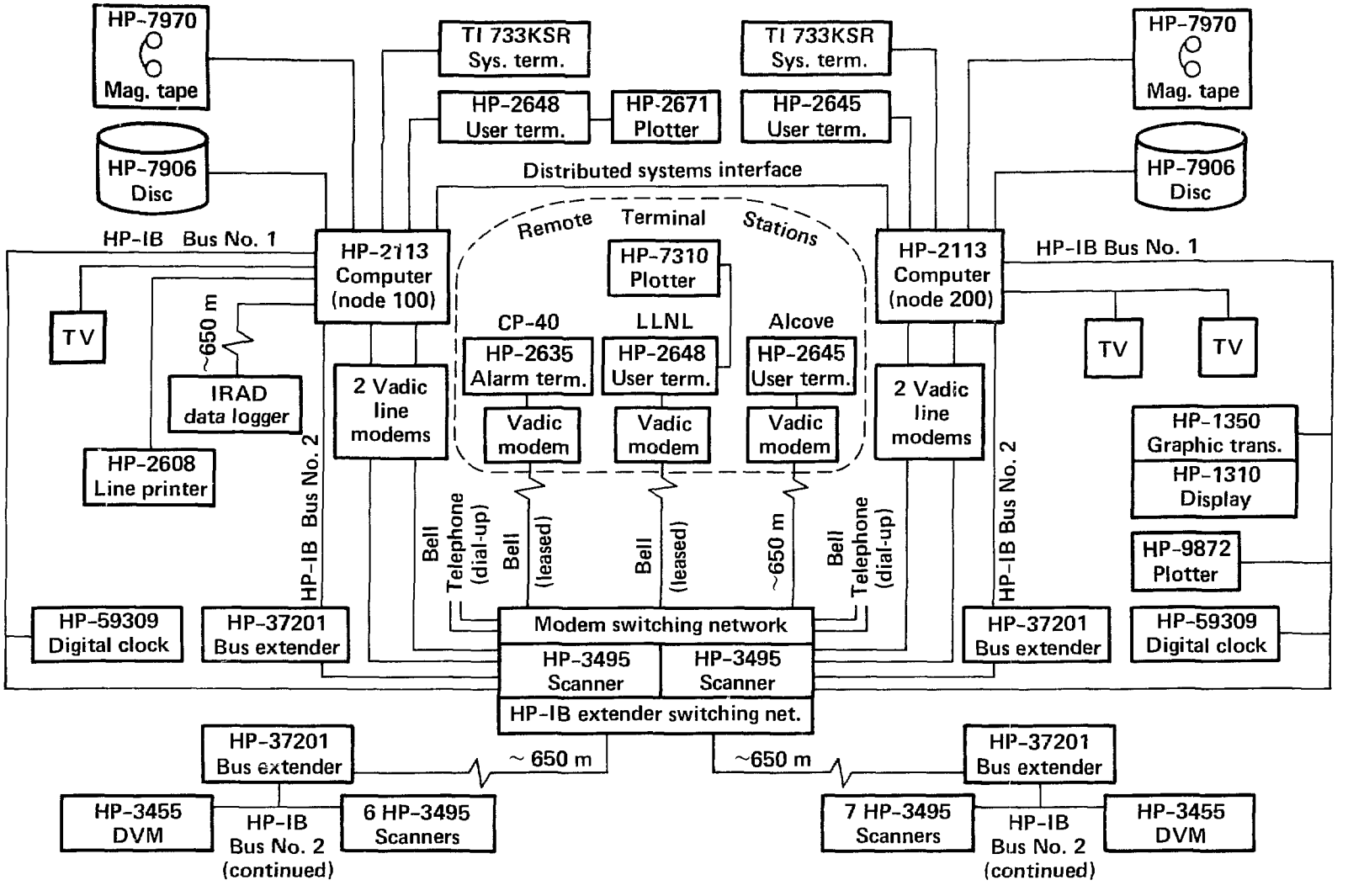

Figure 5-1. SFT-DAS hardware configuration.

~23°C. In addition, several system standard references are measured periodically. These include a precision millivolt source (channels SSR002 and SSR005), two nominally 120-Ω precision resistances (channels SSR003 and SSR006), and several temperature references (channels SSR007, SSR008, RTD200, TRT011, TRT012, and TRT013). The millivolt source is accurate to 1 μV; the resistance values are stable to 0.00018 Ω.

Figure 5-2 illustrates the results obtained from the dc voltage and 4-wire resistance references. The readings provided by the DVMs are guaranteed to 1 μV and 0.0042 Ω with 90-day drifts not to exceed 4 μV and 0.005 Ω, respectively. Resolutions are specified at 1 μV and 0.001 Ω. Examination of those ~20 000 data points/channel collected from 2.7 to 5.0 YOC show that the voltage source is always measured in the envelope 0.996 to 1.004 mV. Minor perturbations are observed as expected at DVM calibration exchanges as indicated by the upward arrows. The 4-wire resistance measurements should be stable to ±0.0092 Ω. However, several periods of out-of-limits readings are noted. Closer examination of that data, coupled with that of the temperature references, reveals that the DVM on node 200 suffered from noise problems after the 4.474 YOC exchange. Similiarly, multiple difficulties with the node 100 DVM are obvious during the period 3.803 to 4.805 YOC. As a result, all DVMs were sequentially routed to the manufacturer for repair and calibration. It is evident from these measurements that variations in 4-wire resistance references are an indicator of potential hardware malfunction, and as such, should be closely scrutinized.

5.2.2 System Reliability

The SFT-C Data Acquisition System has now been operational for more than three years and has proven to perform above the operational specification set forth by Hewlett-Packard. That specification called for a single-point mean-time-between-failure (MTBF) of 30 days, and downtime of at least 2 to 4 days. The relatively long downtime estimate is a function of both the remote siting of the experiment and the availability of qualified service personnel. These figures translate to an average "functionally disabled index" (FDI) of approximately 7%, where the FDI (Nyholm, Brough, and Rector, 1982) is a measure of the likelihood that data cannot be properly recorded and archived on schedule by the DAS as designed. Thus, one node or the other should be capable of acquiring data 93% of the time. The reader should bear in mind

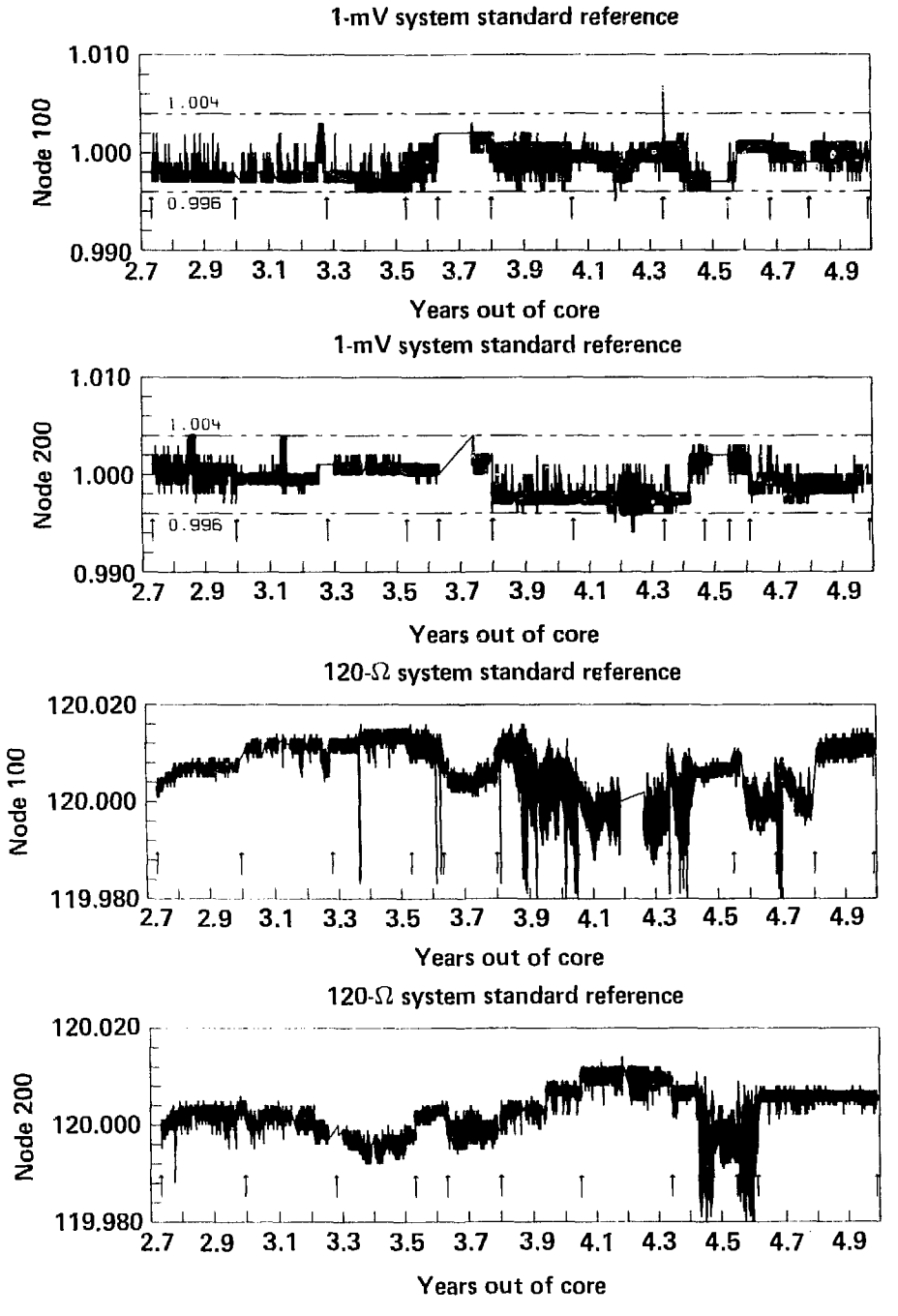

Figure 5-2. SFT-DAS system standard references.

that this statistic was applied prior to development of the modem switching network which allowed each computer node to accomplish the combined functions of both nodes.

Miscellaneous factors that inflate the FDI must be considered if a true estimate of the FDI is to be made. These include:

- Installation and development of software updates.
- Fuel handling operations--data channels of significant interest are scanned rapidly; others may be turned off.
- Hardware maintenance and/or calibration.
- Instrumentation maintenance and/or calibration.
- Cartridge disc unit backup to digital magnetic tape.
- Software failure.
- Computer overburden.

Taken collectively, these factors should account for approximately two additional FDI points, bringing the total FDI to about 9% per computer system.

Figure 5-3 illustrates observed monthly FDIs for the interval May 1, 1980 through November 18, 1982. The upper plot specifies the likelihood that a scheduled data point was not recorded and archived via the front-end data acquisition hardware normally connected to computer node 100 (Fig. 5-1). Similarly, the middle plot reports identical information for data points collected via the acquisition hardware normally connected to computer node 200. The bottom plot presents the likelihood that neither computer node was able to collect a scheduled data point; i.e., both computer nodes were disabled concurrently.

Although examination of Fig. 5-3 shows that no obvious trend is apparent, several points are worth noting. The average observed FDI for node 100, node 200, and the DAS is 15.34%, 9.52%, and 4.13%, respectively. Recording outages through February 1982 have been previously reported and have been basically attributed to software difficulties and a variety of hardware failures. The vast majority of software cures were in place by May 1981. The last was resolved on March 26, 1982 when the IRAD datalogger interface driver was replaced.

Starting in early 1982, the nature of recording failures has been found to have changed. During the latter half of 1981, most outages were related to faulty printed circuit arrangements and/or the hard disc units directly associated with the computer system. Since that time, the front-end data acquisition hardware seems to be the principal source of difficulty. On at

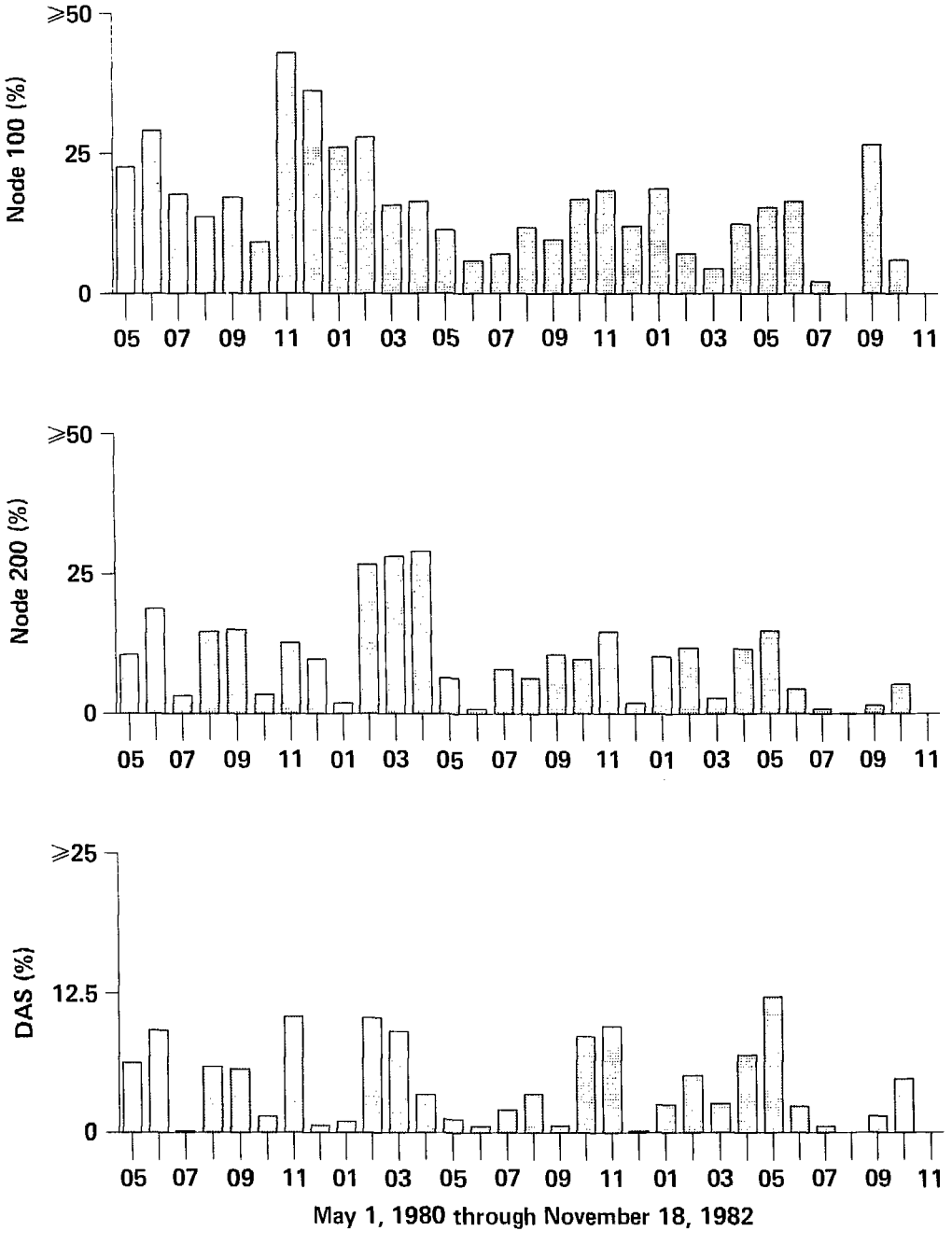

Figure 5-3. SFT-DAS front-end data acquisition hardware monthly FDI.

least two occasions nearby lightning strikes have caused havoc with that equipment. In addition, multiple relay failures in the HP-3495 scanners, as in September 1982, and PCA failures in the HP-37201 bus extenders, have rendered the system inoperable. The major computer-related failure occurred on April 27, 1982 when air conditioners cooling the computer room failed and the area went to 45°C before automatically shutting down via the thermal safety switch. Intermittent equipment difficulties resulted during the subsequent six weeks. That unfortunate incident is obvious in all three plots during April, May, and June of 1982. The thermal safety switch was readjusted to a set point of 40°C.

CHAPTER 6

NEAR-FIELD HEAT TRANSFER MEASUREMENTS

6.1 MEASUREMENT SYSTEM

6.1.1 Reliability

The history of the Inconel 600 Type K thermocouples, as used in the SFT-C, has been flawless. As reported previously (Patrick et al., 1982), the experiment continues without a thermocouple failure. Three thermocouples were destroyed during stressmeter retrievals and one thermocouple was destroyed during a calibration exercise. Another thermocouple was shorted at the isothermal reference block, but a simple separation of lead wires corrected the problem.

6.1.2 Recalibration

To summarize the recalibration effort, only thermocouples that are removed in the normal course of field operations are recalibrated. As reported previously, each fuel exchange exercise allows inspection and recalibration of a small percentage of instruments. During the fuel exchanges in January and October 1981 twelve thermocouples were recalibrated. The third fuel exchange in August of 1982 again gave us the opportunity to perform instrument inspections. Because of a number of activities, involving three fuel-handling operations (Chapter 4), we were able to recalibrate 36

thermocouples from canister emplacement holes 1, 2, 3, 5, 11, and 16. Visual inspection, looking for corrosion damage or mechanical imperfections, has further supported our confidence in the integrity of our measurements. The thermocouples appear as clean and shiny as when they were installed 28 months ago. Calibrations were performed at 0 and 100°C. The results of these calibrations are listed in Table 6-1.

A comparison of these data with previously reported calibration demonstrates that we are maintaining the ability to make precise measurements in the near-field thermal regimes.

6.2 REVISED CALCULATIONS

Several discrepancies between calculated and measured temperatures were discussed in the last Interim Report (Fig. 6-1). We hypothesized that temperature differences in the rock were due to errors in the thermal conductivity and diffusivity of the rock and that temperature differences at the canister and liner were due to errors in the emittances of these surfaces used in the calculations. Although the observed errors were relatively small, we performed a series of calculations using revised input to the TRUMP code to improve the quality of agreement between the measurements and calculations.

Table 6-1. Errors associated with calibrations at 0 and 100°C during August 1982 retrieval operations.

Emplacement hole No.	Error at 0°C		Error at 100°C	
	Mean	Standard deviation	Mean	Standard deviation
CEH01	0.043	0.020	0.134	0.051
CEH02	0.020	0.031	0.162	0.055
CEH03	0.013	0.062	0.064	0.050
CEH05	0.056	0.036	0.003	0.084
CEH11	0.003	0.061	0.167	0.043
CEH16	0.063	0.047	0.176	0.051
Average	0.033	0.024	0.118	0.070

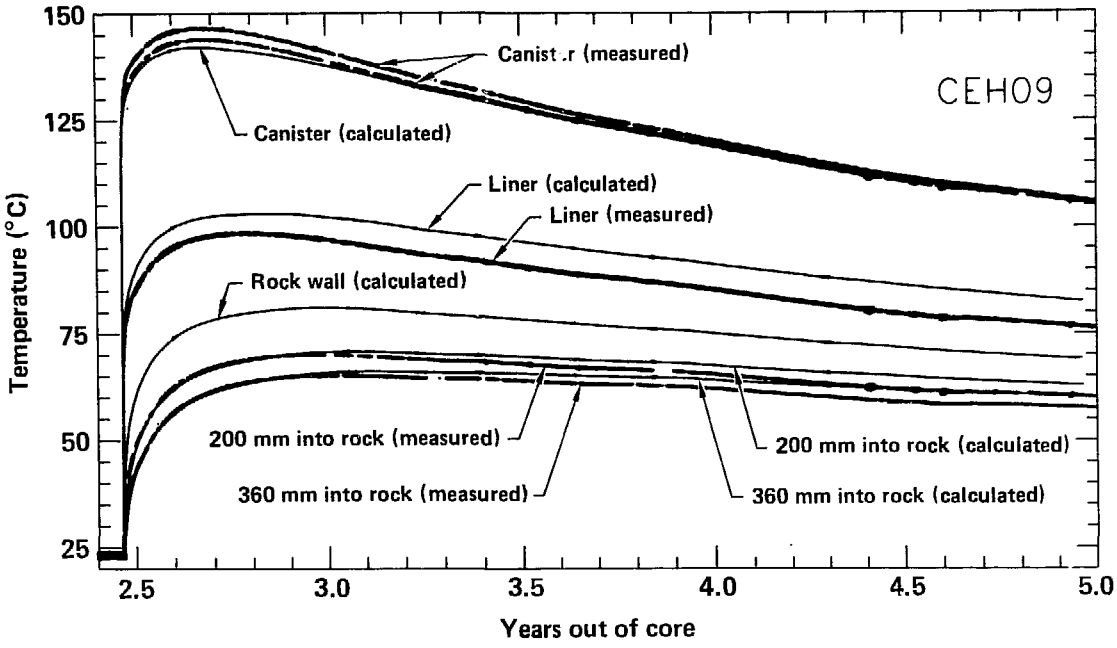

Figure 6-1. Calculated and measured temperature histories at various radial locations at axial midplane of CEH09 (as-built calculation).

The first series of calculations revised the rock thermal conductivity and diffusivity. It was immediately apparent that changes of these properties could shift the calculated temperature-vs-time curves upward or downward, but could not significantly alter the shape of the curves. Even treating diffusivity as slightly temperature-dependent [in accordance with observations by Durham (1982) in other granitic rocks] failed to produce the desired effects.

Using the results of spent-fuel calorimetry (Schmittroth, 1981) and the observed difference between measured and calculated rock temperatures at 5.0 YOC, we proceeded to modify the spent-fuel decay curve in accordance with these observations and to make a second set of revised calculations. The new power curve was developed by gradually reducing the old curve by about 6.5% for times beyond 3.0 YOC. An additional calorimetry will be required to confirm the validity of this approach but it appears that the inventory of short (1- to 2-year) half-life elements was somewhat higher than calculated; leading to a more rapid decay of the power curve at later times. As indicated in Fig. 6-2, agreement between measured and calculated rock temperatures was markedly improved.

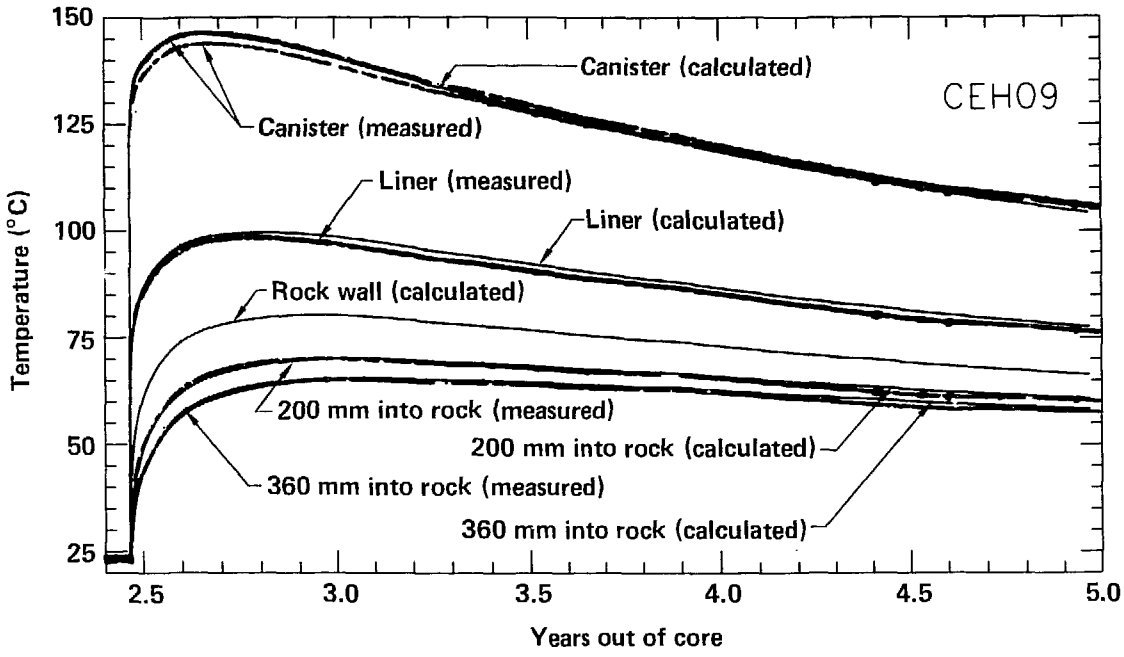

Figure 6-2. Calculated and measured temperature histories at various radial locations at axial midplane of CEH09 (revised calculation).

The third set of revisions is also included in the calculation shown in Fig. 6-2. Here we sequentially modified the emittances of the canister, inner and outer liner surfaces, and emplacement hole wall until satisfactory agreement in temperatures was achieved. Table 6-2 indicates the emittances used in the as-built and revised calculations. Note that all of these values are within the range of available handbook data. Since no direct measurements of emittance have been performed for this project, justification for using the values is founded solely in the fact that it provides better agreement between measured and calculated temperatures.

Table 6-2. Emittances of canister emplacement hole components.

	Emittances			
Calculation	Canister	Inner liner surface	Outer liner surface	Emplacement hole wall
As-built	0.4	0.8	0.8	0.8
Revised	0.4	0.4	0.9	0.9

6.3 COMPARISON OF DATA WITH CALCULATIONAL RESULTS

Figure 6-2 displays the high level of agreement between calculated and measured temperatures at the midplane of the center spent-fuel assembly. More detailed comparisons are possible at various axial and radial positions and selected times for several subsets of the thermal sources present at the SFT-C. Tables 6-3 through 6-5 provide means and standard deviations of differences between measured and calculated temperatures at the top, midplane, and bottom of the thermal sources, respectively. Comparisons are made at the canister, liner, and 360 mm into the rock at fuel ages of 2.6, 4.0, and 5.0 YOC. The subsets treated are the total array of 17 thermal sources, the 11 spent-fuel assemblies, the 6 electrical simulators, and the center 5 spent-fuel assemblies comprising the repository model cell.

Several observations may be made from these tables. First, measured temperatures are consistently higher than calculated at the top and lower than calculated at the bottom of the assemblies at all times and radial positions. As noted last year, this indicates an inadequacy in modeling the very-near-field heat flow. Second, agreement at the midplane in the repository model cell is excellent: within 3°C for the times considered. Third, differences between measurements and calculations are about twice as great for the simulators as for the spent fuel. This may reflect basic differences between the spent fuel and electrical simulators which were modeled to be the same in the calculations. Specific examples are the absence of helium infilling in the electrical simulators and deposition of thermal energy into the rock via γ irradiation from the spent-fuel assemblies. Fourth, the level of agreement, in general, improves with time.

It is apparent that the revised calculations do not yet account for all heat transfer phenomena which are operative in the very-near-field environment. It is also apparent that considerable improvement in the level of agreement between calculated and measured temperatures at the midplane of the thermal sources has been achieved with the noted revisions in input power and emittances. Further modifications to the thermal model and its input will be made in the coming year.

Table 6-3. Differences between measured and calculated temperatures at top of thermal sources.

Radial position	Years out of core	Mean and standard deviations of differences, °C			
		Total array (n = 17)	Spent fuel (n = 11)	Simulators (n = 6)	Repository cell (n = 5)
Canister	2.6	17.94 (8.22)	12.19 (2.07)	28.48 (1.41)	11.93 (1.12)
Canister	4.0	11.46 (5.30)	8.07 (2.38)	17.69 (2.62)	8.35 (0.83)
Canister	5.0	11.22 (6.75)	6.74 (2.85)	19.45 (2.07)	7.30 (1.00)
Liner	2.6	15.64 (5.03)	12.37 (2.25)	21.65 (1.95)	12.73 (1.06)
Liner	4.0	8.11 (3.38)	6.43 (2.32)	11.18 (2.87)	7.03 (1.03)
Liner	5.0	7.34 (3.63)	5.20 (2.02)	11.27 (2.31)	5.86 (0.68)
360 mm	2.6	6.02 (2.15)	5.32 (1.76)	7.48 (2.17)	6.03 (1.35)
into rock	4.0	0.79 (2.37)	0.57 (2.11)	1.19 (2.95)	1.41 (0.33)
	5.0	0.40 (2.14)	0.06 (1.90)	1.03 (2.58)	0.96 (0.19)

Table 6-4. Differences between measured and calculated temperatures at midplane of thermal sources.

Radial position	Years out of core	Mean and standard deviations of differences, °C			
		Total array (n = 17)	Spent fuel (n = 11)	Simulators (n = 6)	Repository cell (n = 5)
Canister	2.6	-4.34 (2.60)	-3.42 (2.33)	-6.03 (2.34)	-2.70 (2.33)
Canister	4.0	-4.55 (4.20)	-2.26 (2.28)	-8.77 (3.61)	-1.21 (1.65)
Canister	5.0	-2.29 (2.75)	-1.77 (2.95)	-3.25 (2.24)	-0.22 (1.37)
Liner	2.6	-1.51 (2.09)	-1.53 (2.10)	-1.46 (2.26)	-1.17 (0.59)
Liner	4.0	-4.53 (2.98)	-3.52 (2.31)	-6.22 (3.39)	-2.82 (0.93)
Liner	5.0	-3.30 (2.51)	-3.21 (2.48)	-3.46 (2.79)	-2.15 (0.81)
360 mm	2.6	0.67 (2.25)	0.95 (2.25)	0.16 (2.37)	2.17 (1.54)
into rock	4.0	-3.22 (3.02)	-2.53 (2.64)	-4.48 (3.49)	-1.29 (0.56)
	5.0	-2.92 (2.66)	-2.51 (2.51)	-3.66 (2.99)	-1.17 (0.33)

Table 6-5. Differences between measured and calculated temperatures at bottom of thermal sources.

Radial position	Years out of core	Mean and standard deviations of differences, °C			
		Total array (n = 17)	Spent fuel (n = 11)	Simulators (n = 6)	Repository cell (n = 5)
Canister	2.6	-19.45 (7.44)	-15.49 (6.17)	-26.71 (1.84)	-12.82 (3.21)
Canister	4.0	-15.06 (7.49)	-10.20 (3.13)	-23.98 (3.51)	- 8.75 (1.67)
Canister	5.0	-11.75 (5.99)	- 8.14 (3.50)	-18.36 (3.01)	- 6.63 (0.95)
Liner	2.6	-13.09 (6.79)	-10.94 (7.52)	-17.02 (2.37)	-10.96 (2.33)
Liner	4.0	-11.77 (5.01)	- 9.38 (3.90)	-16.15 (3.79)	- 8.86 (0.80)
Liner	5.0	- 9.58 (4.17)	- 7.81 (3.50)	-12.82 (3.40)	- 6.54 (0.70)
360 mm	2.6	- 2.87 (2.40)	- 2.24 (1.78)	- 4.02 (3.09)	- 1.41 (1.60)
into rock	4.0	- 5.18 (3.03)	- 3.95 (1.92)	- 7.43 (3.54)	- 3.56 (0.69)
	5.0	- 5.28 (2.85)	- 4.58 (2.57)	- 6.56 (3.13)	- 3.22 (0.42)

CHAPTER 7

INTERMEDIATE-FIELD AND FAR-FIELD HEAT TRANSFER MEASUREMENTS

7.1 REVISED CALCULATIONS

The revised calculations described in Chapter 6 were used to generate the temperature contours discussed here. The changes in emittances influence only the temperatures of materials inside the canister emplacement holes: the same thermal flux is seen by the borehole wall and the rock conductive properties are unchanged in the revised calculations. Revision of the spent-fuel decay curve is seen throughout the rock mass.

A ventilation effects test was conducted during the third quarter of this fiscal year, as described briefly in Chapter 8. Data from that test have not yet been analyzed to the point that they can be used to revise the ventilation model used in these calculations.

7.2 COMPARISON OF DATA WITH CALCULATIONAL RESULTS

Two stations (2+83 and 3+45) are heavily instrumented and thus provide a cross section of temperatures at two locations down the drifts. Figures 7-1 through 7-6 display TRUMP results for times of 3.0, 4.0, and 5.0 YOC together with measured temperatures at the two stations. The TRUMP results are displayed as temperature contours with the outermost contour at 24°C and a contour interval of 2°C. The initial rock temperature was taken as 23°C. Measured temperatures are shown as numerals adjacent to "plus" marks where the measurements are made. The south heater drift is to the left in these figures.

Several observations may be made for these figures. First, there is excellent agreement between measured and calculated temperatures throughout the two cross sections and at all times: generally within a few degrees Celcius. Measured temperatures are, in general, cooler than calculated. Second, in comparing the as-built (Patrick et al., 1982) and revised calculational results, we see only slight differences, as expected with the modest change in power input. Third, there is a high degree of symmetry in the measured temperatures on either side of a vertical plane passing through the canister (center) drift. This is a strong indication of the homogeneity of the rock with respect to heat flow. Although agreement between measured and calculated results is more than adequate, we discuss and investigate

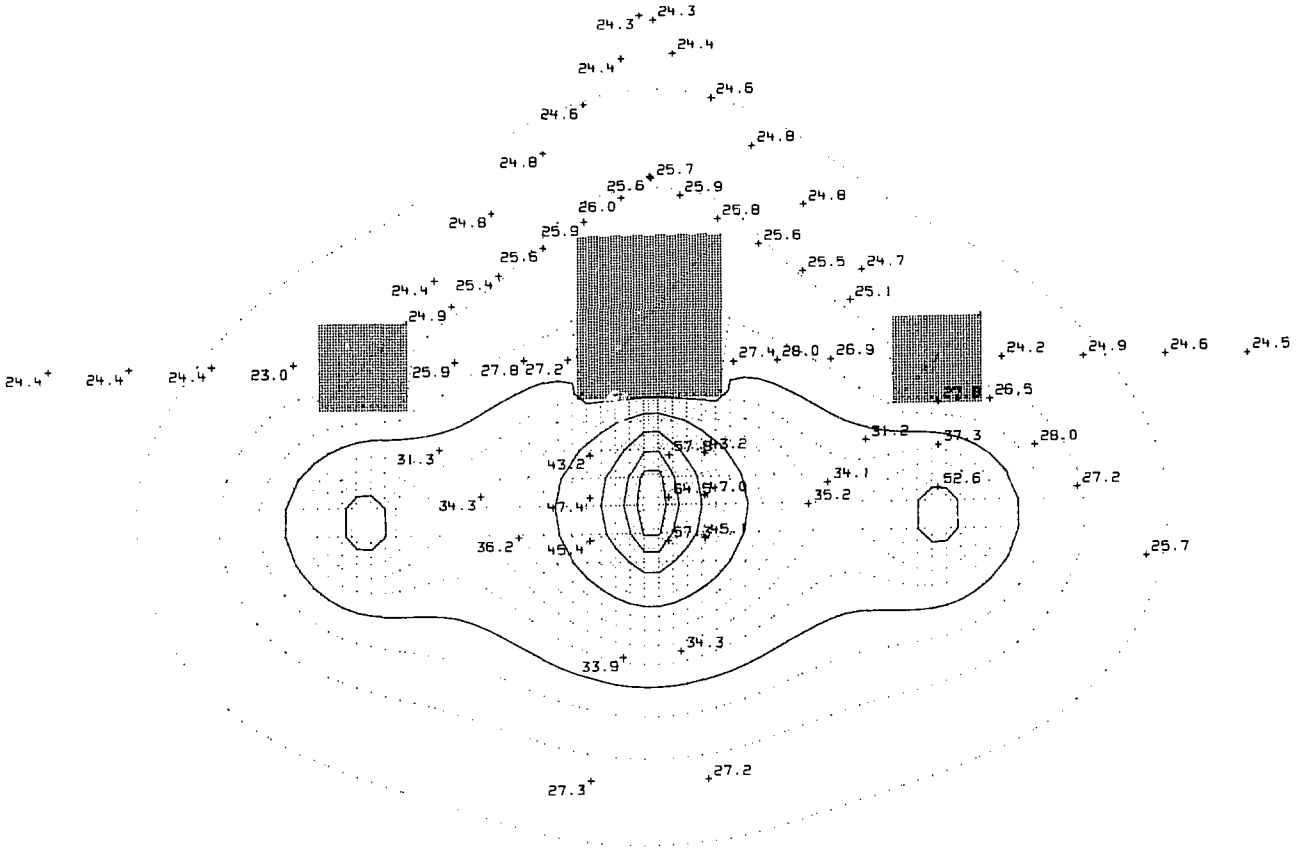

Figure 7-1. Comparison of measured temperatures with TRUMP-calculated temperature contours at 3.0 YOC at station 2+83 (first solid contour at 30°C, contour interval at 2°C).

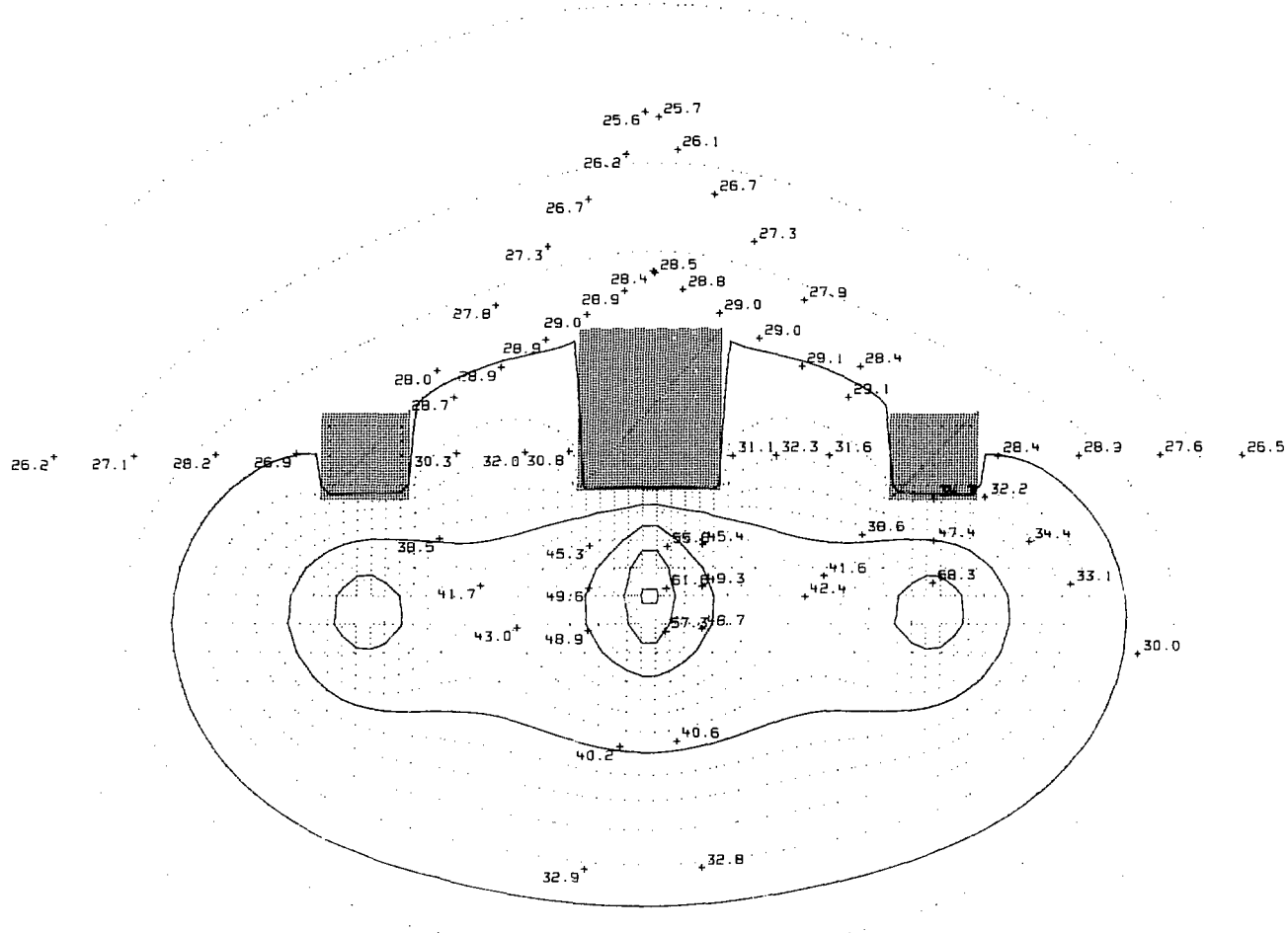

Figure 7-2. Comparison of measured temperatures with TRUMP-calculated temperature contours at 4.0 YOC at station 2+83 (first solid contour at 30°C, contour interval at 2°C).

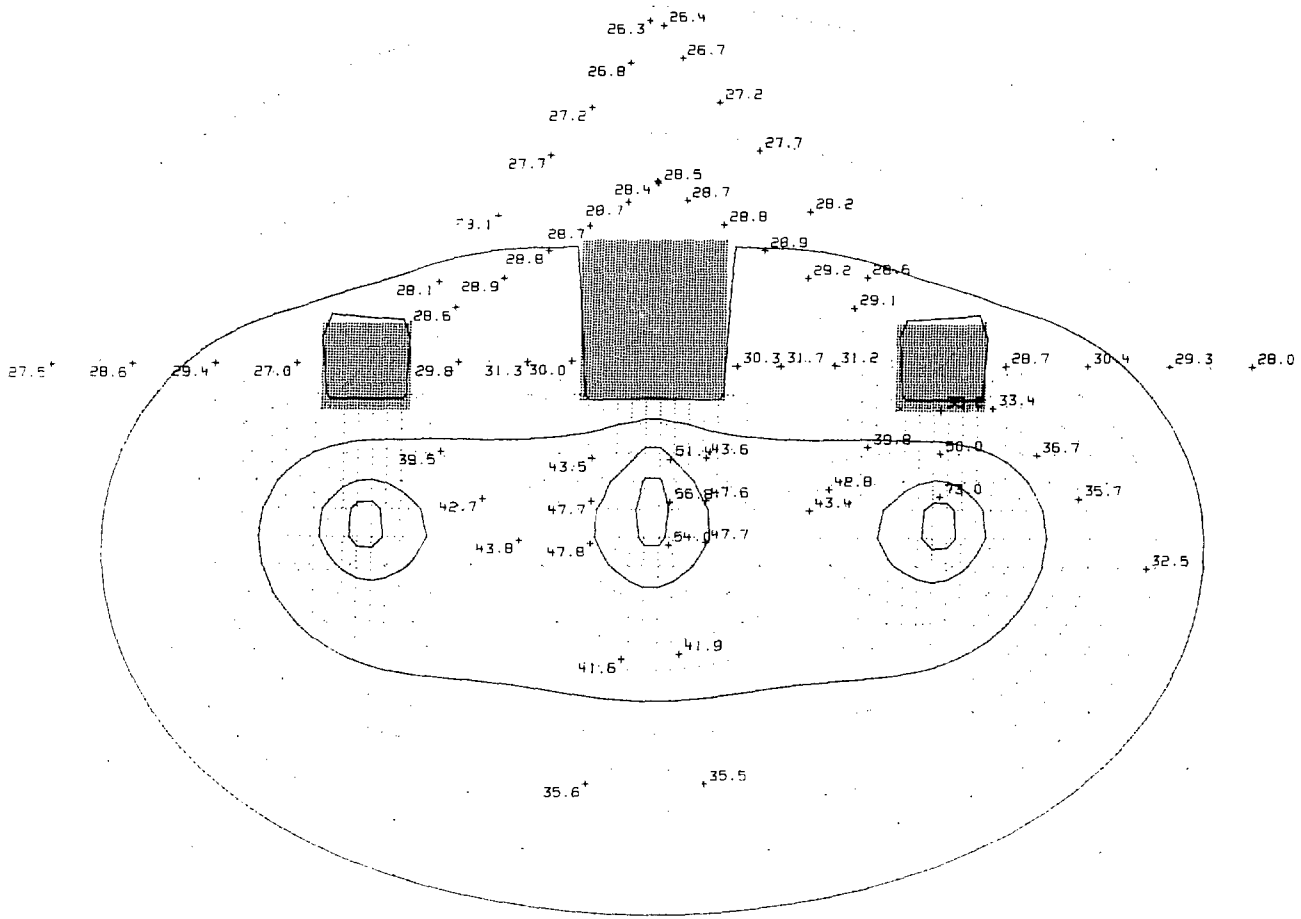

Figure 7-3. Comparison of measured temperatures with TRUMP-calculated temperature contours at 5.0 YOC at station 2+83 (first solid contour at 30°C, contour interval at 2°C).

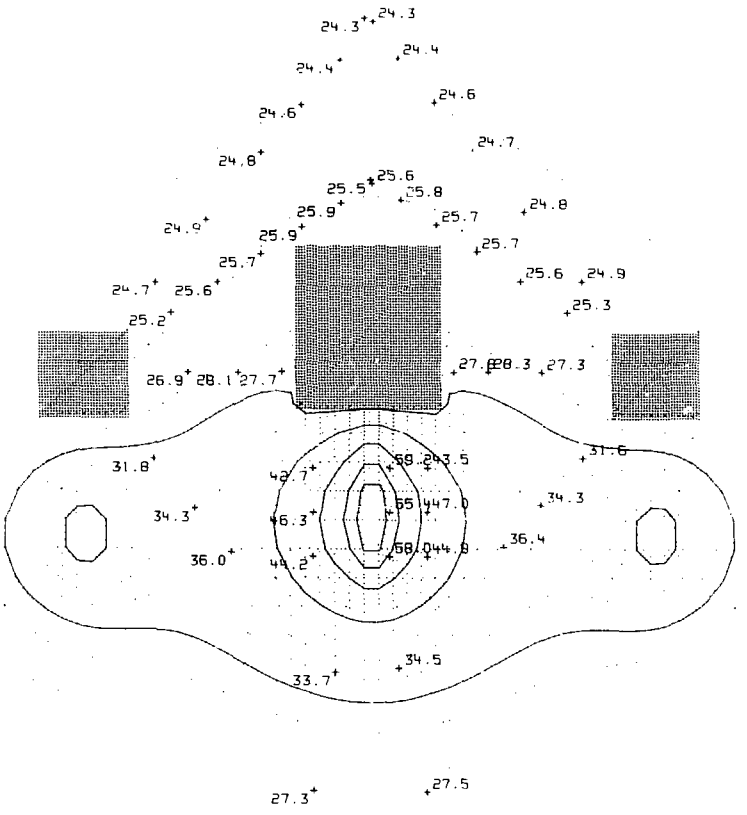

Figure 7-4. Comparison of measured temperatures with TRUMP-calculated temperature contours at 3.0 YOC at station 3+45 (first solid contour at 30°C, contour interval at 2°C).

possible sources of differences to improve our understanding of heat flow in a repository environment.

We now have three observations which are seemingly in conflict. First, the revised calculation provides excellent agreement with measured temperatures within the first few hundred millimetres of rock, indicating that the proper quantity of energy is being deposited in the rock. Second, we observed above that the measured temperatures in the intermediate field are, in general, less than calculated, indicating that either too little energy is being input or too much is being removed from the facility. Third, as discussed in Chapter 8, the measured energy removed in the ventilation airstream is significantly less than calculated. The latter observation should lead to rock temperatures higher than calculated when in fact we see the opposite.

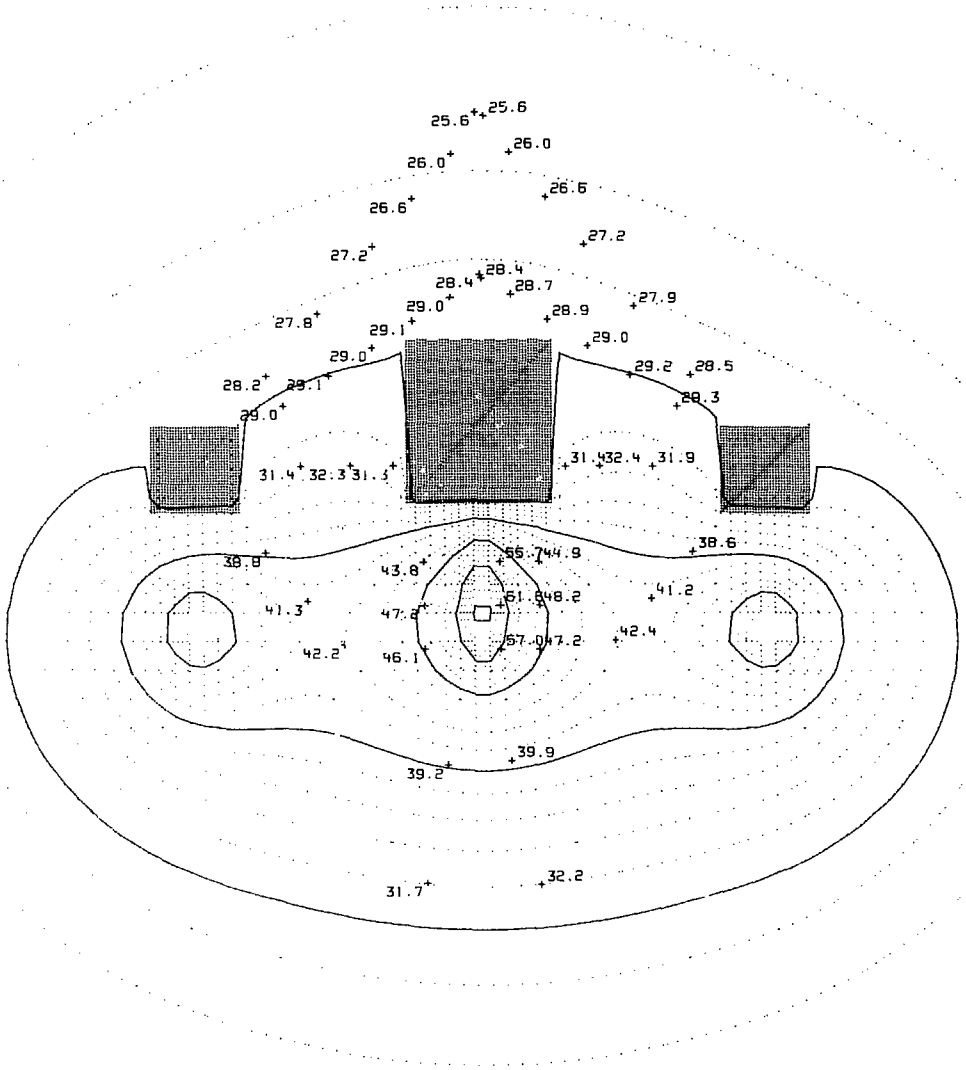

Figure 7-5. Comparison of measured temperatures with TRUMP-calculated temperature contours at 4.0 YOC at station 3+45 (first solid contour at 30°C, contour interval at 2°C).

A potential source of the observed inconsistencies is hypothesized here. The calculation assumes that the thermal sources in the canister and heater drifts continue to infinity, thus permitting two-dimensional analysis of heat flow. This is not true in the test facility since the actual array of thermal sources is only 50 m long. Heat is thus permitted to flow out of the cross-sectional plane whereas it is not permitted to do so in the calculation. This could result in somewhat lower temperatures in the intermediate field.

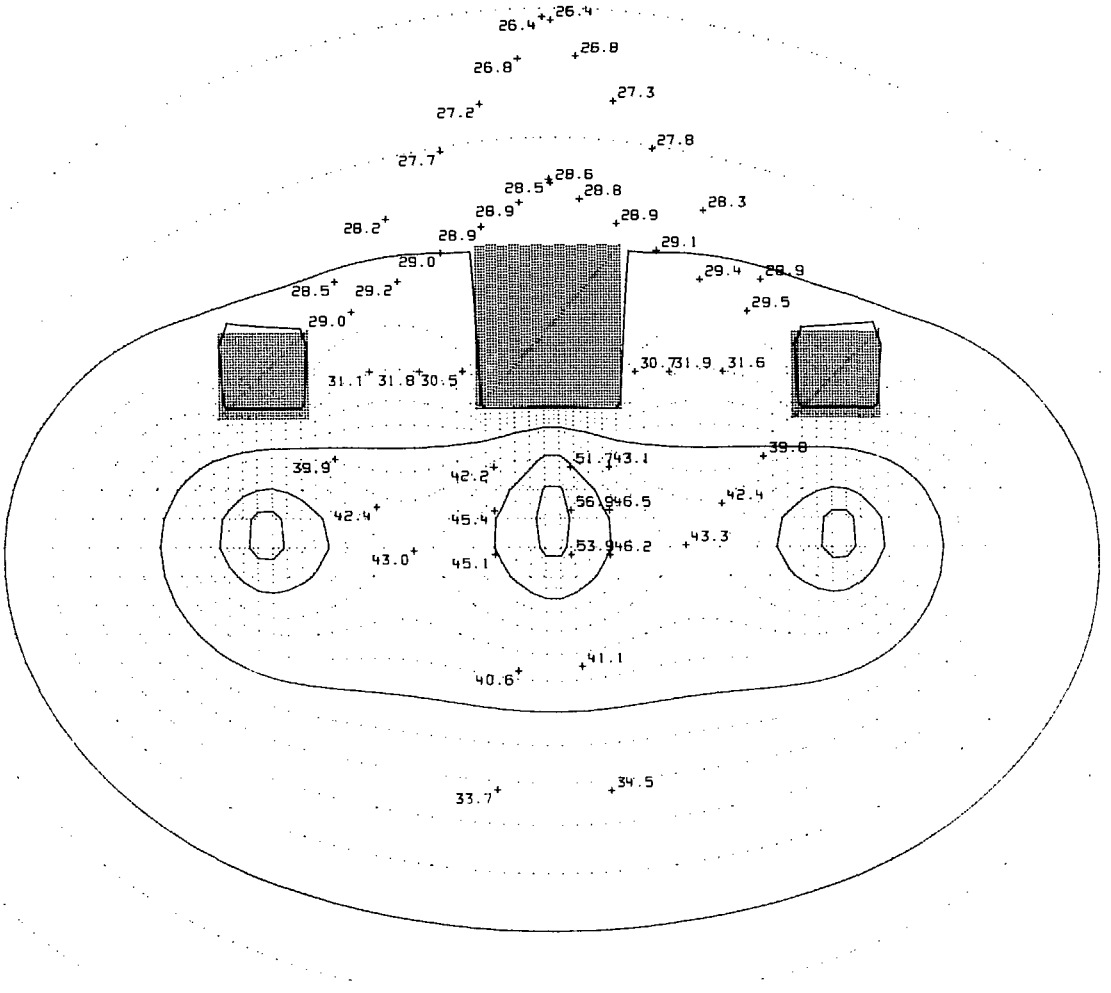

Figure 7-6. Comparison of measured temperatures with TRUMP-calculated temperature contours at station 3+45 (first solid contour at 30°C, contour interval at 2°C).

CHAPTER 8

VENTILATION SYSTEM MEASUREMENTS

8.1 INSTRUMENTATION RELIABILITY

The insertion turbine flowmeter used in monitoring ventilation rate has provided a continuous record with only two exceptions. First, the turbine

signal conditioner failed and was repaired September 1981 (3.8 YOC). Second, the turbine flowmeter was replaced June 8, 1982 (4.55 YOC) after failure of the jewel bearings.

Figure 8-1 represents ventilation rates for all time. Turbine flowmeter data from both AFM001 and its replacement AFM201 are combined here in a single plot. The three fuel exchanges as well as the three ventilation tests are readily discernible.

The dewpoint sensors, DPM001 (inlet) and DPM002 (outlet), are continuing to report data (Fig. 8-2). The cyclic seasonal pattern of dew point is

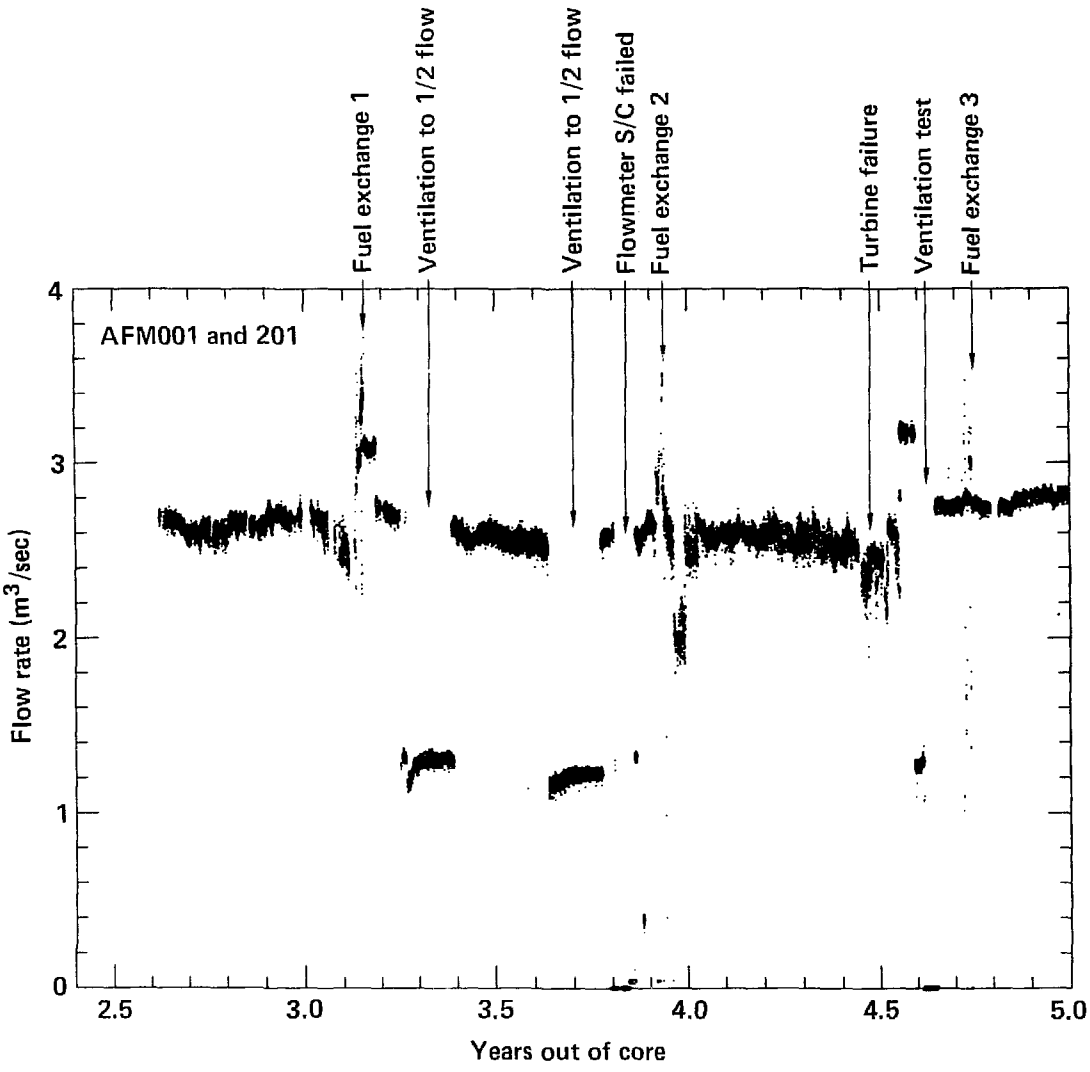

Figure 8-1. Ventilation flow rates recorded by turbine flowmeters.

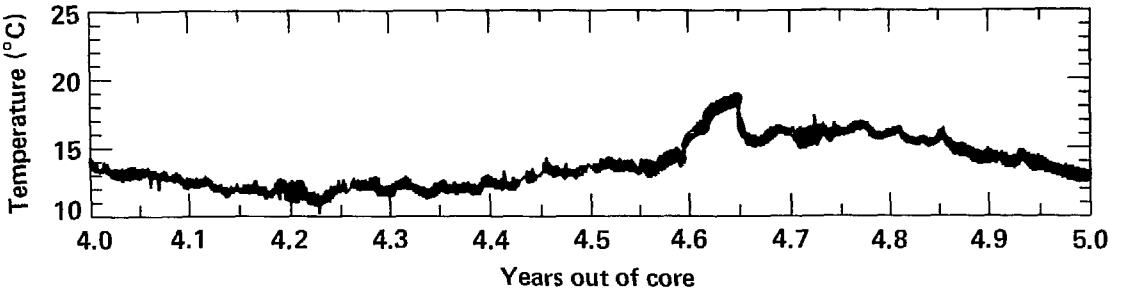

(a). Inlet air dewpoint temperature

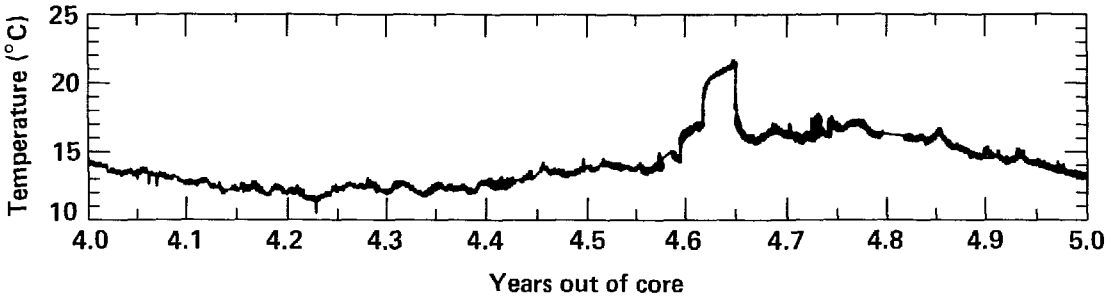

(b). Exhaust air dewpoint temperature

Figure 8-2. Dewpoint sensors: DPM001 (inlet) and DPM002 (outlet).

evident in the plots. The effects of the ventilation tests carried on during July 1982 are very pronounced.

8.2 VENTILATION MEASUREMENTS

As with the previous reports, we discuss the data from the ventilation measurement instruments in a compressed form of 10-day averages. In order to display trends, we are reporting data for all time instead of only the last year.

8.2.1 Input Power

We will discuss the effects of the various thermal input power sources here. Details of individual sources were discussed in Chapter 4.

Figure 8-3 displays the power input and removal history. Planned ventilation tests are readily identified and annotated. The data have been compressed and are displayed as a 10-day running average.

8.2.2 Heat Removed from Test Area

The heat removed from the test area is of two types. Figure 8-4 indicates that the sensible heat comprises about 75% of the total heat removed while the latent heat of vaporization of water comprises 25% of the total. The energy contributed by the test area lighting is included in the calculations and plays a sizeable role in the sensible heat factor in the curve structure. The test area continues to receive a small amount of moisture from seepage through the rock mass and the associated fracture system.

Figure 8-5 represents the latent heat of vaporization of the above-mentioned moisture seepage. The reduction of ventilation rates has a distinguishable effect on latent heat removal.

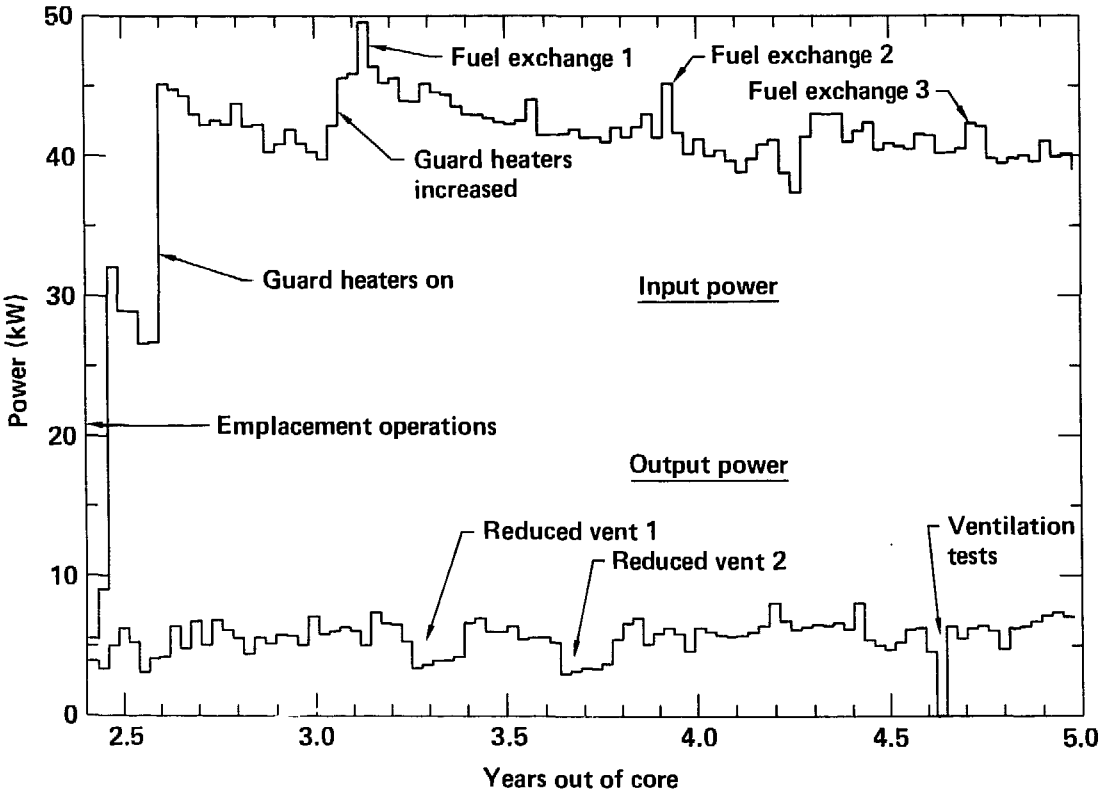

Figure 8-3. Power input and removal history annotated for significant events.

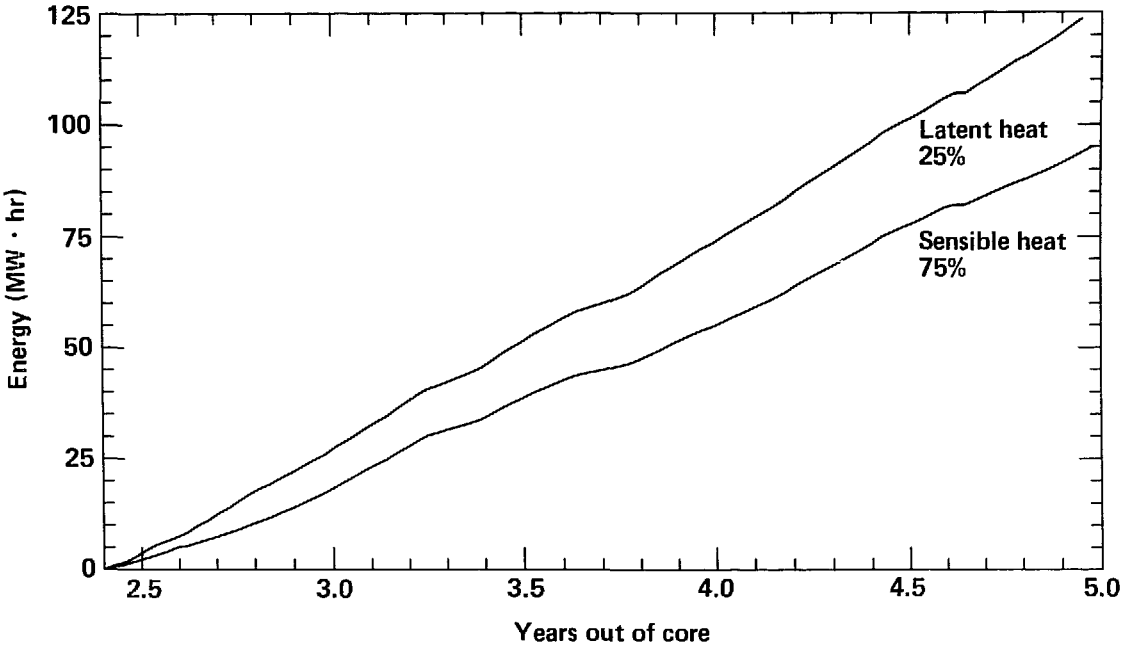

Figure 8-4. Cumulative thermal energy removed by ventilation.

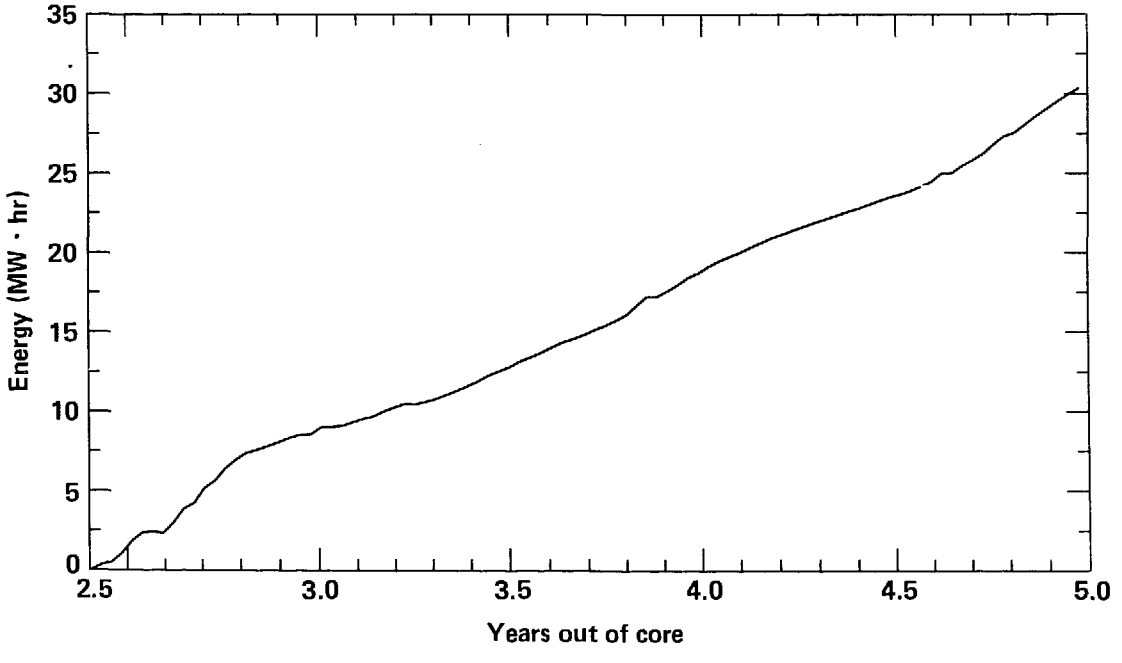

Figure 8-5. History of cumulative thermal energy removed by vaporization of water.

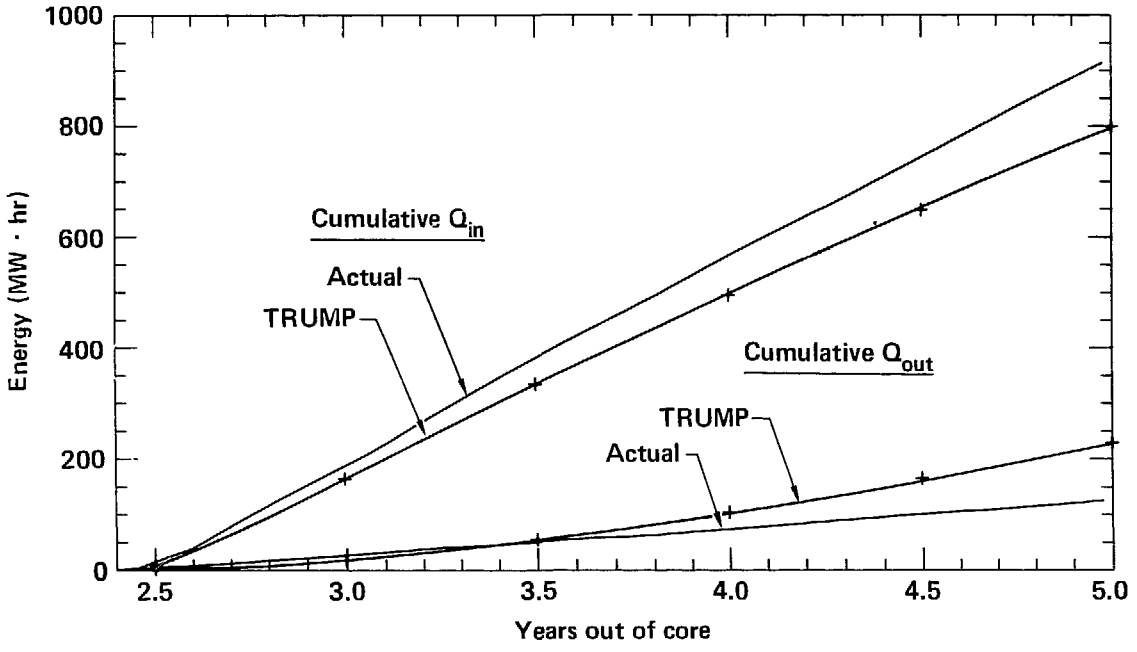

Figure 8-6. Comparison of calculated and actual cumulative thermal energy input and removal.

The ventilation system performance as evaluated by the TRUMP program (Montan and Patrick, 1981) continues to have little or no agreement with acquired data (Fig. 8-6). As reported last year the calculation yields a time-dependent increasing fraction of the input power being removed by the ventilation, with that fraction being about 44% at 5.0 years. The measurements, on the other hand, indicate that while the heat removal rate is directly proportional to the air-flow rate, it is otherwise essentially constant and averages about 15%. The initial spike in Fig. 8-7 is an artifact of construction water vaporizing because the facility began heating up after spent-fuel emplacement and energizing the heaters.

The disagreement between the modeled and measured input power (Fig. 8-6) is explained by the computational model having an insufficient number of guard heaters. This is due to end effects, the overpowering of the electrical simulators early in the test, and the neglecting of the area lighting load. Clearly, the ventilation aspect of our thermal modeling effort is deficient and we will continue working on this problem during the coming year.

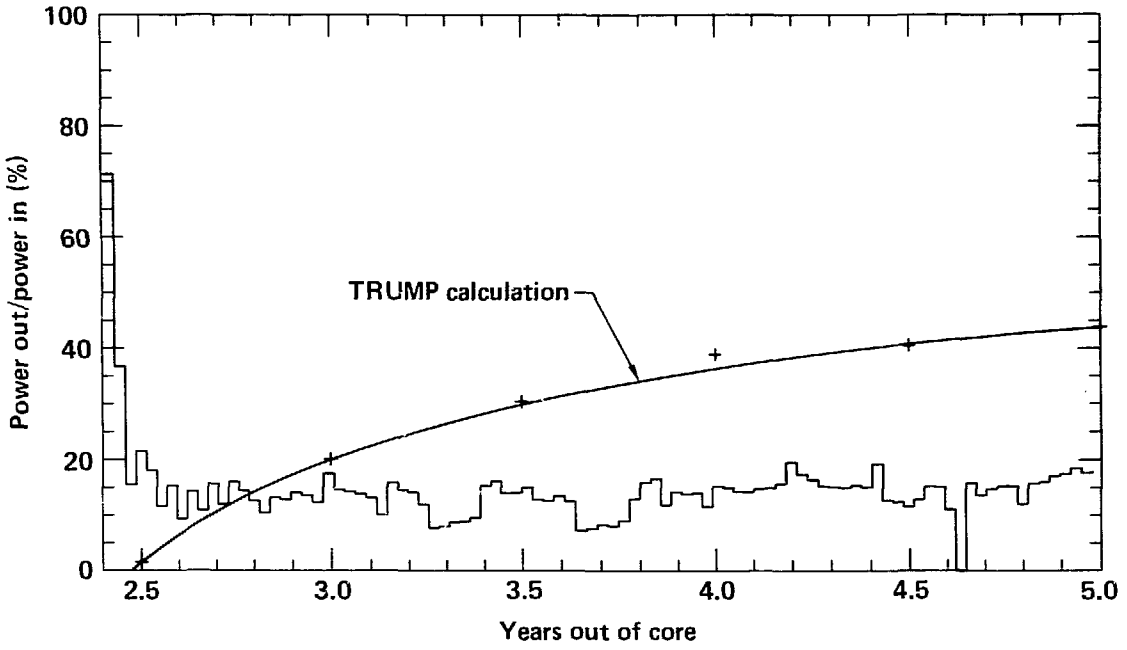

Figure 8-7. Comparison of calculated and actual percentage of input energy removed by ventilation.

CHAPTER 9

RADIATION MEASUREMENTS

9.1 RADIATION DOSE TO GRANITE

9.1.1 Dose Measurements

Dosimeters have been emplaced in 5 of the 17 canister emplacement holes to measure the radiation dose to the granite (Carlson et al., 1980). This work is being performed by EG&G-Santa Barbara Operations. Dosimeters are located at the borehole wall in stainless-steel tubes within four holes containing spent-fuel assemblies and one hole containing an electrical simulator. Furthermore, dosimeters are located at radii 508 and 660 mm from canister centerline in CEH03. Emplacement was made in the hole with the electrical simulator to study the effects of thermal annealing on the dosimeters. These units were exposed to 4×10^6, 3×10^7, and 3×10^8 rad prior to emplacement.

The 7 dosimeter assemblies contain 25 gamma dosimeter subassemblies and 5 neutron subassemblies. Optical grade ^{7}LiF was selected for gamma dosimetry, based on its response above 10^{8} rad and its insensitivity to fading at temperatures above 50°C (Quam and Devore, 1982). The measurement is based on peaks in the photo-absorption spectrum of LiF generated by ionizing radiation. The companion neutron dosimeters consist of Co foils and the Ni present in the 303-type stainless-steel parts of the subassembly. These are used to compensate for the neutron sensitivity of the gamma dosimeters.

Data collected during the first year of the test indicated that a thermal effect influenced the response of one or more of the peaks used in the analysis. This finding was contrary to previously published data but was supported by data obtained from the SFT-C (Quam and DeVore, 1982). To investigate this effect, temperature-controlled exposure holders were fabricated and deployed at a ^{60}Co source to obtain calibration curves over a range of exposures from 10^{4} to 2×10^{7} rad-LiF at a temperature of 70°C. Note that this calibration source did not permit extension of the elevated temperature calibration curve to the maximum required--about 5×10^{7} rad-LiF. This study showed that (1) the calibration curve for the 443-nm peak exhibits a large shift between 25 and 70°C, (2) the 374-nm peak is essentially unaffected by elevated temperature exposure, and (3) the calibration curve for the 247-nm peak showed a minor temperature effect and could be extended to overlap the 374-nm peak data, thus eliminating the need to utilize the temperature-sensitive 443-nm peak. Fabrication of a high-intensity mercury arc lamp was required to extend the calibration data for this peak.

In addition to the concern for the effect of simultaneous heating and irradiation, there was uncertainty with regard to post-irradiation annealing over extended times at elevated temperature. To address this concern, CaF_2 and MgB_4O_7 thermoluminescence dosimeters (TLDs) were installed for a short exposure during the August 1982 spent-fuel exchange (Quam, DeVore, and Sever, 1982). Following calibration, two of each kind of TLD were placed in the capsules normally used to hold the LiF chips. Emplacement at CEH03 permitted measurements at three axial and three radial positions. Exposure times were nominally 1 h.

9.1.2 Comparison of Dose Measurements and Calculations

Armed with the temperature-insensitive, extended calibration curves, Quam and DeVore (1982) were able to reanalyze the previous and current data sets. Van Konynenburg (1982) utilized these data and the short-term TLD data in a comparison with previously reported radiation transport calculations (Wilcox and Van Konynenburg, 1981). Figures 9-1 through 9-3 display the calculated absorbed doses, ±25% error bands, and the three sets of field data.

In general, the data and calculation are in good agreement; both in time and in space. Some of the observed disagreement is believed to be the result of using 25°C calibration data for the 374-nm peak rather than 70°C data because of the previously noted limitations of the calibration source.

9.2 RELIABILITY AND AVAILABILITY OF RAM/CAM SYSTEM

The radiation monitoring systems continue to operate in a very reliable mode.

The Remote Area Monitors (RAMs) have continued to function with only minor problems. Continued calibration testing using the "internal calibrate mode" has identified small errors caused by photomultiplier aging as well as high voltage problems in the detector heads. These types of problems are detected early and corrected with very short down times. Dedicated instrument spares are on hand to bridge the service times for these detectors.

The Continuous Air Monitors (CAMs) have continued to operate without any malfunctions. Monthly inspections using the "internal calibrate mode" has disclosed no problems.

Table 9-1 represents the results of calibrations performed July 20-28, 1982. Calibrations of both systems using a ^{60}Co source for the RAMs and a ^{90}Sr source for the CAMs have determined that the systems are operating within the manufacturers, design limits.

9.3 SUMMARY OF RADIATION LEVELS ENCOUNTERED DURING HANDLING AND STORAGE PHASES

During the August 1982 fuel exchange no exposures were reported. The personnel dosimeters, with a minimum detectable gamma and neutron exposure of 30 mRem, indicated zero for all personnel.

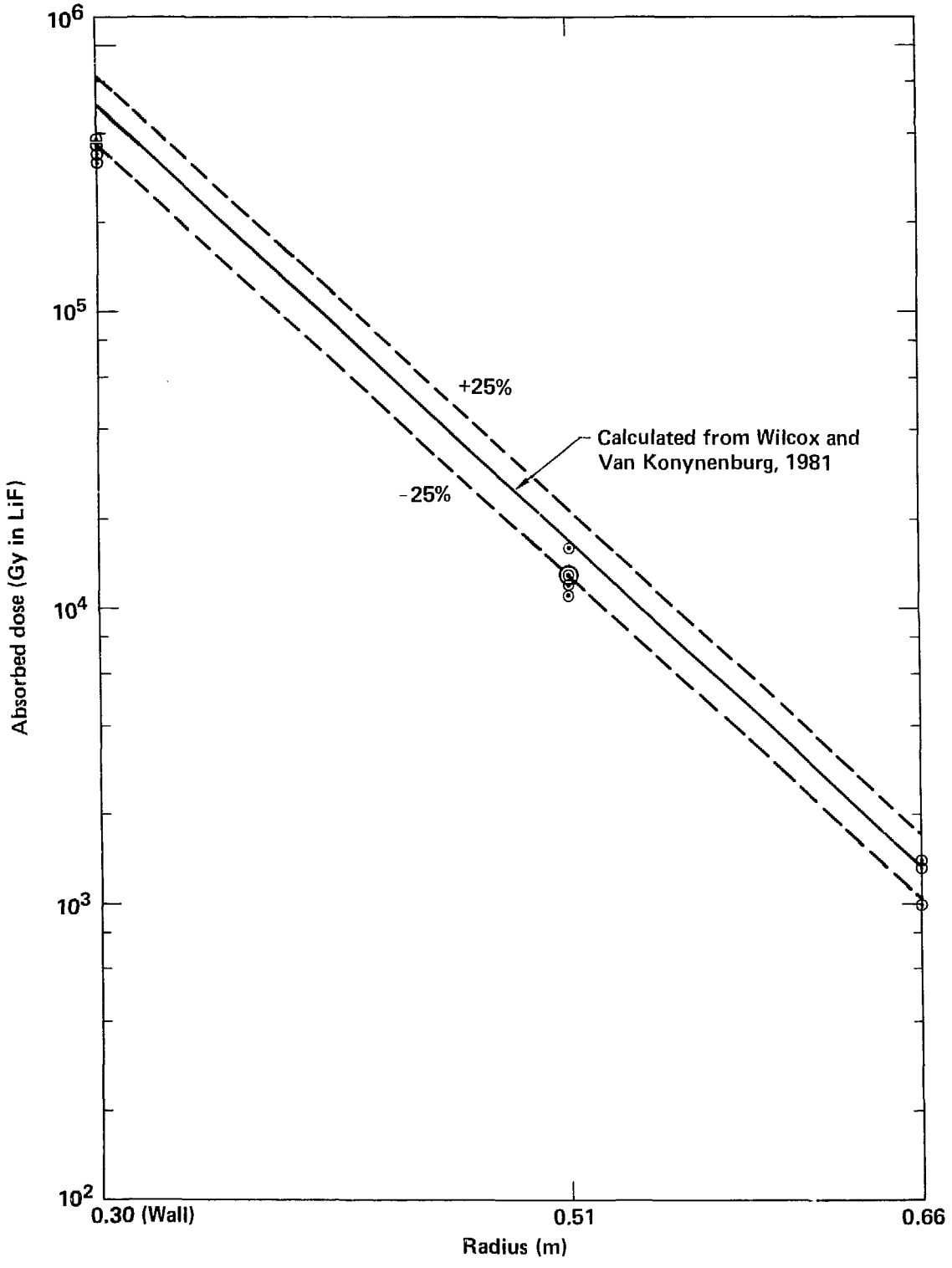

Figure 9-1. Comparison of calculated and optical-absorption measured doses for Hole CEH3 for first period from April 1980 to 12 January 1981 (measured data are from W. Quam and T. DeVore of EG&G--after Van Konynenburg, 1982).

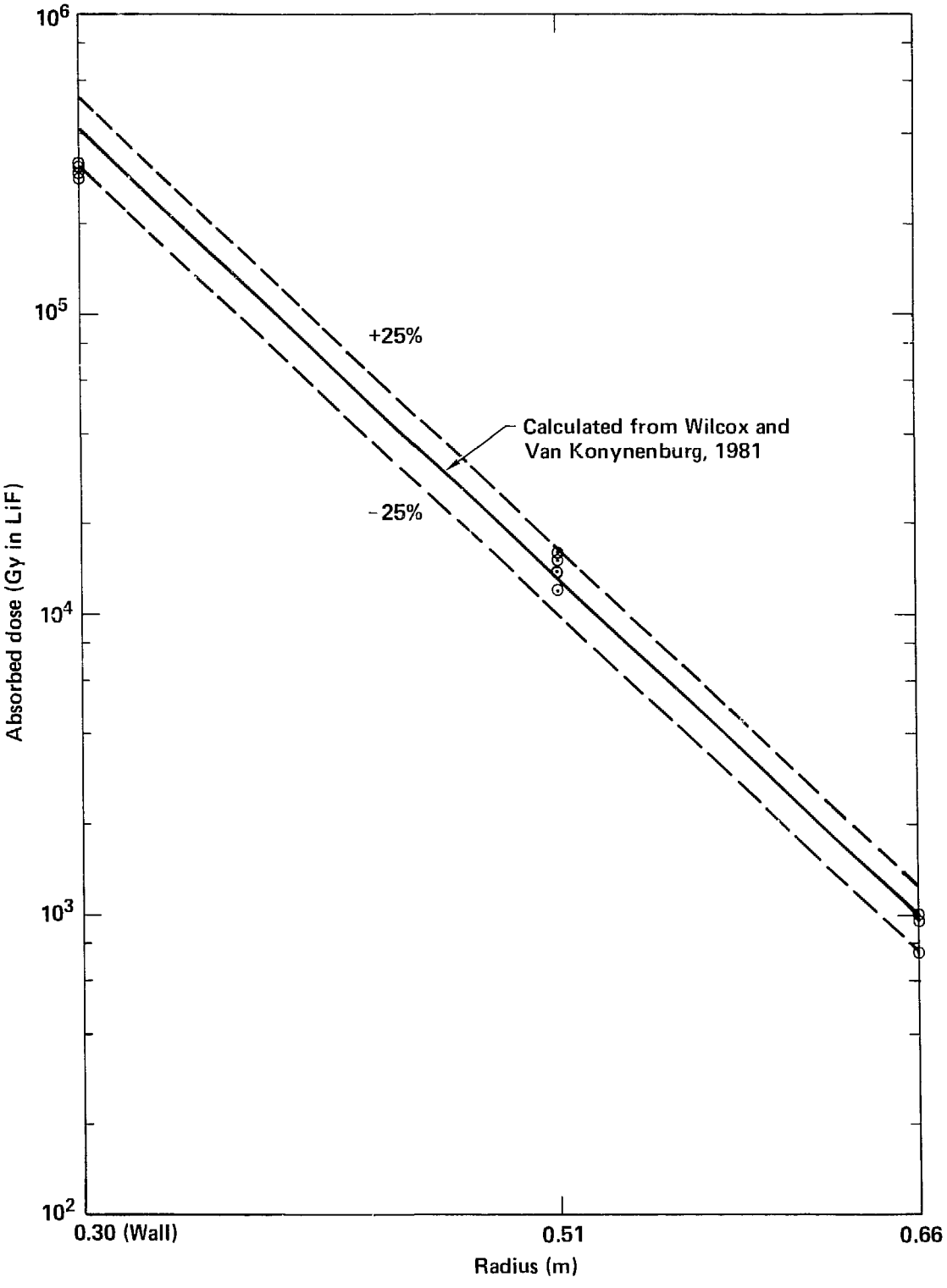

Figure 9-2. Comparison of calculated and optical-absorption measured doses for Hole CEH3 for second period from 12 January to 23 October 1981 (measured data are from W. Quam and T. DeVore of EG&G--after Van Konynenburg, 1982).

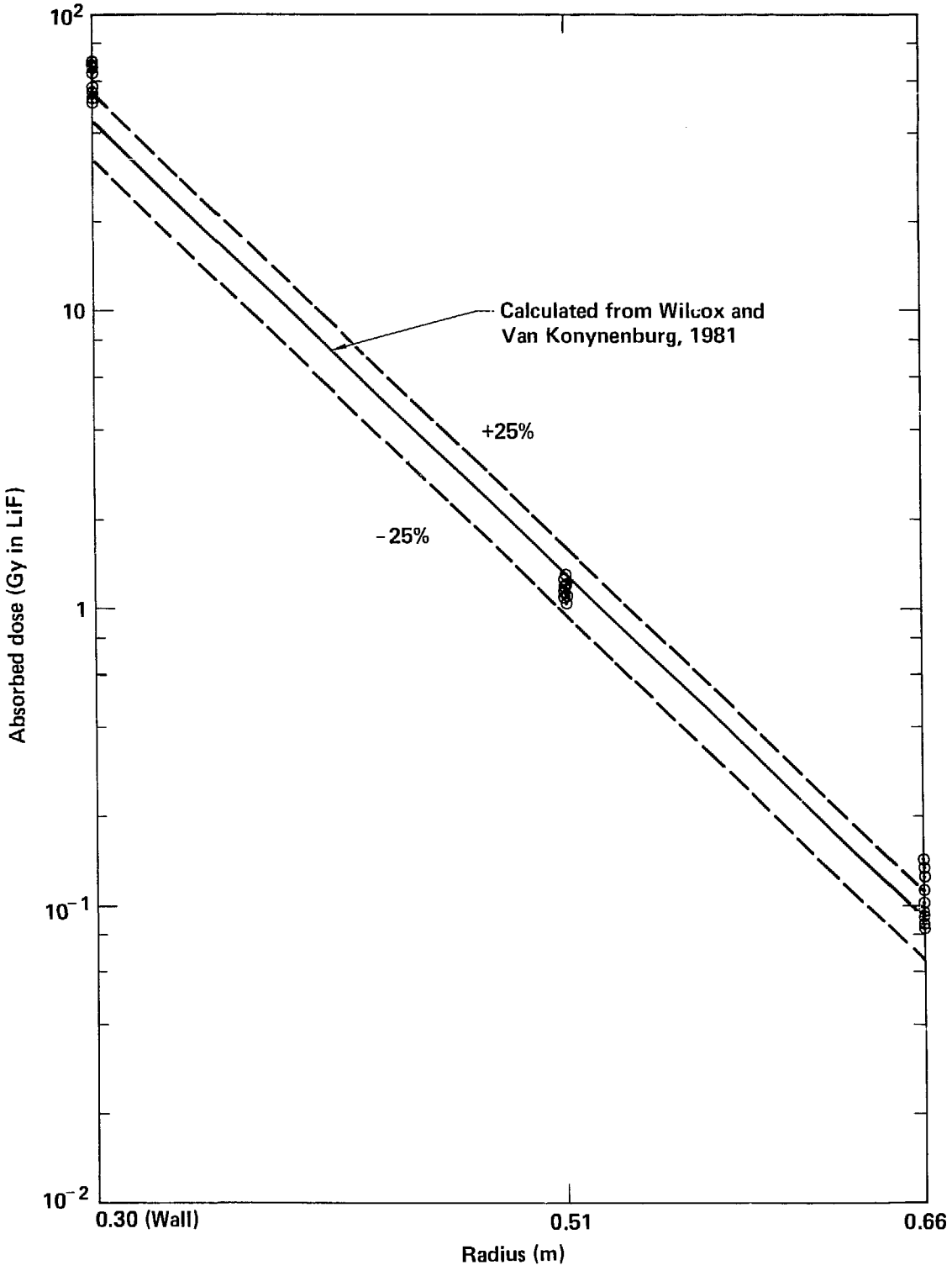

Figure 9-3. Comparison of calculated and thermoluminescence-measured doses for Hole (CEH3) for Hole CEH3 on 13 August 1982 (data measured by Quam, DeVore, and Sever of EG&G--after Van Konynenburg, 1982).

Table 9-1. RAM and CAM calibrations, July 20-28, 1982.

Instrument	"K" value	Old "K" Value	Instrument	"K" value	Old "K" value
RAM 001	2.19	2.13	CAM 101	2.48	2.48
RAM 002	2.29	2.35	CAM 201	2.53	2.46
RAM 003	2.38	2.40	CAM 102	2.55	2.52
RAM 005	2.18	2.19	CAM 103	2.53	2.47
RAM 006	2.29	2.24	CAM 203	2.46	2.46
RAM 007	2.25	2.26	CAM 104	2.48	2.46
RAM 008	2.00	a	CAM 204	2.49	2.47
RAM 009	2.00[b]	2.00	CAM 105	2.46	2.61
RAM 010	2.21	2.13	CAM 205	2.46	2.45
RAM 011	2.17	2.13	CAM 106	2.52	2.45
RAM 012	2.00[b]	2.00	CAM 206	2.42	2.42
RAM 013	2.00[b]	2.00	CAM 007	2.23	2.23
			CAM 008	2.03[c]	2.05

[a] Because RAM 008 is a replacement RAM, no old "K" value exists.
[b] RAM 009, 012, 013 are high level RAM and were not calibrated.
[c] CAM 008 is the Krypton monitor and the "K" value converts the voltage to counts per minute.

CHAPTER 10

ROCK STRESS MEASUREMENTS

10.1 INSTRUMENT RELIABILITY

It was reported in the previous Interim Report that 13 of the 18 stressmeters had failed. Nine instruments were replaced. Since that time, the remaining five instruments failed. The failed instruments were removed and inspected to determine the failure mechanism. As expected, the gauges all failed in the same manner as the original 13; moisture penetration of the seals and corrosion of the vibrating wire.

None of the modified gauges that were installed in the June 1981 activities has failed to date.

Table 10-1. Vibrating-wire stressmeter data for October 1982 installation.

License	Serial number	IRAD channel	Depth, cm	Orientation	Emplacement reading			
					Zero	Tool set	Tool slack	Tool out
NSG231	6-15	1	325	CW60°	2110	2313	2312	2307
NSG232	6-3	2	335	Vertical	2121	2334	2334	2325
NSG233	6-46	3	345	CCW60°	1928	2133	2132	2115
NSG234	6-47	4	95	CCW60°	1790	1997	1993	N/A
NSG235	6-2	5	105	Vertical	2120	2332	2329	2313
NSG236	6-13	6	115	CW60°	1983	2180	2178	2174
NSG244	6-53	10	75	CCW60°	1776	1979	1984	1975
NSG245	6-20	11	85	Vertical	2145	2347	2354	2342
NSG246	6-11	12	95	CW60°	2121	2329	2320	2318

Note: CW = clockwise looking down drill hole,
CCW = counterclockwise looking down drill hole.

Nine additional stressmeters of the modified version were installed October 25-27, 1982. Table 10-1 represents the locations and orientations of the replacement stressmeters. The boreholes were inspected with a borescope prior to stressmeter installation to precisely position the stressmeters to avoid fractures, voids, and foam debris remaining from the previous installation.

CHAPTER 11
DISPLACEMENT MEASUREMENTS

This chapter describes the status and interpretation of rock displacement measurements and calculations at the SFT-C. A description of the instrumentation and the locations of the various instruments are given in Brough and Patrick (1982). The three sections of this chapter present data on instrument reliability and modifications, a study of the influence of boundary conditions on calculational results, and comparisons of available measured and calculated displacements.

11.1 INSTRUMENT RELIABILITY AND MODIFICATIONS

Four activities were completed this fiscal year to enhance our understanding of the performance of geotechnical instrumentation in a simulated repository environment. Additional temperature measuring devices were installed to improve temperature compensation of displacement-measuring devices, coefficient of thermal expansion data was acquired for the superinvar deployed on near-field extensometers, failure of two superinvar connecting rods was investigated, and the investigation of transducer failures was extended to include replacement potentiometers which have failed this year. These four activities are described below.

11.1.1 Temperature Compensation Instrumentation

At the outset of the test, we anticipated that fairly uniform temperatures would exist in the three-drift complex. This anticipation was supported by calculational results (Montan and Patrick, 1981). Ventilation and convective heat transfer within the airstream produced significant temperature gradients. This necessitated installation of additional temperature sensors to facilitate adequate compensation of displacement data for the effects of thermal expansion of instrument components.

First, thermocouples were attached to the interior surface of each rod extensometer head assembly, a total of 26 units. The thermocouples are of the same design as used throughout the test: Type K, Inconel sheathed, MgO insulated, and grounded at the junction. These were calibrated at 0 and 50°C prior to installation. Mean errors at the two calibration temperatures were 0.0477 and -0.0613°C, respectively, and standard deviations of errors were 0.0542 and 0.0444°C, respectively, well within the ISA special limits of error.

The thermocouples produce a substantial improvement in the head assembly temperature compensation applied to the acquired data. Since an individual head assembly may have a temperature several degrees different from nearby devices (which were originally thought to be adequate) and the distance to the first anchor point thermocouple is typically 1.5 to 1.7 m, it was not unusual to see fairly large errors in the temperature-distance product. This measurement also supports compensation for thermal expansion of the extensometer rods, adding the end point temperature at the head to existing temperature measurements at each anchor. Compensation of the rods is unique

in that temperature varies along the rod. The amount of thermal expansion is proportional to the area under a graph of temperature vs distance along the rod. Since the temperature is not known everywhere along the rod, but just at the head and anchor positions, the area is obtained by trapezoidal approximation. This is equivalent to assuming that the temperature at any point lies on a straight line between the known points.

Second, a thermocouple was attached to each fracture monitor system (FMS). These thermocouples are the same as described above and the associated calibration errors are reported in the above statistical data.

The FMS units have relatively short components; therefore associated temperature-related errors are quite small. Offsetting this apparent advantage is the disadvantage of the small gauge length over which the FMS measures displacements. Since total displacements are very small, even minor thermally induced errors are significant and, thus, we have implemented thermal corrections.

Third, a four-wire resistance measuring scheme was developed and deployed to measure the average temperature of the convergence wire extensometers (CWE). The CWE units, while measuring displacements of 1 to 3 mm over distances of 3 to 7 m, have relatively long, temperature-sensitive components.

The four-wire resistance scheme used commercially in resistance temperature devices (RTD) was applied to the CWE units to measure average wire temperatures. As applied at the SFT-C, two wires are attached near each end of the 304L stainless steel measurement wire. Current is applied across the outer pair of leads and the resulting voltage drop is measured across the inner pair to determine the resistance of the wire. Total resistance of the wires ranges from about 6 to 18 Ω, depending on wire length. Circuit sensitivity ranges from 0.06 to 0.16°C/mΩ, again depending on wire length. Given the observed stability of 4-wire resistance measurements of ±0.0092 Ω, we conclude that system accuracy ranges from ±0.55 to ±1.47°C.

11.1.2 Superinvar Coefficient of Thermal Expansion

Superinvar alloy was utilized for the connecting rods of the vertical extensometers deployed in the canister storage drift. Manufacturer's data indicated that the coefficient of thermal expansion (CTE) of this material varied from 0.22 to 0.27 × 10^{-6}/°C over the temperature range of interest

(20 to 60°C). We contracted with Professor S. Jacobs of the University of Arizona to provide an independent measurement of the CTE.

Using excess material remaining from extensometer assembly, Jacobs prepared three etalons, each consisting of three 6.35-mm-diam by 100-mm long rods to be used in the CTE determinations. These rods, stabilized at each end with clamping fixtures, were used to space the Fabry-Perot mirrors, thus producing a vertical optical axis (Fig. 11-1). The technique involved locking a tunable laser to the etalon resonant frequency. Frequency changes

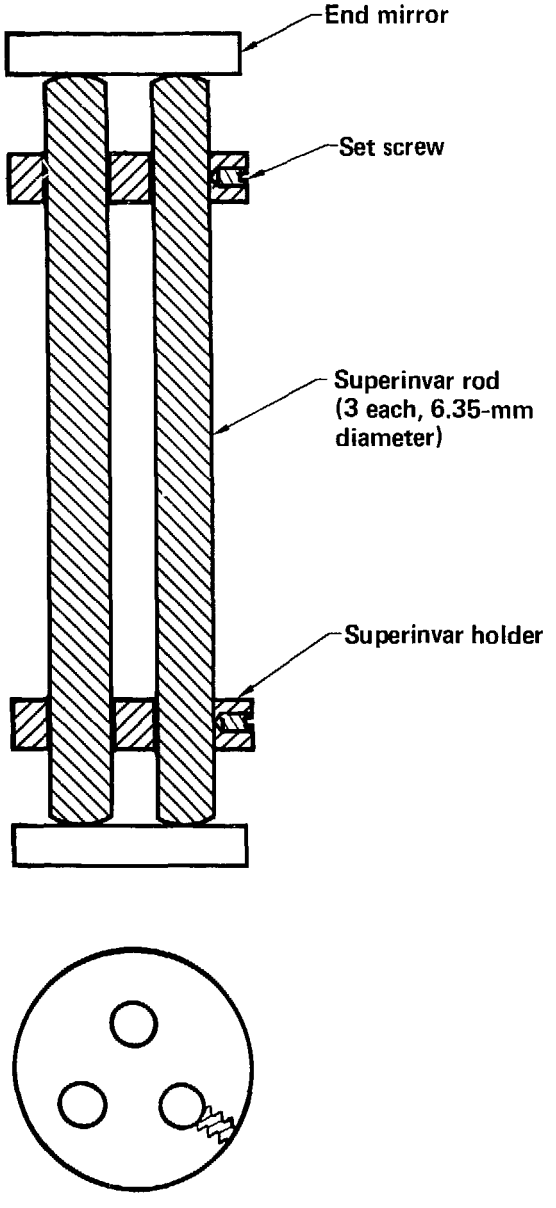

Figure 11-1. Geometry of coefficient of thermal expansion test.

associated with changes in etalon length were determined by comparing the frequency of the tunable laser to the frequency of a frequency-stabilized laser (Jacobs, 1982).

Etalon frequencies were measured in 20°C increments over the range of 20 to 100°C. Two etalons were subjected to one cycle of heating and cooling while the third was cycled several times over various temperature intervals to examine hysteresis effects.

Figure 11-2 displays the "instantaneous average" CTE values recorded in the tests. "Instantaneous" is used here to mean the CTE recorded during one increment or decrement in temperature. "Average" means that the CTE is evaluated over the current temperature interval and is plotted at the midrange of the temperature interval. Several interesting observations may be made. First, the CTEs are all small but are opposite in sign to those reported by the manufacturer. Second, the first and second etalons appear to be distinctly different from the third. Third, although linear relationships are plotted in the figure, significant hysteresis is evident in the third data set (the numbers on Fig. 11-2 indicate the order of the measurements). Further note that the hysteresis is most pronounced at an average temperature of 30°C. Fourth, CTE values were both positive and negative, depending on temperature.

For our application at the SFT-C, we needed to know the cumulative effect of expansions or contractions on instrument components. Therefore, we calculated "cumulative average" CTE values from Jacobs data. These values reflect the net CTE associated with heating from ambient to a specific elevated temperature and are reported at the midrange of the latest increment or decrement in temperature (Fig. 11-3). Note that where the laser system was reset or a measurement was missing, a break in the cumulative history occurred.

Figures 11-2 and 11-3 display the high degree of variability present in the data set. Statistical analysis of the data and attempts at curve fitting led to the conclusion that the mean cumulative CTE was as good a predictor of CTE as any other model tried because of the high variability in the data. This approach indicated a CTE of -33.2×10^{-8}/°C ± 23.3×10^{-8}/°C. Using this mean, the observed extreme range of CTE (+1.8 to -82.2×10^{-8}/°C), and calculated temperature rises along the rods, we calculated the ranges of errors indicated in Table 11-1.

We conclude that errors associated with observed variations in CTE will be within a $\pm 25 \times 10^{-6}$ m envelope for differential displacements between

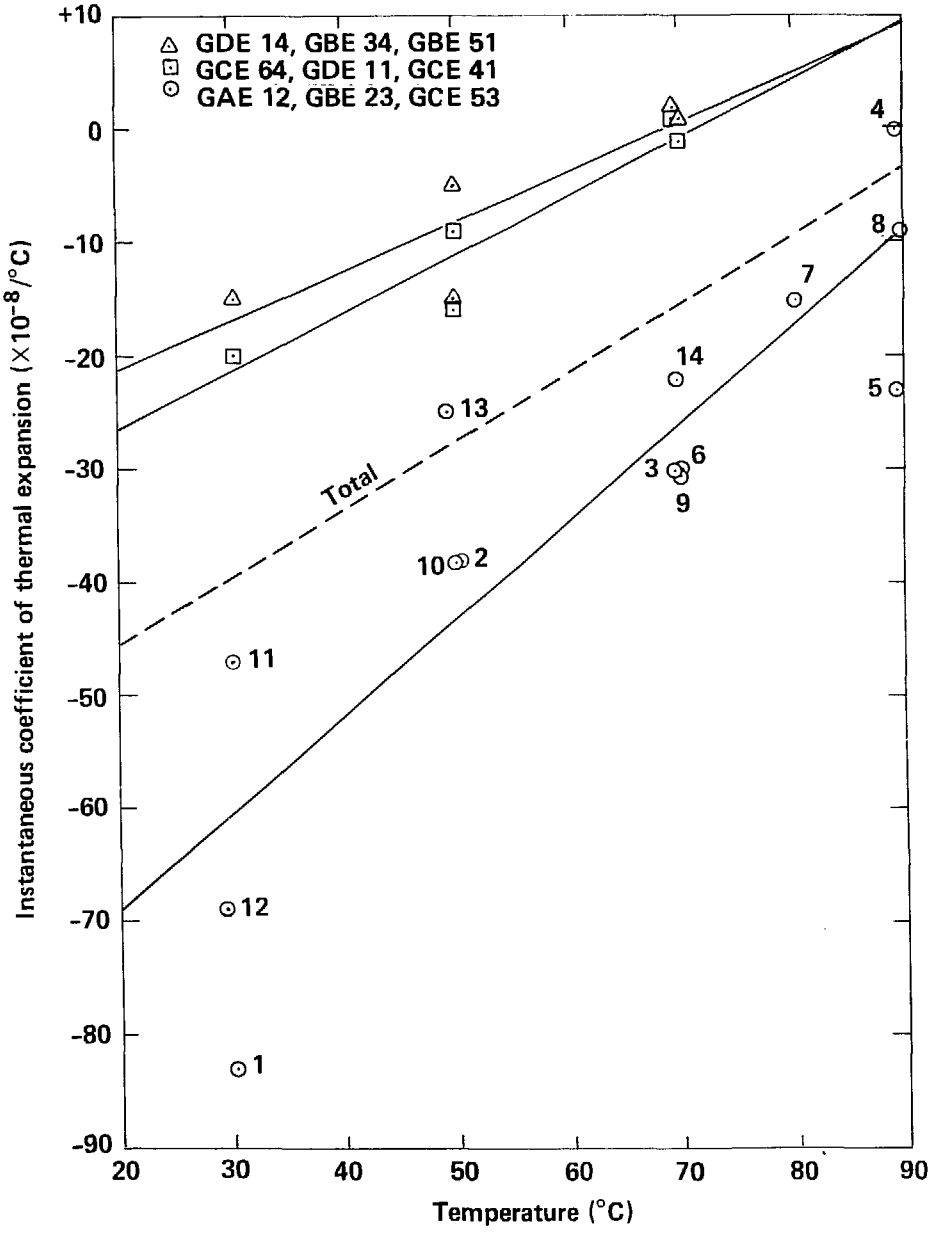

Figure 11-2. Instantaneous average coefficient of thermal expansion of SFT-C superinvar.

the upper three anchors or a $\pm 150 \times 10^{-6}$ m envelope for relative displacements between the head assembly and any of the anchor points. Although these errors are about a factor of 3 larger than the advertised precision of the rod extensometer at constant temperature (0.02 to 0.05 mm), they are small compared to the 1- to 3-mm displacements calculated to occur at these anchor points (Butkovich, 1981).

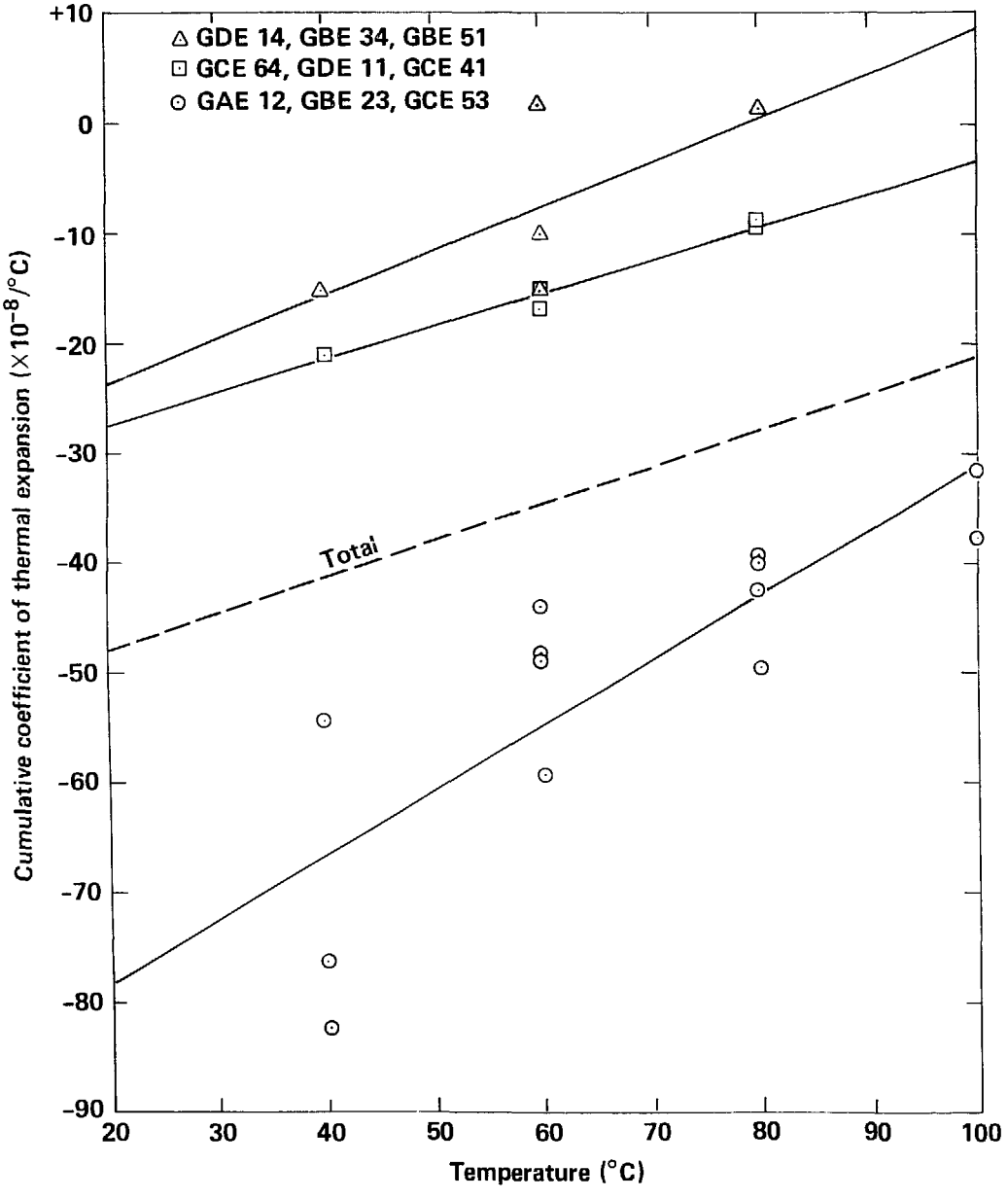

Figure 11-3. Cumulative average coefficient of thermal expansion of SFT-C superinvar.

11.1.3 Failure of Superinvar Rod Stock

As noted above, the vertical extensometers in the canister drift utilized Superinvar alloy for the connecting rods. Two of these rods (instruments GCE223 and GCE251) were observed to fail within 2 mo of each other after being in place about 34 mo.

Table 11-1. Range of errors in displacement associated with an average CTE of -33.2×10^{-8}/°C.

Measurement interval, m	Range of error, $\times 10^{-6}$ m
0 - 1.95	-18, +13
1.95 - 3.48	-23, +16
3.48 - 5.00	-25, +18
5.00 - 13.45	-88, +62
0 - 13.45	-154, +108

The conditions to which these rods were subjected were not particularly severe and are also present for an additional 54 rods. Temperatures gradually increased with time after spent-fuel emplacement but were more or less constant at temperatures not exceeding 50°C.

The sealing of the extensometers is believed to exclude liquid water from contact with the rods although water vapor is present. Partial confirmation is that the failed rods were dry to the touch when removed from the instruments. Analysis of gas samples taken from the extensometer head assemblies revealed no measurable contaminants.

Radiation dose at these locations is insignificant since they are about 2.2 m from the radiation sources. Calculations estimated a total dose 1 m from the sources of about 10^3 rad during the approximately 3-yr period since installation.

The rod tensioning assembly provides a nominal load of 50 kg to the rod. Laboratory testing of this assembly indicated actual loads of 35-40 kg, thus confirming the low-stress condition for the 6.4-mm-diam rod. Other tests confirmed the relatively high strength of the rod.

Metallographic analyses of the two failed rods were conducted to determine the type and possible cause of failure. Several observations were made. First, one rod failed perpendicular to the rod axis, apparently near the root of a thread, while the second failed at about a 45°C angle to the rod axis, indicating a combined tension-torsion loading. Second, SEM studies revealed transgranular cleavage with preferential attack along grain boundaries. Third, optical microscopy of a section parallel to the rod axis

showed fractures typical of stress-corrosion cracking; being both intergranular and transgranular in nature. The base alloy appeared to be clean and free of inclusions under these inspections.

Our tentative conclusion is that these rods failed due to stress-corrosion cracking. This phenomenon was not expected in view of the seemingly benign environment, the relatively short 3-yr test duration, and the high (38%) nickel content of the alloy.

11.1.4 Failure of Linear Potentiometers

We reported previously that 41% (23) of the transducers associated with the vertical rod extensometers in the canister drift failed (Patrick, Carlson, and Rector, 1981). These failures were expressed as nonlinear changes in resistance. All failing units were M5184 Bourns rectilinear potentiometers.

The 48 affected units were replaced with equal numbers of Bourns potentiometers, Vernitron potentiometers, Kaman electromagnetic proximeters, and Schaevitz LVDTs. Each of these groups were in turn subjected to three different environments: normal sealed head assembly, nitrogen flushed, and vacuum purged.

This year we observed four transducer failures, all on one head assembly. The transducers were Vernitron potentiometers and the environment was the normal sealed head assembly. The mode of failure was the same as observed with the earlier failures.

As in the case of previous failures, we proceeded to analyze the failures. Gas samples drawn from the head assembly indicated that only warm, moist air was present. Hydrocarbons were absent and chloride, sulfate, and nitrate were all of ambient levels. Microscopic analysis of the resistive elements revealed significant fracturing in a random pattern near one end, gradually decreasing to a few minor fractures along each edge of the element at the other end. Associated with the fracturing was an apparent slight debonding between the resistive element and the substrate.

It is significant that the mode of failure (nonlinearity of resistance), environmental condition (sealed head assembly), time to failure (6 mo in the former case, 1 yr in this case), and transducer type (continuous thin film potentiometer) were involved in both series of failures. A definitive explanation has yet to be formulated for either series of failures despite

rigorous testing and investigations by both the SFT-C staff and the respective manufacturers. Research in the evaluation of these instruments is continuing.

11.2 EFFECTS OF BOUNDARY CONDITIONS ON THERMOMECHANICAL CALCULATIONS

The effects of varying certain boundary conditions on the results from a finite element calculation were studied in relation to the SFT-C (Butkovich, 1982). In a calculation that is later used for comparison with data, a number of boundary conditions are imposed on the finite element mesh, such as a fixed temperature on a heat flow calculation, or imposing stress loadings on the outer boundaries of the mesh. These boundary conditions affect the results of the calculations.

The study employed a thermoelastic model with the ADINA (Bathe, 1978) structural analysis code. Nodal temperature histories were generated with the compatible ADINAT (Bathe, 1977) heat flow code. The calculations were made with a damaged zone around each excavation; i.e., with the same input as used with the as-built calculations (Butkovich, 1981).

Three boundary conditions were studied:

- The effect of isothermal boundaries on a smaller mesh as compared with a significantly larger mesh.
- The effect of stress loading on three progressively larger meshes.
- Plane strain vs plane stress conditions.

Figure 11-4 shows the meshes employed, which were made up of eight-node elements. The smaller mesh consists of 274 elements, exclusive of the degenerated four-node elements used in the excavation of the openings. Because of the symmetry of the drift geometry, only half the region is modeled. Figure 11-5 shows the elements around the drifts and the relative position of the spent fuel canisters below the floor of the spent-fuel drift and the electrical heaters below the heater drift floors. A region 0.5-m thick was included around each opening so that different properties could be assigned the material identified as being explosively damaged during the excavation.

The first outer layer of the mesh consists of 52 elements and the outermost layer 56 elements, with an effective size of 140 × 140 m for the largest mesh, contrasted to an effective mesh size of 80 × 80 m for the smallest mesh.

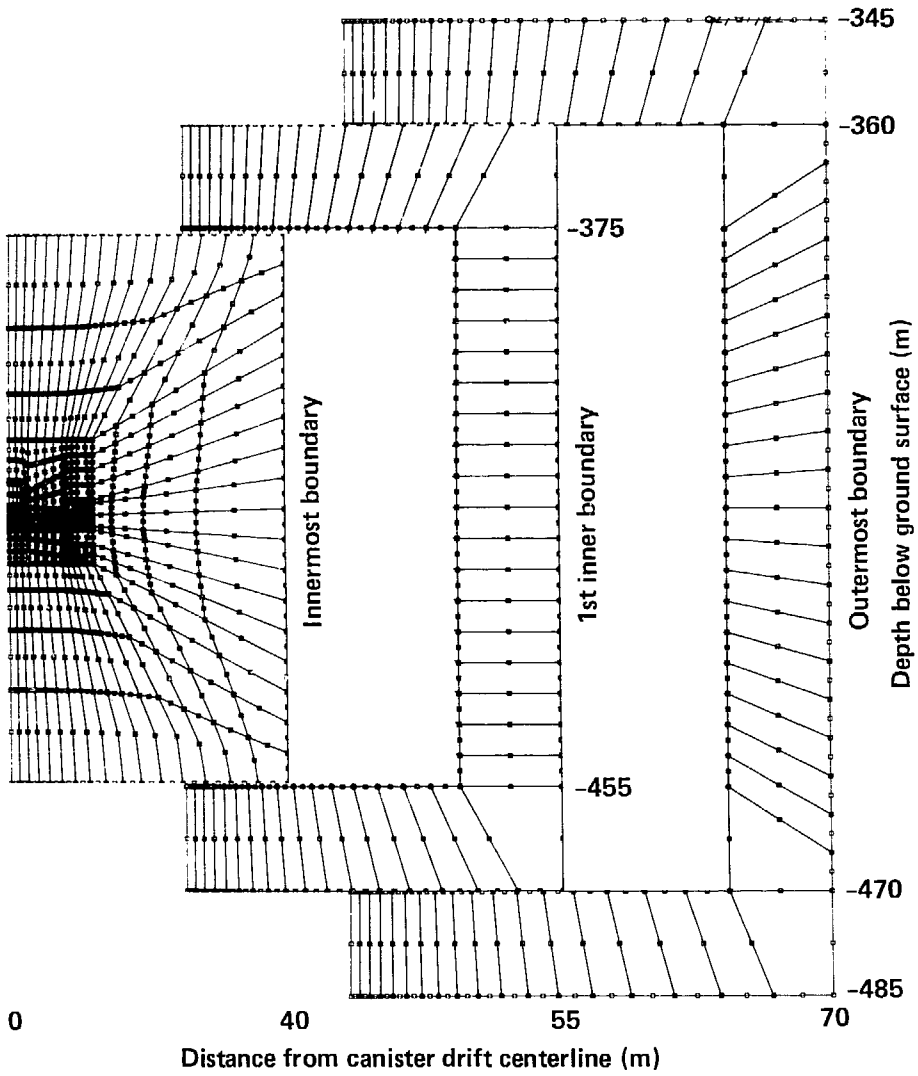

Figure 11-4. Mesh construction allows layers to be peeled off like onion skins (boundary coordinates in metres).

The effect of isothermal boundary conditions on mesh size was obtained by running two ADINAT heat flow calculations and imposing ambient temperature conditions on the smallest mesh and the largest mesh outer boundaries.

The constant temperature boundary can become a heat sink at times greater than it takes for the outgoing heat pulse to arrive there; i.e., as the heat pulse approaches this temperature boundary, the boundary remains at constant temperature rather than increasing in temperature. Figure 11-6 shows a comparison of temperature contours at 5.0 yr after the emplacement of the spent fuel (7.45 YOC) for the innermost region defined by the smaller mesh.

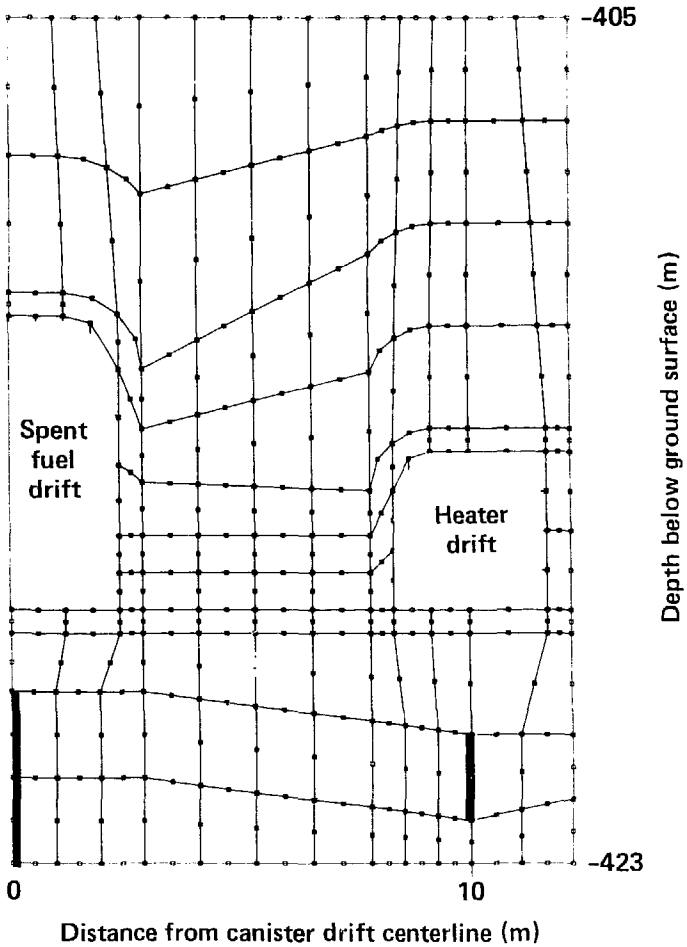

Figure 11-5. Finite-element mesh in vicinity of openings (positions of heat sources are shown by heavy lines beneath openings--all dimensions in metres).

This figure indicates the effect of the different locations of the ambient temperature boundary. Obviously, the mesh size must be large enough that the thermal boundaries will not influence the region of interest near the excavation and heat sources during the time span being calculated. For the 3-yr time span for the SFT-C, a small mesh (80 × 80 m, effective size) was sufficient. For longer times a larger mesh would be required.

The effect of boundary loading on progressively larger mesh sizes was studied by doing three thermoelastic ADINA calculations with the same thermal histories for the common nodes in the three different meshes. The difference was that the outer boundary loading was ρgh in the vertical direction and

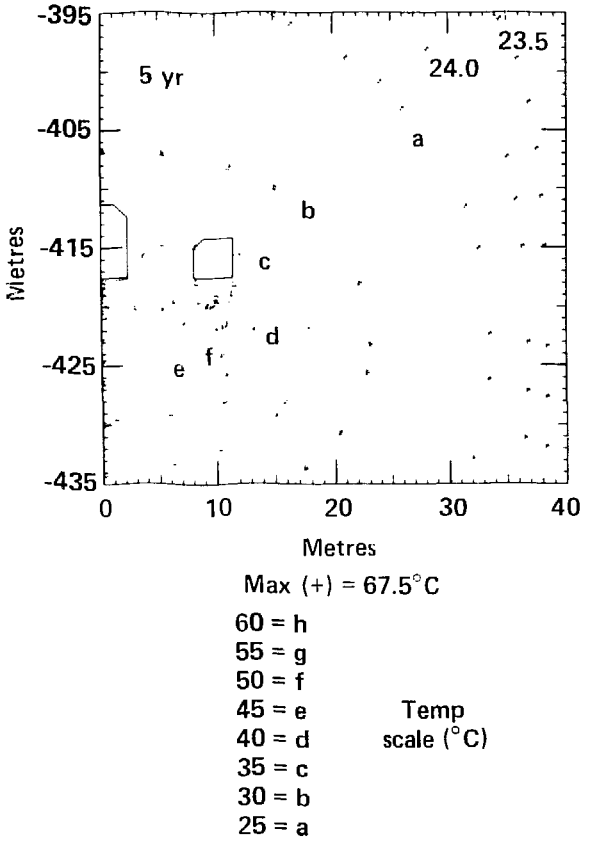

Figure 11-6a. Temperature profiles at 5.0 yr (temperature is 23°C at innermost boundary.

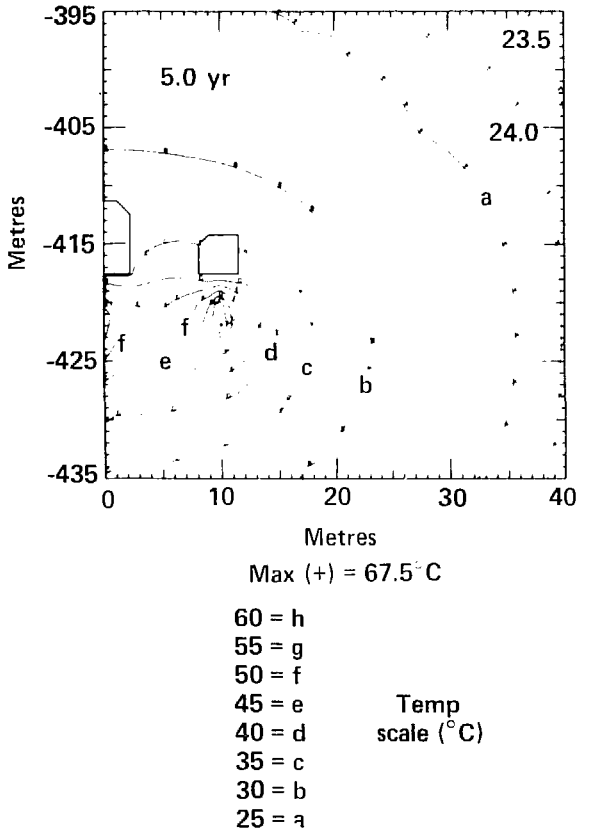

Figure 11-6b. Temperature profiles at 5.0 yr (temperature is 23°C at outermost boundary).

1.2 ρgh in the horizontal direction on different outer boundaries. The left vertical (Y = 0) and the lower horizontal boundaries were roller boundaries.

Stress fields and displacements in the region of interest around these excavations were compared. The differences in both stresses and displacements in the three calculations were extremely small and could be better discerned by numerical rather than a graphical analyses of the results. As an example, horizontal and vertical drift closures calculated with the three meshes are shown in Table 11-2.

Because of constraints on computer size and running time, all calculations utilized two-dimensional (planar) geometry. Three-dimensional calculations of the SFT-C would require extremely coarse zoning if one were to model the drifts, with loss of resolution in the innermost region near the excavation.

Table 11-2. Drift closures from heating calculated in plane strain with different mesh size.

Time since emplacement, yr	Full[a]	Full--1[a,b]	Full--1 and 2[a,b]
	A. Spent Fuel Drift		
	(Horizontal)		
0.25	3.23	3.36	3.38
0.5	3.57	3.69	3.70
0.75	3.72	3.84	3.83
1	3.84	3.95	3.93
	(Vertical)		
0.25	3.17	3.18	3.19
0.5	3.40	3.42	3.42
0.75	3.41	3.42	3.42
1	3.37	3.38	3.37
	B. Heater Drifts		
	(Horizontal)		
0.25	0.95	0.97	0.97
0.5	0.90	0.92	0.92
0.75	0.83	0.82	0.84
1	0.79	0.80	0.78
	(Vertical)		
0.25	1.70	1.72	1.74
0.5	1.87	1.89	1.90
0.75	1.97	1.99	1.99
1	2.03	2.05	2.04

[a] Closures in mm.
[b] Full--1 refers to full mesh minus the outermost layer. Full--1 and 2 refers to full mesh minus the two outermost layers.

When a planar calculation is made, plane-strain or plane-stress boundary conditions must be imposed. In a plane-strain calculation no out-of-plane motion is allowed. At a given point in the mesh, the out-of-plane stress attains a value dependent on the in-plane stress and Poisson's ratio. In a

plane-stress calculation, the out-of-plane stress equals zero everywhere in the mesh.

In this comparison, an ADINA plane-stress calculation was made to 1 yr, and compared with a similar plane-strain calculation. The differences noted were again more discernible from a numerical rather than from a graphical comparison.

Table 11-3 shows the horizontal rib motion resulting from the mine-by at various points in the rib relative to a hole collar at midheight in the heater drifts. Table 11-4 shows a comparison between horizontal and vertical stresses calculated at two points in the largest mesh at various times during the mining and heating phases of the SFT-C. The differences in the calculated horizontal and vertical stresses are about 9% higher with the plane-stress boundary condition.

Table 11-3. Mine-by rib motion at various points in rib relative to hole collar at midheight in heater drifts.

Distance from hold collar, m	Relative displacements, mm		
	Full	Full--1[a]	Full--1 and 2[b]
	A. Plane-Strain Calculations		
1.72	0.458	0.471	0.469
2.94	0.636	0.656	0.653
4.16	0.681	0.807	0.802
5.38	0.918	0.948	0.942
	B. Plane-Stress Calculations		
1.72	0.510	0.526	0.524
2.94	0.693	0.716	0.713
4.16	0.845	0.874	0.869
5.38	0.991	1.025	1.019

[a] Full--1 refers to full mesh minus the outermost layer.
[b] Full--1 and 2 refers to full mesh minus the two outermost layers.

Table 11-4. Horizontal and vertical stresses calculated for two points in full mesh at various times during mining and heating phases.

	Near spent fuel canister		Midrib	
	Horizontal, MPa	Vertical, MPa	Horizontal, MPa	Vertical, MPa
A. Plane-Strain Calculation				
Mesh loading	12.83	10.70	11.83	11.17
Heater drift mining	12.77	10.74	10.93	11.90
Spent-fuel drift mining	13.42	10.22	8.89	13.63
0.25-yr heating	17.25	11.34	6.78	16.33
0.5-yr heating	18.15	11.40	6.74	17.13
0.75-yr heating	18.60	11.37	6.77	17.60
1.0-yr heating	18.85	11.33	6.80	17.91
B. Plane-Stress Calculation				
Mesh loading	12.74	10.80	12.18	10.86
Heater drift mining	12.69	10.82	11.30	11.53
Spent-fuel drift mining	13.30	10.36	9.29	13.16
0.25-yr heating	18.09	12.08	7.08	16.21
0.50-yr heating	19.28	12.21	7.09	17.23
0.75-yr heating	19.87	12.17	7.15	17.93
1.0-yr heating	20.21	12.13	7.20	18.34

In summary, the size of the mesh should be sufficiently large so that the effect on the thermal pulse by the thermal boundary condition does not significantly affect the region of interest. The boundary stress loading on different size meshes apparently has a small effect on the stresses and displacements calculated in the region of interest. That is not to say that different stress distributions on the outer boundaries will not affect this region. Calculations of the type conducted for the SFT-C are usually done with a plane-strain boundary condition. It is expected that plane-stress results will be somewhat higher.

11.3 COMPARISON OF MEASURED AND CALCULATED DISPLACEMENTS

This section is divided into three parts, each of which compares measured displacement values with calculated displacements. Part 11.3.1 describes the rock displacement data available from the rod extensometer systems, part 11.3.2 discusses drift deformation data available from the convergence extensometers, and part 11.3.3 presents fracture behavior data available from the fracture monitor and Whittemore gauge measurements. In each case, the instrument systems and their operation and location have been described previously by Patrick et al. (1982). As before, all measurements are referenced to years out of core.

11.3.1 Rock Deformation from Rod Extensometer Measurements and Calculations

Relative displacements are being measured with rod extensometers during the SFT-C. These are compared with results from the as-built thermoelastic finite element calculation (Butkovich, 1981). Rod extensometers had been installed in boreholes drilled from both the north and south heater drifts at two locations along the length of the drifts. One set was oriented horizontally into the pillars, and two other sets were inclined at 34° and 50° from horizontal above the canister drift. These instruments provide for measurement of relative displacements between the hole collars in the heater drifts and anchor points located at various positions in the boreholes. In addition, vertically oriented rod extensometers were emplaced from the canister drift. Data from these units are not reported here because the thermal correction algorithms for these units are not yet operational. Temperatures are monitored with thermocouples emplaced near each anchor point.

Displacement measurements from the heater drift extensometers were not available before 3.0 YOC, and all relative displacements that are compared are with respect to those measured since that time. Temperature corrections to the data were made with hand calculations. These show the temperature correction to be from two to many times greater than the indicated displacement. This is because the expansion coefficients of the rock and the carbon steel rods of these instruments are very similar. As a result, temperature changes induce rod expansions and rock displacements of the same order of magnitude. The displacements recorded prior to temperature compensation are thus primarily due to inelastic rock responses.

Comparisons between temperature-corrected relative displacements from the hole collars were made with the as-built calculation which included a damaged zone around each excavation. The calculational results used in these comparisons were obtained by projecting the calculated vector displacements of the nodes intersected by a given rod extensometer anchor point to the angular orientation of the extensometer. Figures 11-7 and 11-8 show the comparisons at 4.5 and 5.0 YOC at Station 2+83 and Figs. 11-9 and 11-10 for 4.5 and 5.0 YOC at Station 3+45. The upper number at each anchor point is the temperature-corrected measurement and the lower value is the corresponding calculational result. The "x" symbol indicates that the data are unavailable. In general, the agreement between calculations and measurements is quite good, especially when one considers the relative displacements are less than 1 mm over as much as 13 m in length of the rod extensometer (<75-μ strains).

An analysis of these results and those at 3.5 and 4.0 YOC that were reported earlier (Patrick et al., 1982) show, in general, that except in the region immediately over the canister drift, the measurements and calculations

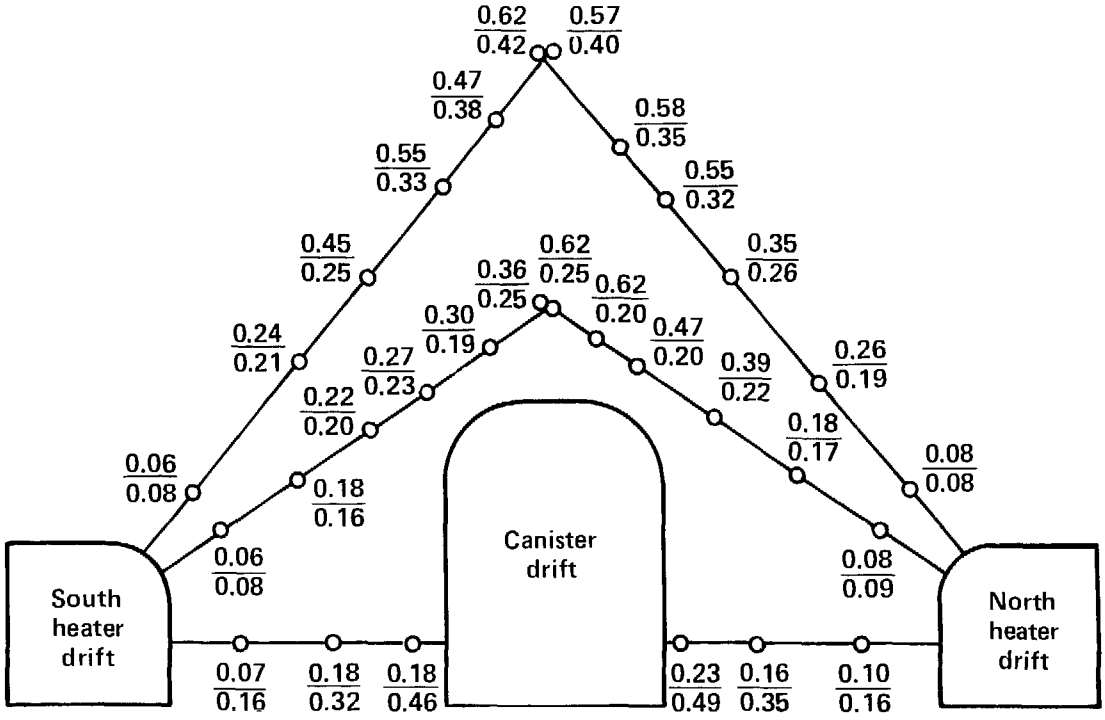

Figure 11-7. Relative rock displacements in mm at station 2+83 between 3.0 and 4.5 YOC (upper numbers measured; lower numbers calculated).

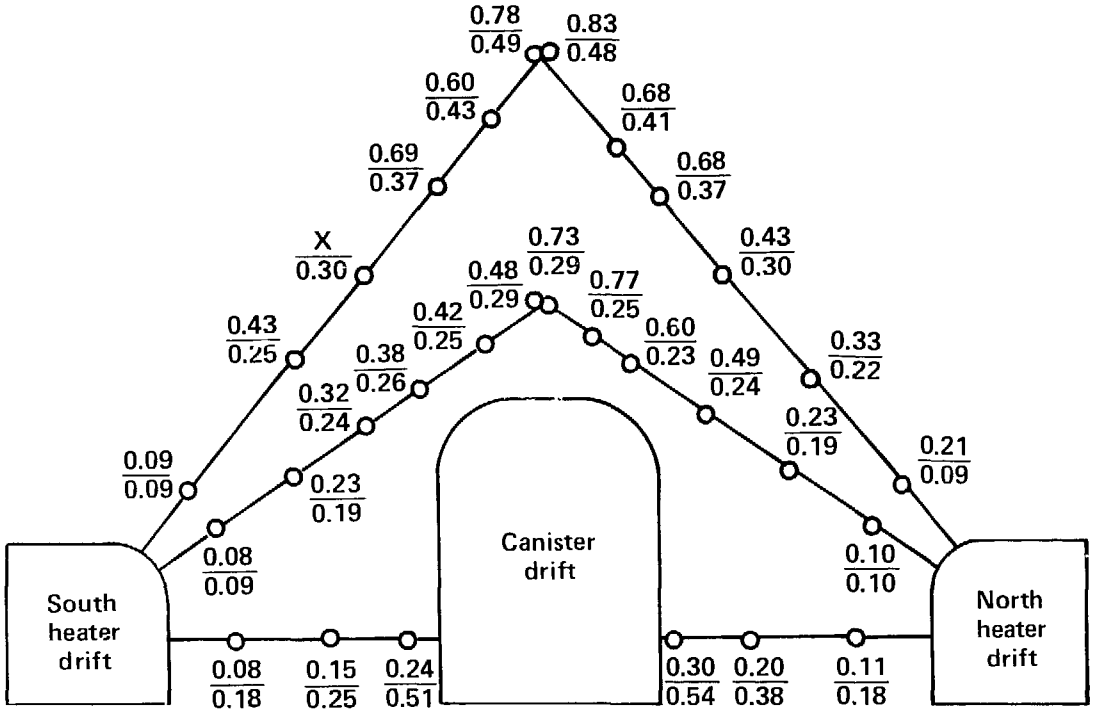

Figure 11-8. Relative rock displacements in mm at station 2+83 between 3.0 and 5.0 YOC (upper numbers measured; lower numbers calculated).

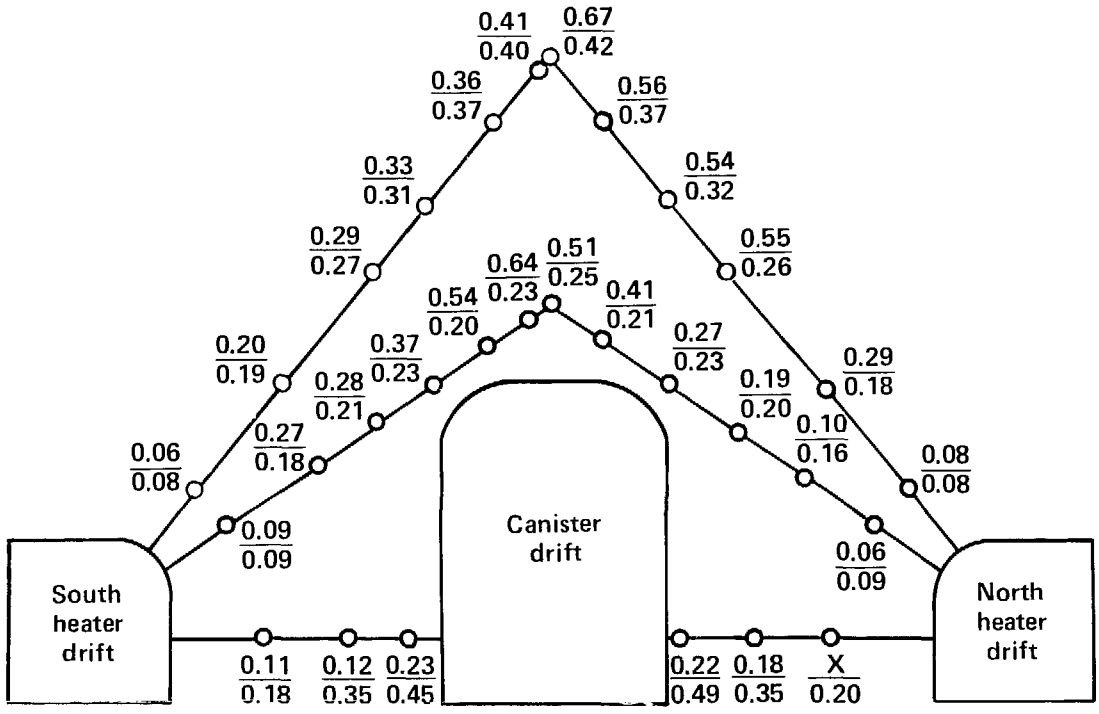

Figure 11-9. Relative rock displacements in mm at station 3+45 between 3.0 and 4.5 YOC (upper numbers measured; lower numbers calculated).

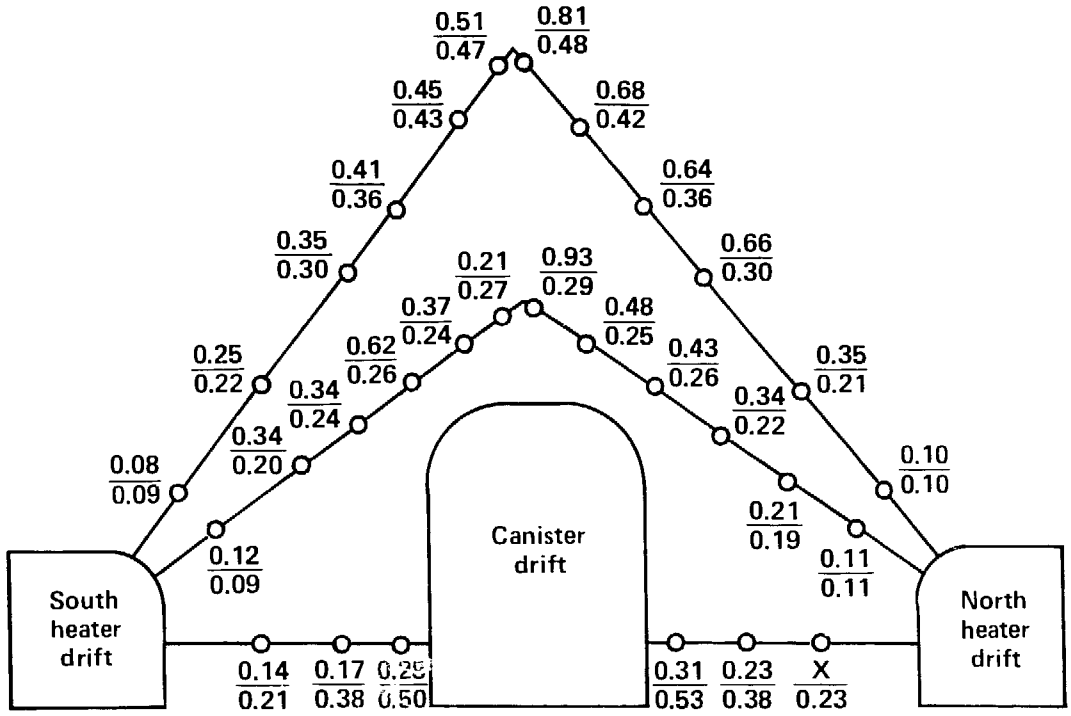

Figure 11-10. Relative rock displacements in mm at station 3+45 between 3.0 and 5.0 YOC (upper numbers measured; lower numbers calculated).

agree within a factor of 2 or much better. Another observation is that the measured displacements are larger than those calculated except for the horizontal extensometers in the pillar. A third observation is that there are regions where a given group of measurements on one side of the canister drift is in better agreement with the calculations than a given group on the other side.

It must be emphasized that the as-built finite element calculations from which the calculational results were extracted assumed the rock mass surrounding the excavations to be a thermoelastic continuum in which no jointing or other discontinuities were present. In reality the Climax stock is moderately-to-highly jointed, with several shear zones identified as extending throughout the excavation region. At Station 3+45, two shear zones intersect just above the north pillar while there are no shear zones identified above the south pillar. At Station 2+83, one shear zone extends into the region above the north pillar, and four separate shear zones extend and intersect in the region above the south pillar where the rod extensometers were installed. Better agreement between measurements and calculations occurs where there is an absence of these shear zones. This effect may be expected

since the measured displacements contain a component of the inelastic rock response from movement along a joint.

The excavations were made using standard mining practices. These practices employ high explosives to break the rock. A damaged region around each excavation has been observed during in situ measurements of elastic modulus (Heuze, et al., 1981a). This region has an effective modulus of about one half that of the rock mass and extends 0.5 m or more from the walls of the drifts. Even though an 0.5-m thick region around each excavation with a lower modulus was modeled, other blast damage effects not specifically modeled may be the reason for the relatively poor agreement between measurement and calculation immediately above the crown of the canister drift.

The observation that the calculated results are larger than those measured only for the horizontal rod extensometers within the pillars may also be due to the jointing and the presence of shear zones. The rod extensometers were installed prior to the excavation of the canister drift. Displacement measurements during the mine-by indicated that the pillar thickness decreased at both locations, and additional instrumentation indicated that the stresses within the pillars also decreased. These observations suggested an arching phenomenon (Wilder and Patrick, 1981b) which was not observed in a finite element linear elastic calculation (Butkovich, 1981) or a jointed rock model calculation (Heuze, Butkovich, Peterson, 1981b) of the mine-by process. Apparently the presence of jointing and shear zones affects the thermoelastic response to a different degree in the midpillars as compared with the area above them.

11.3.2 Drift Deformations from Calculations and from CWE, THE, and TX Measurements

As reported before, the height and width of the SFT-C drifts are monitored at 16 stations by convergence wire extensometer (CWE) instrument systems. Tape extensometer (TX) measurements are made at these same locations periodically to provide redundancy. In addition, two through-hole extensometer (THE) systems monitor the width of the entire SFT-C facility. Unfortunately, thermal correction of CWE and THE data has not been possible thus far because of the complexities of the temperature regime within the drifts. TX data are currently available for use, but it must be kept in mind that the TX temperature corrections are only approximations, as the actual

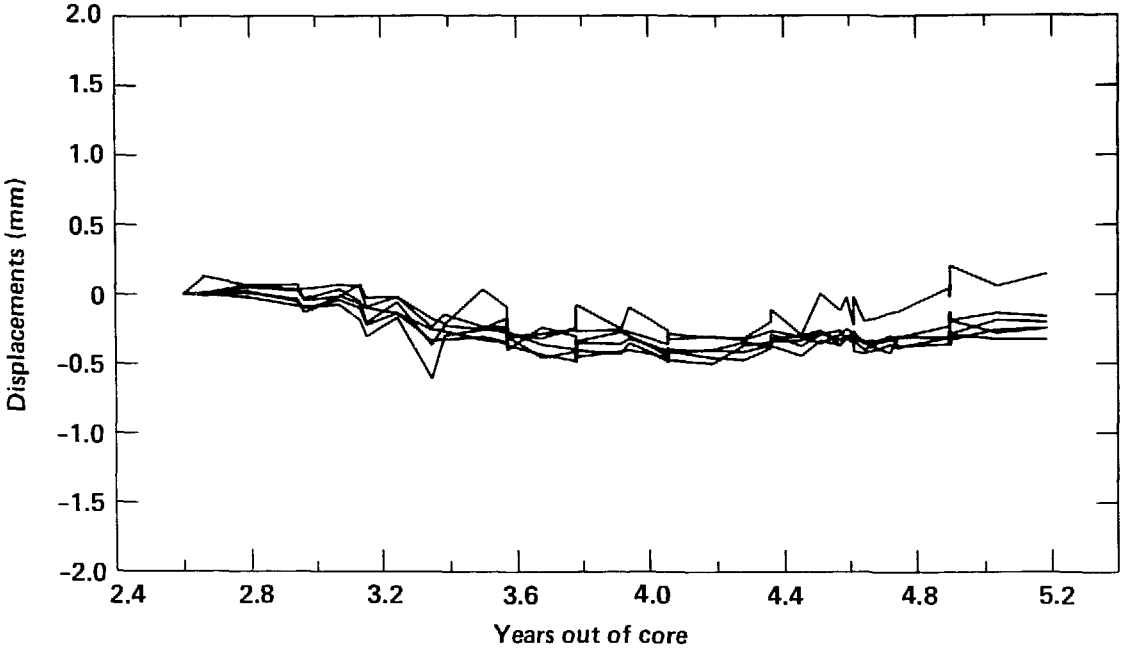

Figure 11-11. Canister drift horizontal tape extensometer data.

instrument temperature distribution is unknown at present. This and other sources of error in the TX data have been described here previously.

Figures 11-11 through 11-16 show displacements monitored since the start of the TX measurement program. Displacement values on each plot are related to an arbitrary initial value of zero assigned to the time TX measurements commenced. Negative values of displacement indicate convergence of the drift at the given station; positive values indicate divergence. The data have been modified before plotting by temperature corrections and adjustments described in Patrick et al. (1982). The relatively large vertical offsets and "seesaw" effects seen in the plots reflect the influences of different operators making readings on the same or consecutive days. No attempt has been made to smooth the data by means of curve-fitting or other techniques.

Station-by-station comparisons of TX-measured displacements have not been made due to the level of accuracy of the data. Six data plots (which average measurements of like orientation within each drift) are used for comparison with the calculations. As these plots were prepared, the TX stations in the receiving room were omitted because of their proximity to apparently significant known faults in the receiving room. TX stations at the northwest

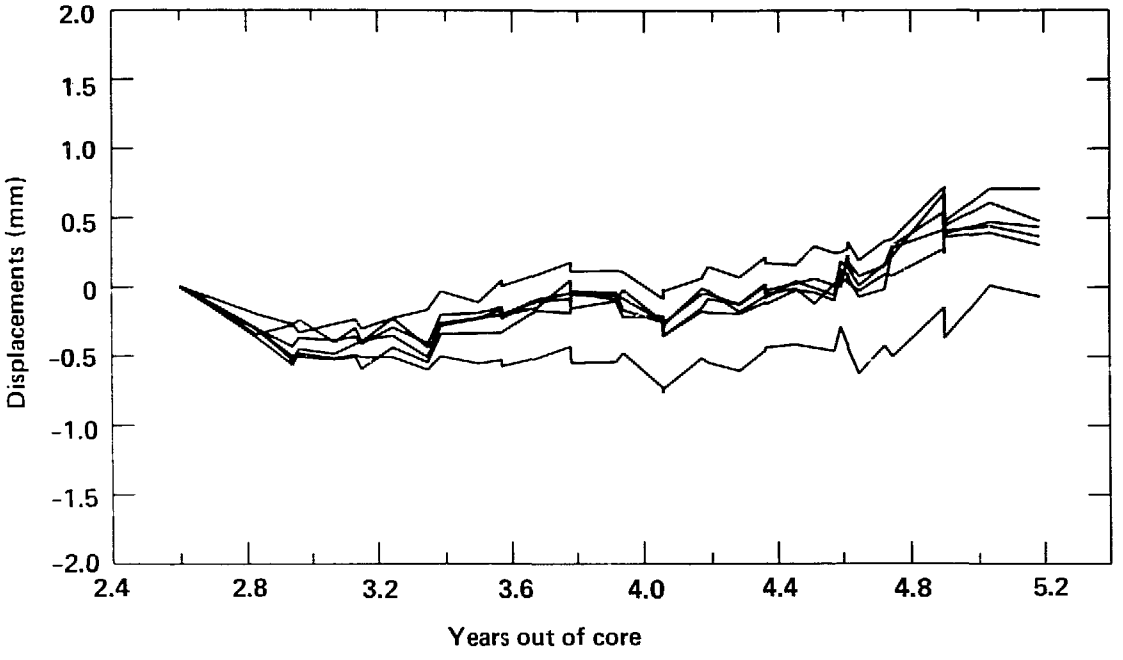

Figure 11-12. Canister drift vertical tape extensometer data.

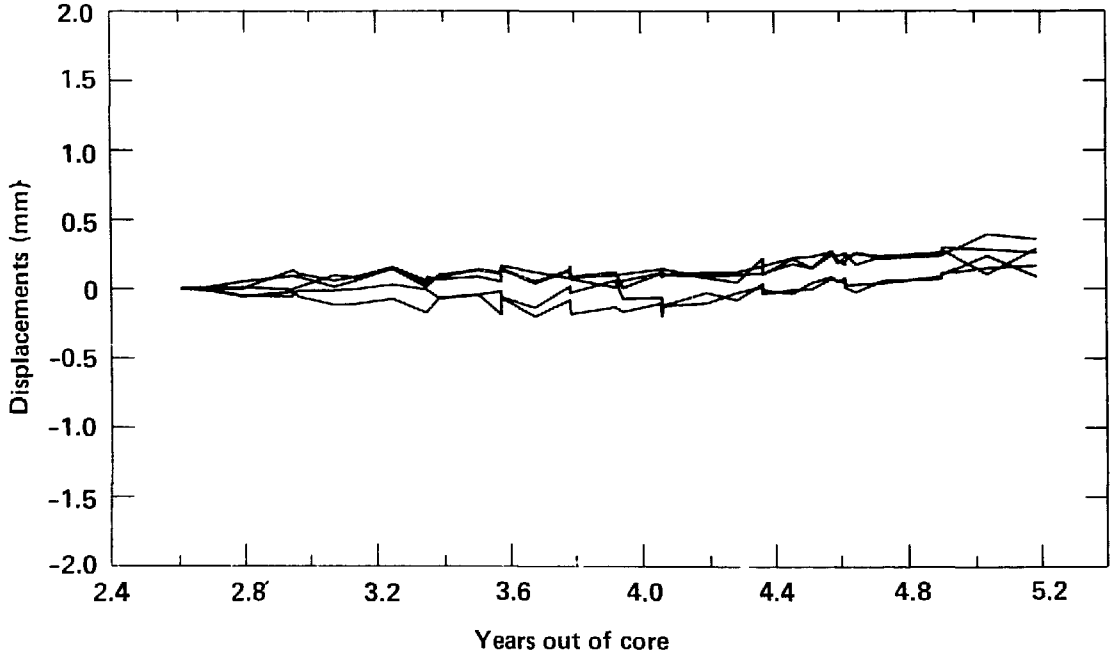

Figure 11-13. North heater drift horizontal tape extensometer data.

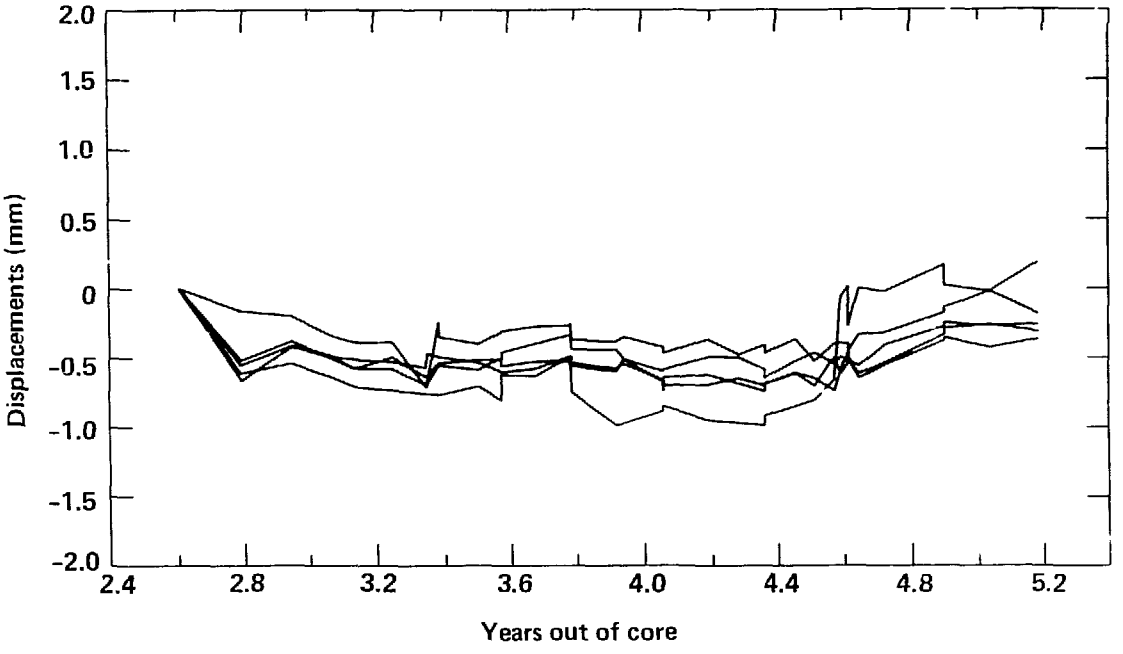

Figure 11-14. North heater drift vertical tape extensometer data.

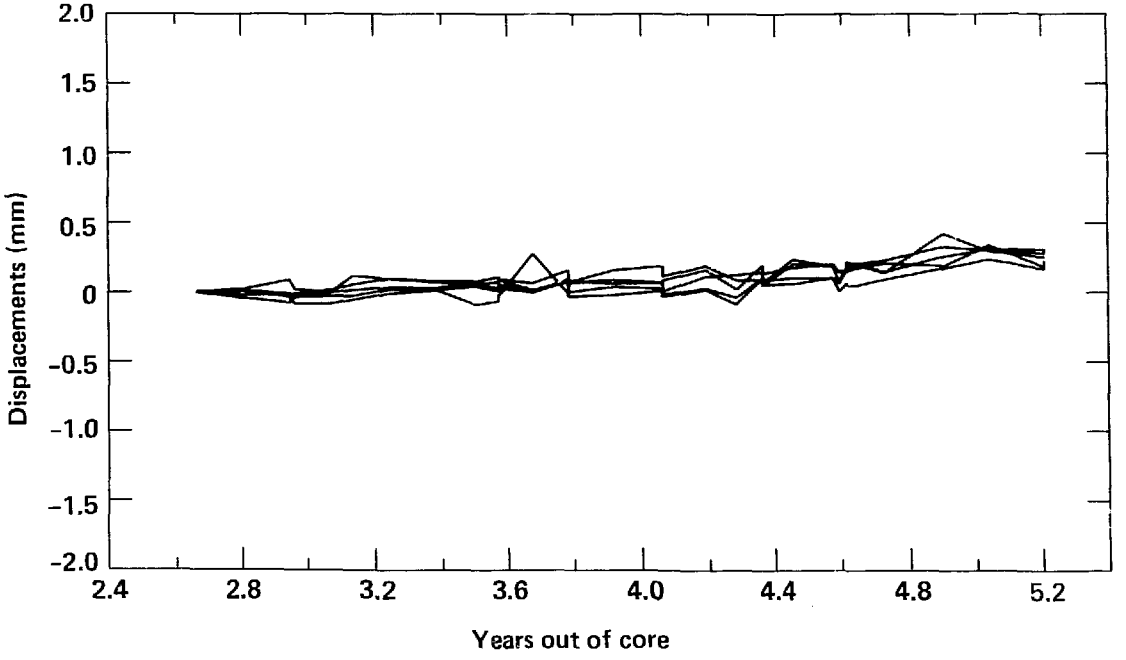

Figure 11-15. South heater drift horizontal tape extensometer data.

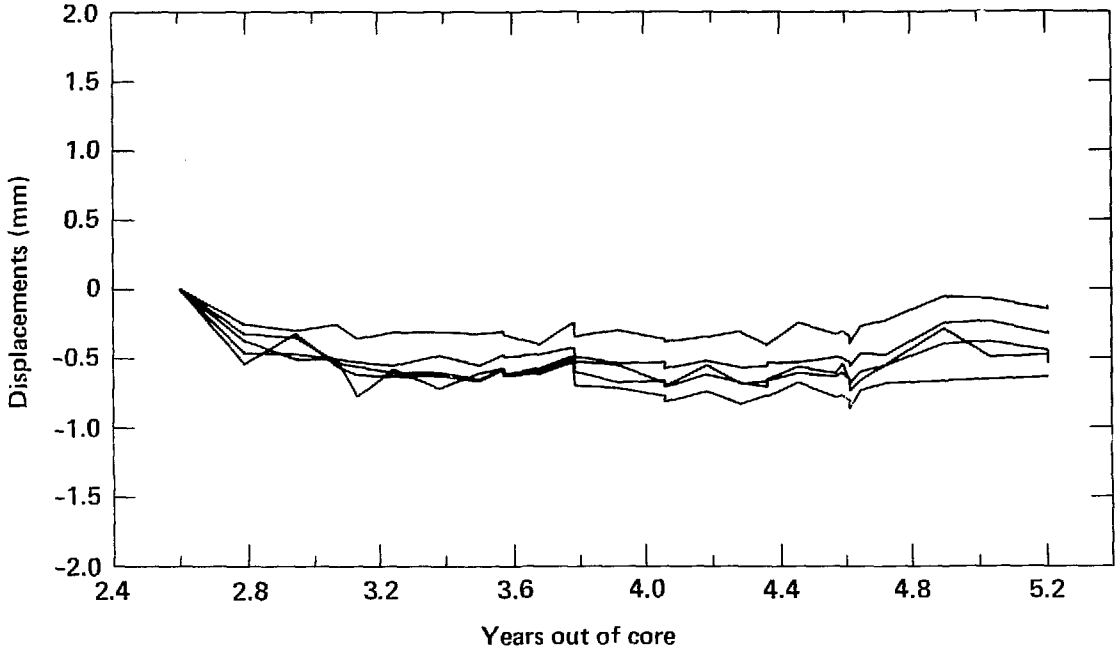

Figure 11-16. South heater drift vertical tape extensometer data.

end of the south heater drift were also omitted because of their location at the curved end of the drift.

These averaged TX records of the drift closures are compared with the calculated displacements at the floor and ceiling centerlines and at the midheights of the walls in each drift. The calculations used in this comparison are those which included no explosively damaged region. In other words, the modulus is 27 GPa throughout the finite element mesh because prior to instrument installation, damaged rock was scaled from the walls to ensure sound instrument anchorage. Figures 11-17 and 11-18 show the average of measurements of horizontal and vertical closure of the canister drift. Measurements were begun on June 26, 1980 (2.6 YOC). The TX zero value was adjusted for this time, and shows closure from the beginning of the calculation out to about 5.0 YOC. Figures 11-19 and 11-20 show a similar comparison for the south heater drift, and Figs. 11-21 and 11-22 for the north heater drift.

General trends in the TX data from 2.6 YOC to about 4.0 YOC were described in Patrick et al. (1982). All vertical TX measurements indicated convergence of the roof and floor of each drift. The horizontal TX measurements in both heater drifts indicated displacements ranging from

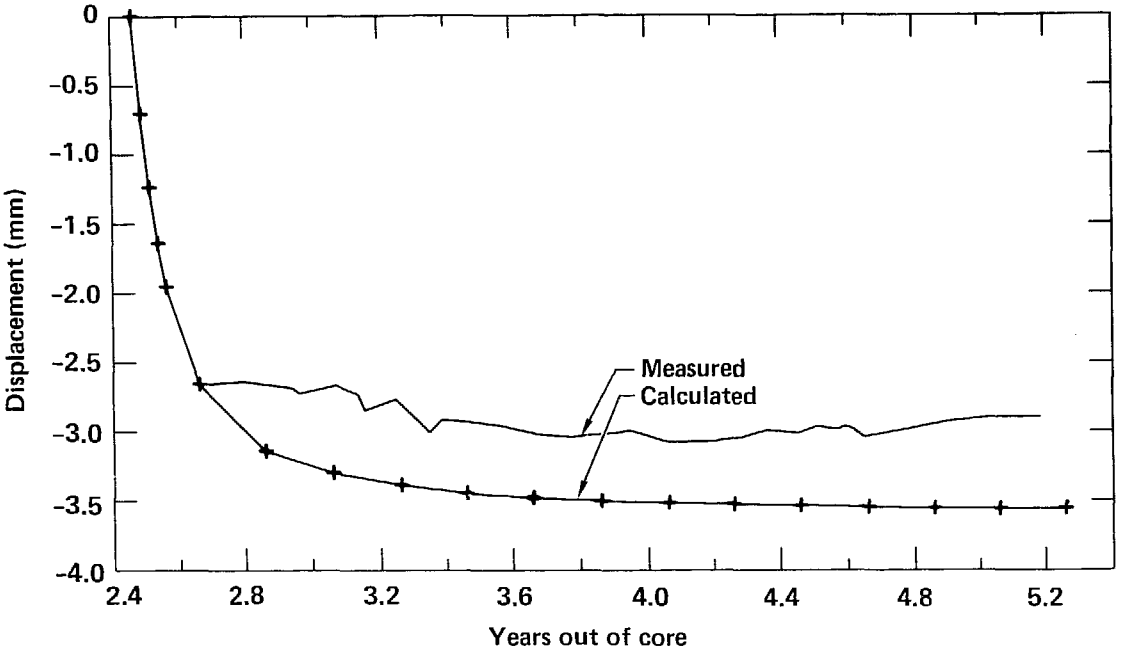

Figure 11-17. Horizontal measured and calculated canister drift convergence.

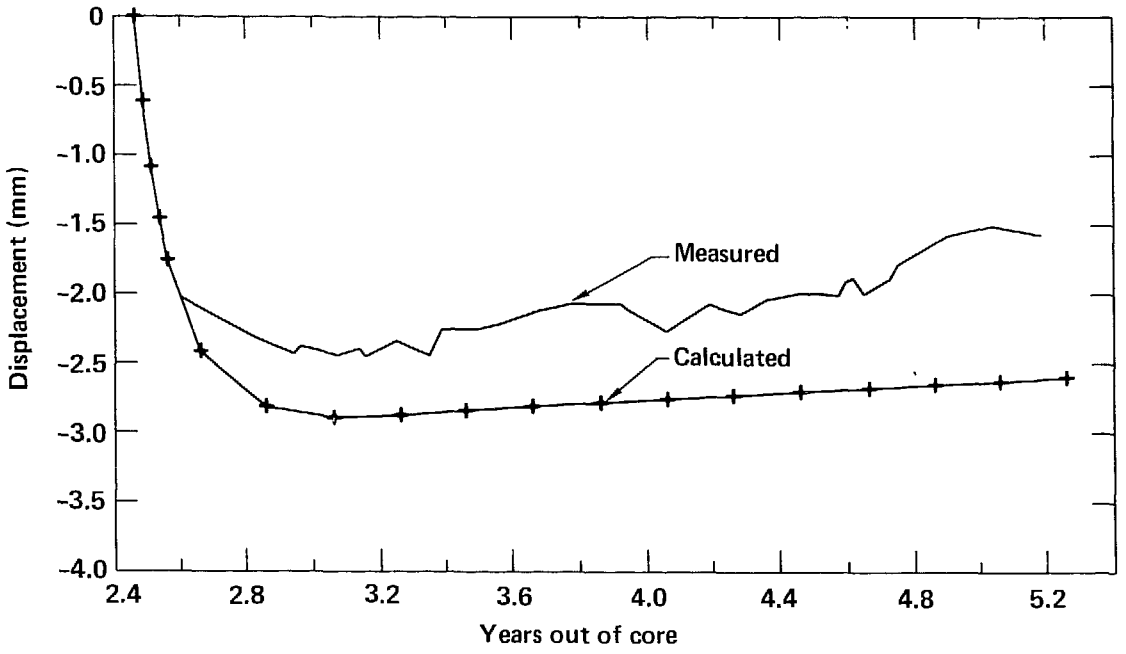

Figure 11-18. Vertical measured and calculated canister drift convergence.

essentially zero to a very slight divergence of the drift walls, while the horizontal canister drift measurements indicated an increasing net closure of the drift from the thermal load.

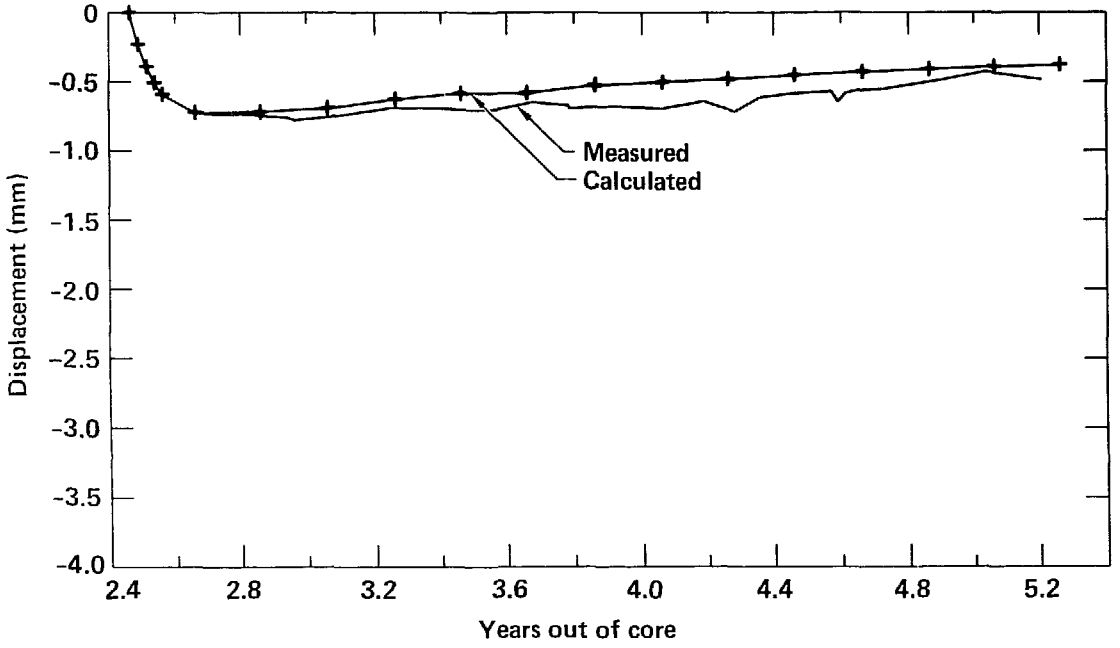

Figure 11-19. Horizontal measured and calculated south heater drift convergence.

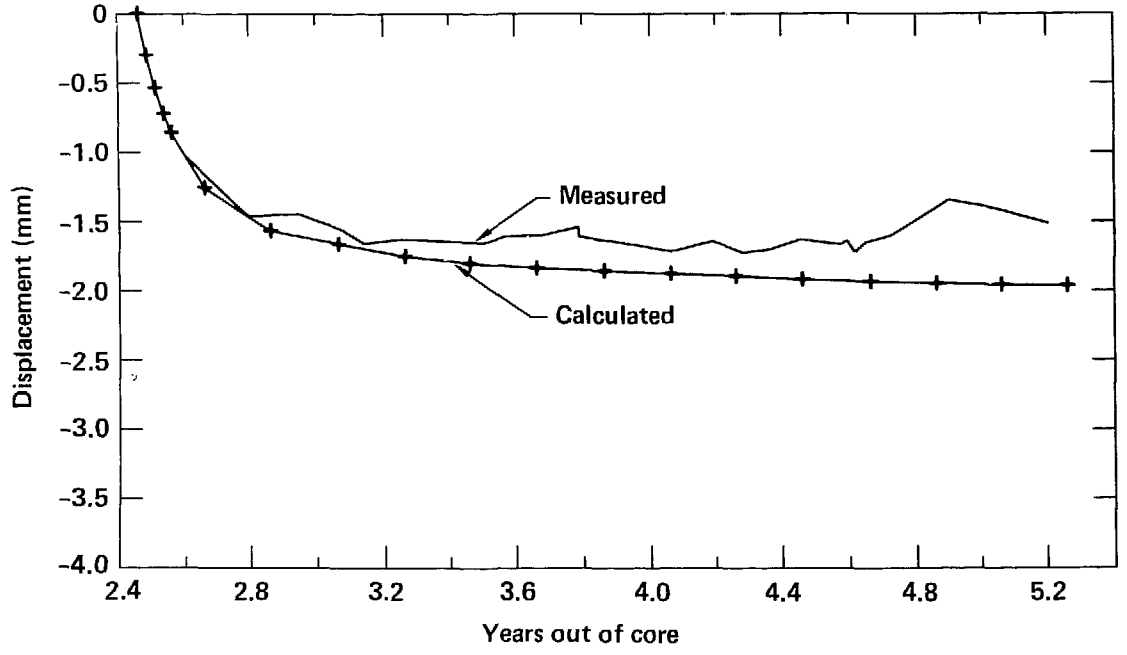

Figure 11-20. Vertical measured and calculated south heater drift convergence.

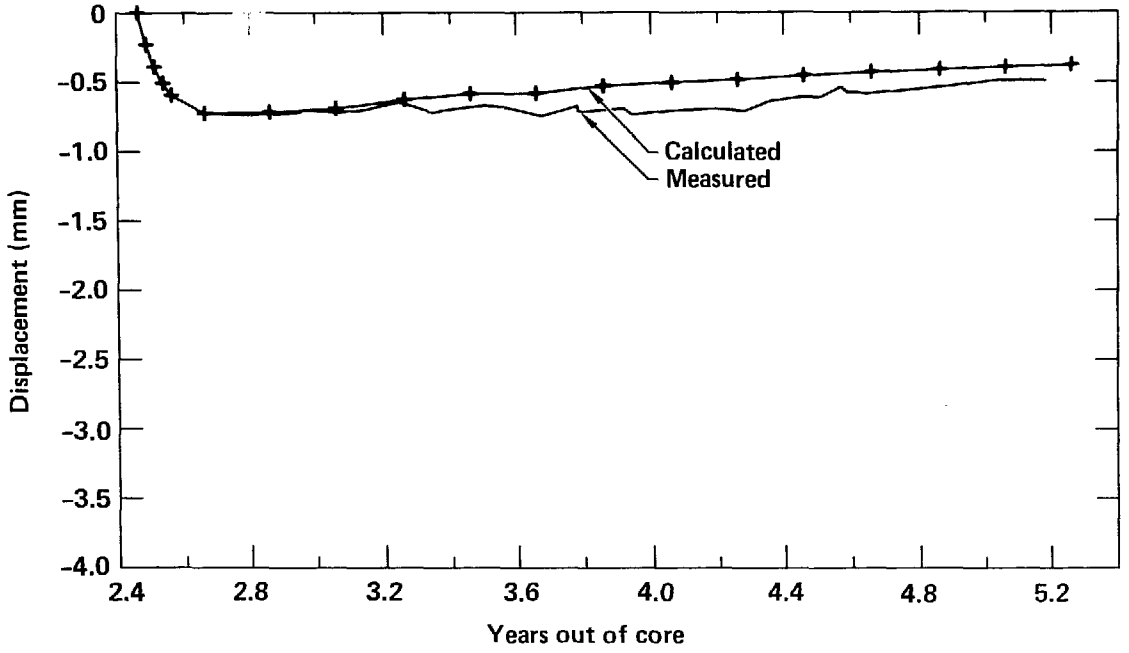

Figure 11-21. Horizontal measured and calculated north heater drift convergence.

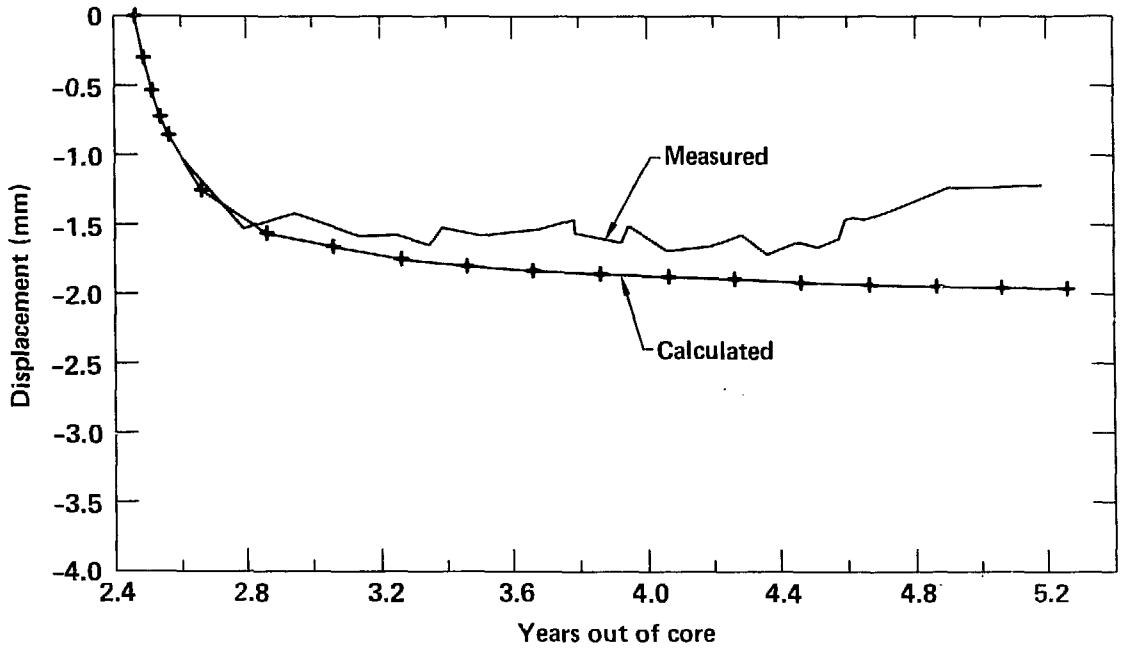

Figure 11-22. Vertical measured and calculated north heater drift convergence.

The trends in the measured and calculated drift convergences tracked each other quite well through about 4.0 YOC, as was pointed out by Yow and Butkovich (1982) and by Butkovich, Yow, and Montan (1982). However, there has since appeared somewhat of a deviation of TX-measured values from calculated trends. This deviation is particularly evident in the vertically oriented TX measurements and represents an apparent divergence of the drift relative to the previously measured deformations. In the heater drifts the apparent deviation seems to begin at about 4.5 YOC, while in the canister drift it begins at about 4.2 YOC. If valid, this data trend would imply greater vertical expansion of the pillars than was calculated, along with essentially no lateral expansion of the pillars since about 4.2 YOC.

As stated earlier, the two largest problems with the TX measurement program are the lack of TX data from the first weeks of the test, and the use of one-point temperature measurements to represent an average TX temperature for temperature correction purposes. Data available from CWE instrumentation and supplementary temperature data should resolve these problems and enable us to verify the TX data trend.

11.3.3 Fracture Monitor System and Whittemore Gauge Measurements

Most displacement instruments at the SFT-C measure integrated rock displacements, including movement of the rock mass as well as movement along discontinuities within the rock mass. The fracture monitor system (FMS) and Whittemore gauge data, however, reflect movement on selected discrete fractures in the rock and in the concrete floor of the canister drift, respectively. Because no FMS data have been corrected for temperature effects, no further discussion of FMS data will be included here. The Whittemore gauge is being used to monitor displacements on discrete fractures at six locations in the concrete floor of the canister drift. The fractures monitored were reported here last year initially to be radial features fanning out from canister emplacement holes. Cracking had continued even after the original features coalesced, and the character of the cracking gradually changed from a radial pattern in the immediate proximity of each hole to a roughly rectangular pattern in the regions between the canister emplacement holes.

Figures 11-23 through 11-28 show the change in crack aperture with respect to YOC for each of the six measurement stations. Some of the "seesaw" effect seen in the plots results from differing instrument operators. Positive displacements represent opening of the crack following commencement of measurements; negative displacements indicate closure. Shear movements along each crack are not illustrated, but are usually less than half the magnitudes of the aperture movements. In all cases some unknown amount of opening was not measured before the initial gauge readings were made since the cracks had already formed before the measurement locations were selected. Three of the cracks (Figs. 11-23, 11-25, and 11-26) show a distinct continued opening or widening trend with time, while the other three do not.

All of the plots show some closure at about 4.6 YOC corresponding to the time at which drift ventilation was at a significantly reduced rate and drift air temperature was correspondingly higher (Chapter 8). The associated increase in the near-surface temperature of the concrete floor produced a temporary partial closure of the cracks. The overall long-term behavior of the cracks, which has gradually become reestablished since the normal ventilation rate was resumed, seems to result from material expansion below the immediate floor surface, and probably represents both heave (or rise) and lateral expansion in the floor of the canister drift.

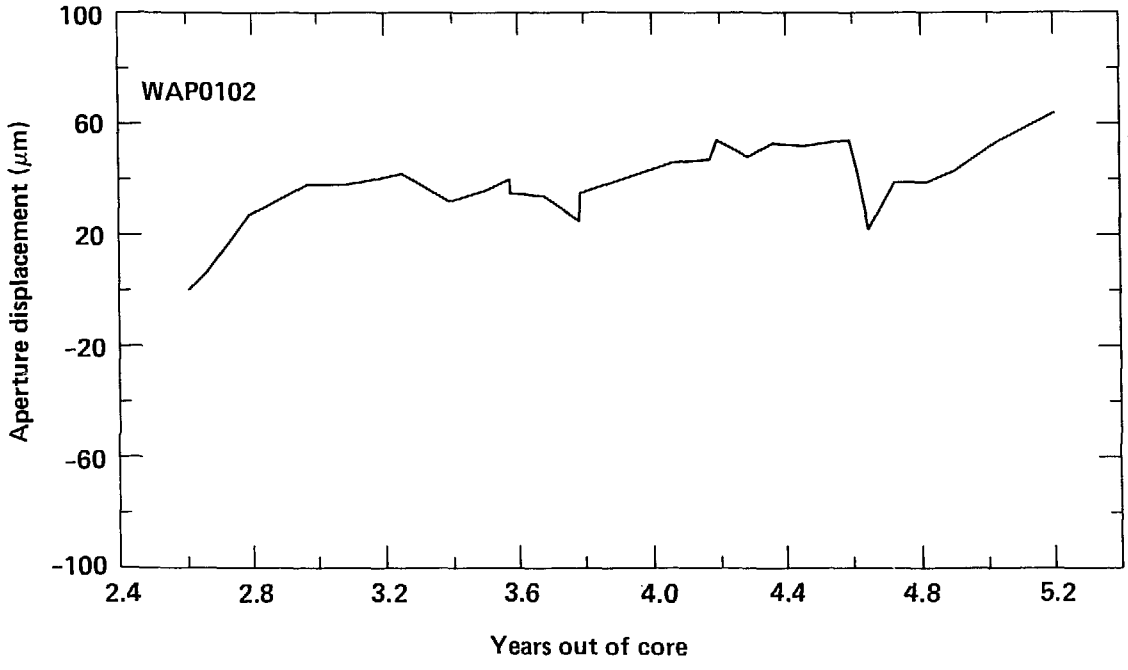

Figure 11-23. Whittemore measurements--aperture vs time (WAP0102).

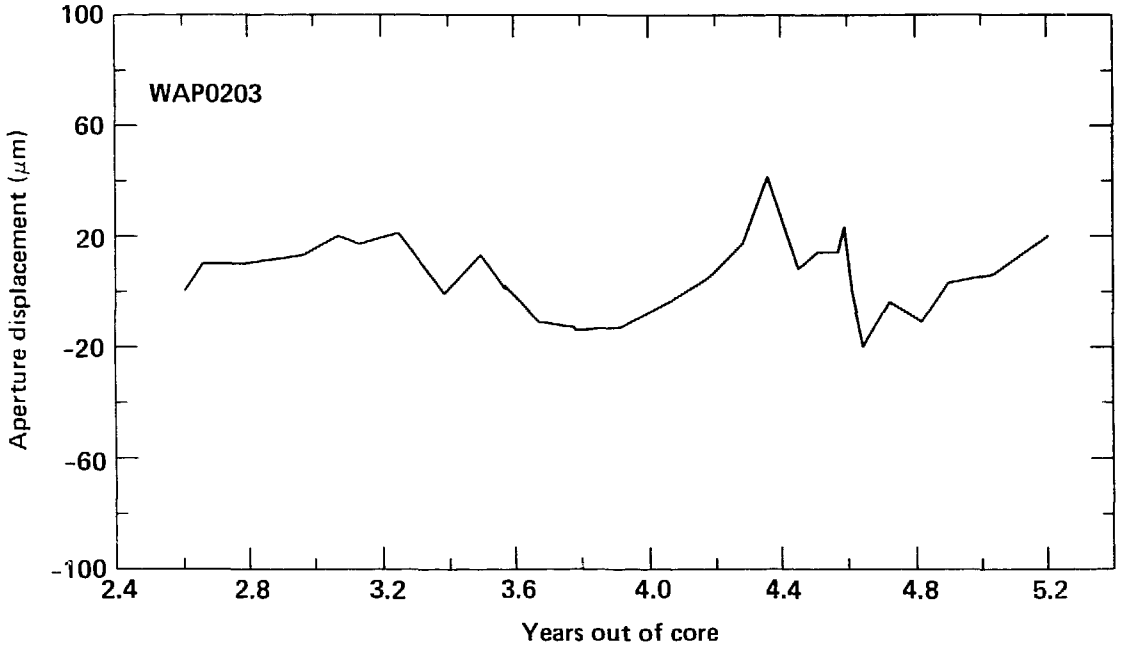

Figure 11-24. Whittemore measurements--aperture vs time (WAP0203).

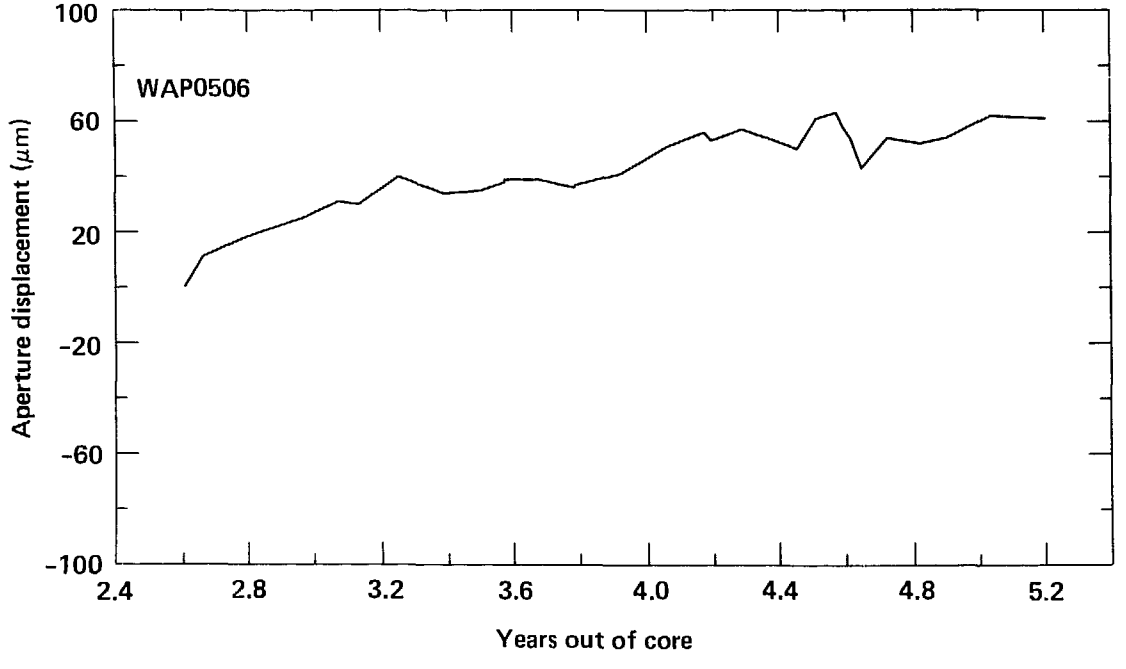

Figure 11-25. Whittemore measurements--aperture vs time (WAP0506).

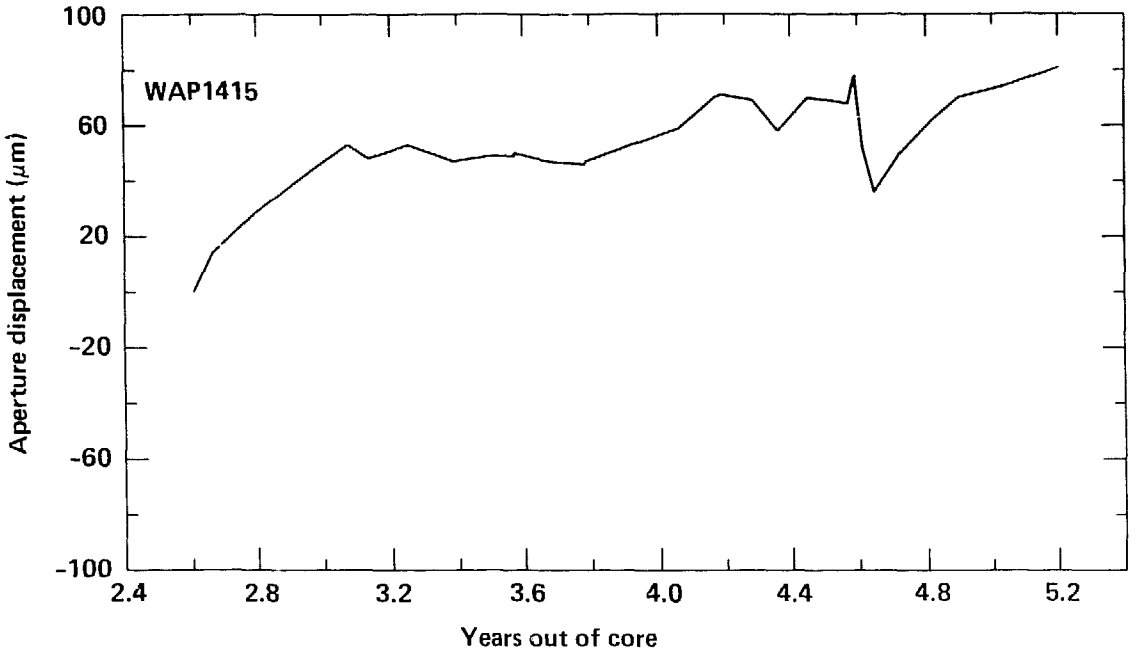

Figure 11-26. Whittemore measurements--aperture vs time (WAP1415).

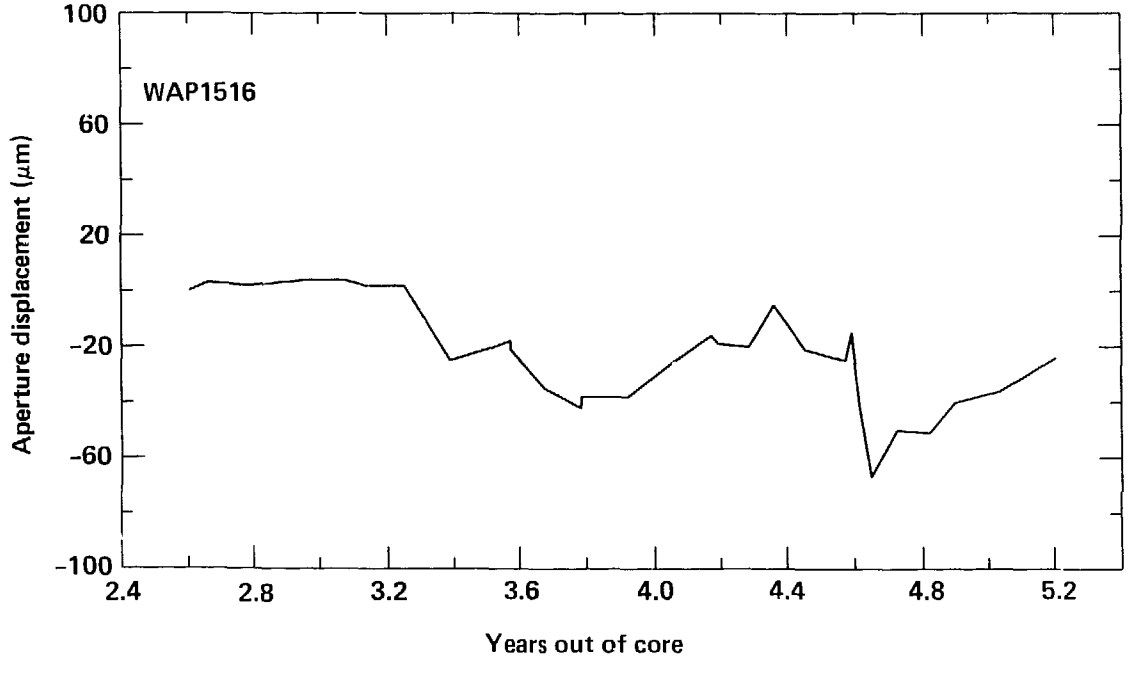

Figure 11-27. Whittemore measurements--aperture vs time (WAP1516).

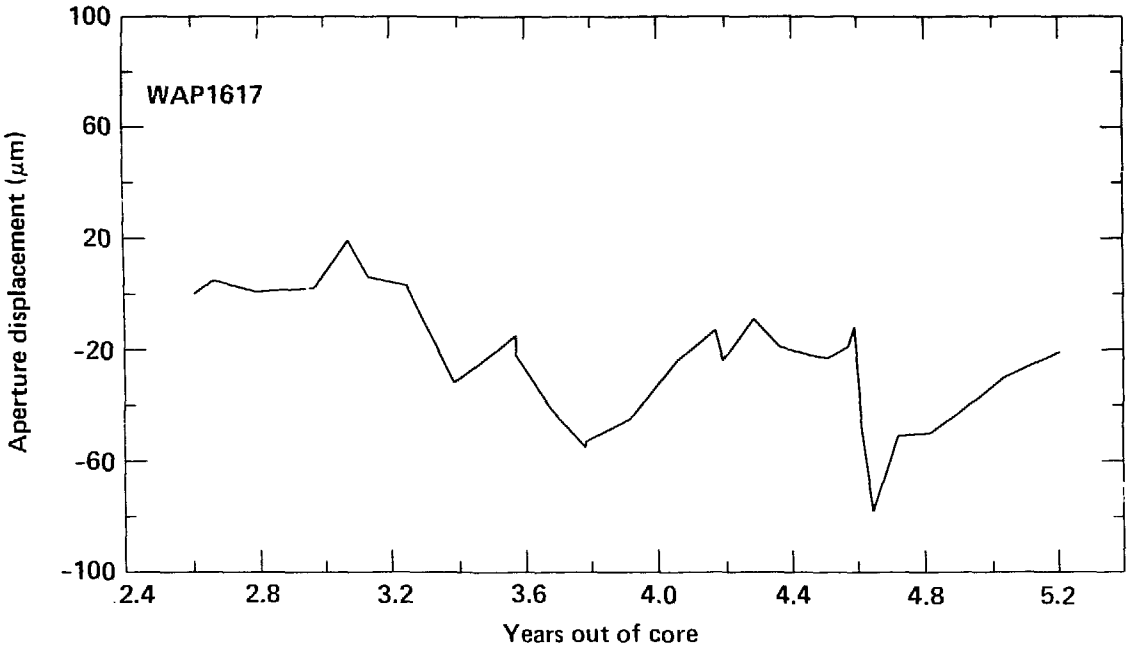

Figure 11-28. Whittemore measurements--aperture vs time (WAP1617).

CHAPTER 12

ACOUSTIC EMISSION AND WAVE PROPAGATION MONITORING

Since January of 1980, acoustic emission activity (AE) and wave propagation characteristics (velocity and amplitude of P- and S-waves) have been measured on a weekly basis. The objective of this part of the measurement program is to determine the applicability of seismic techniques for monitoring the integrity of an underground repository during storage of nuclear waste. This chapter describes the work during FY 1982 and presents some conclusions relative to the utility of the techniques. For a detailed description of equipment setup and the techniques used please refer to Majer et al. (1981).

12.1 INTRODUCTION

Prior to this experiment there have been few long-term studies on this scale of seismic activity or on the behavior of P- and/or S-waves in granite. Previous studies on rock falls (Blake et al., 1974) and the Stripa heater

tests (Paulsson and King, 1980) indicate that AE activity and changes in elastic wave behavior could be expected. However, it was not known to what extent AE activity or velocity and attenuation of the elastic waves would be affected at the scales (50 × 20 × 20 m array) and temperatures (maximum 85°C) involved. If changes in these phenomena did occur, the question remained whether they could be detected reliably for long time periods over reasonable bandwidths. In addition, and most importantly, could these data be useful for inferring such parameters as stress changes, fluid content, rock properties, and/or other critical parameters of importance using techniques developed for larger scales and lower frequencies? Lastly, was the rate of data collection (i.e., digitization rates, AE occurrence, etc.) such that the data reduction and analyses could be performed using in-field equipment and in close to real time?

12.2 AE MONITORING

The Climax AE experiment is designed to determine the relative importance of such factors as mine geometry, thermal effects (cooling and heating), pore content, and tectonic stress in the generation of AE activity. Radiation degradation and rock type and heterogeneity will also provide other factors influencing failure rates and mechanisms. In addition to the question of radioactive material containment, there also remained the confirmation of overall mine stability and safety. The intention was to employ as many seismological techniques as practical to characterize the AE activity in more complete terms relative to the continuing physical processes.

Because of the potentially wide range of fracturing involved (microfracture to small scale faulting), careful consideration was given to the frequency range monitored. Such factors as physical dimensions of the repository, noise sources, and attenuation properties led to the selection of the 1- to 10-kHz range. Assuming a static dislocation model, these frequencies correspond to fractures on the order of several centimetres. Although much higher frequencies would be generated by microfracturing near the canister surfaces, it was the larger fracture dimensions that would occur throughout the repository that were of interest in determining overall stability and integrity of the mine.

12.2.1 AE Results

Figure 12-1 shows the general layout of the experiment and the areas of principal seismic activity. Shown in Fig. 12-2 is the rate of AE activity vs time (events/week) and temperature at various points within the rock.

Several interesting aspects of the observations can be noted. The events located and shown in Figs. 12-1 and 12-2 are those which have been detected at four or more stations and could be reliably located (±1 m). During the entire survey (1979 to present), the principal areas of AE activity have been confined to the areas shown in Fig. 12-1. However, the activity in 1982 was mainly located near hole AE15, as was the peak in activity near the end of 1981. All of the events in this area are of similar character; i.e., impulsive with clearly defined P and S phases, indicating shear failure. All events were located 2 to 5 m beneath the canister drift floor, aligned in approximately an east-west direction. In addition to these shear failure events, which appear to be occurring within the intact rock, there are numerous "abnormal" events. These events are usually of lower frequency content (1 to 4 kHz) and often "harmonic" in appearance; they contain relatively little S-wave energy. These events are typically emergent in their onsets, making them difficult to locate; however, they seem to be occurring principally near the mine walls or near instrument installations. One such example is the "emergent type" events, thought to be due to concrete cracking, reported here last year.

Because of the automated processing being carried out in the field, the most reliable results are for those events which are impulsive. Attention will be focussed on these events, although all types of activity will be discussed later.

The dominant frequencies of the impulsive events range between 7 and 12 kHz for the P-wave and 6 to 12 kHz for the S-wave. In general the S-wave corner frequencies (f_0) are 80 to 90% of the P-waves, sometimes equal, but almost never significantly greater. The moment of these events (M_0) varies from 10^{10} to 10^{12} dyne-cm. Although it may be meaningless to extrapolate moment-magnitude relations developed for microearthquakes, these events would be magnitude -4.5 to -3.0, using $\log_{10}(M_0) = 16.5 + 1.5\ M_l$. The most interesting aspects of these events are the stress drop and fault plane solutions. The stress decrease (initial minus final stress) for these events ranges from 0.1 to 5 MPa. One must keep in mind that these stress drops are

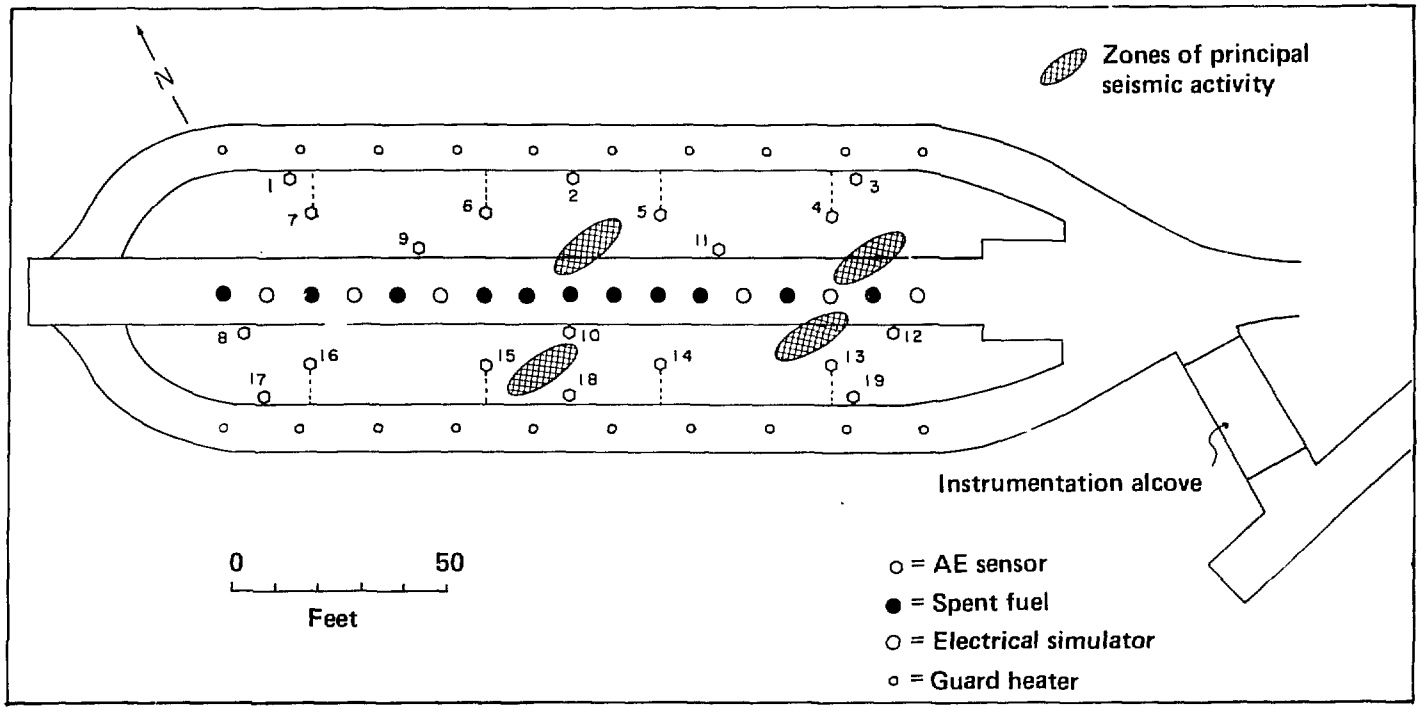

Figure 12-1. Plan view of acoustic emission instrumentation locations and zones of principal seismic activity.

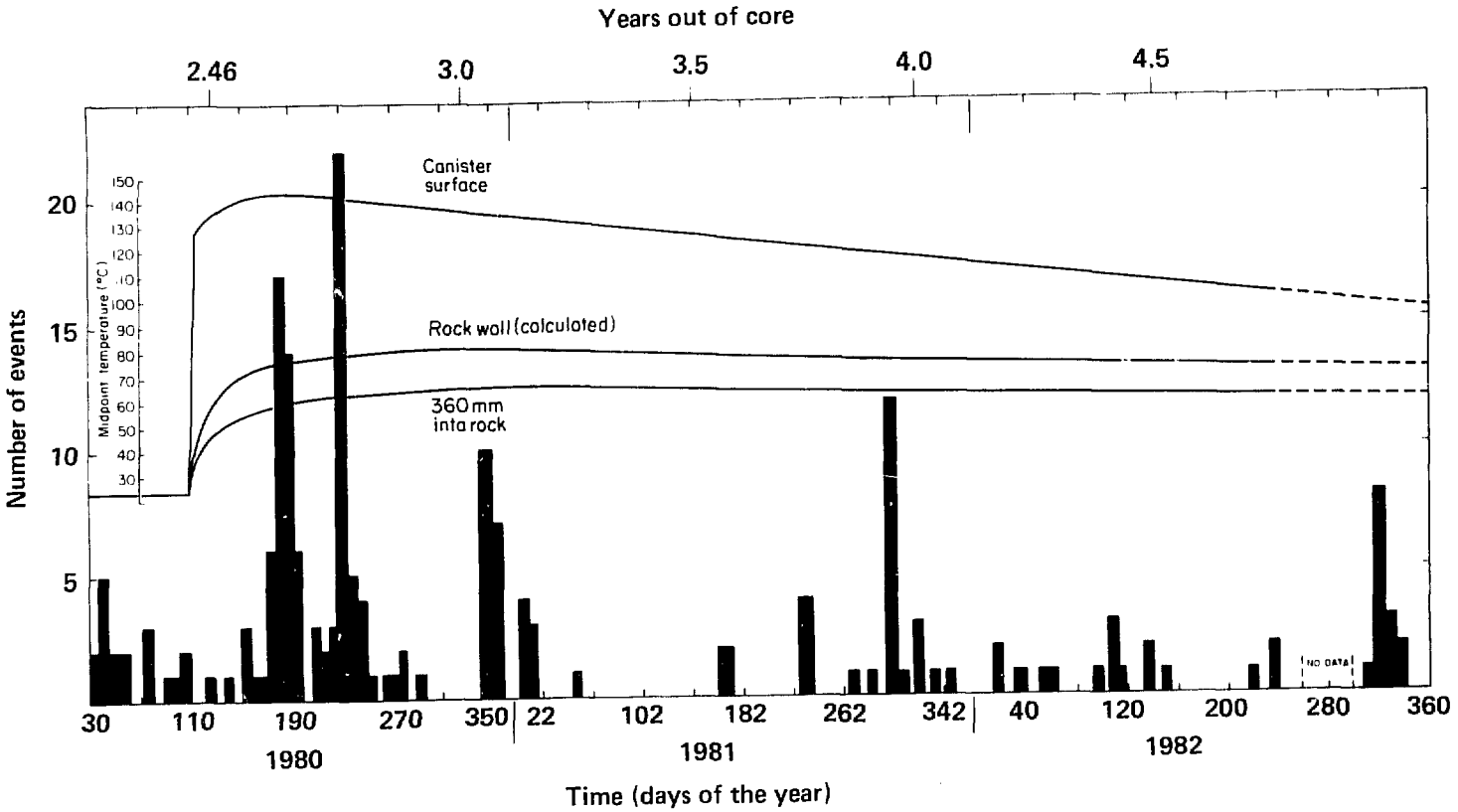

Figure 12-2. AE activity and temperatures from January 1980 through December 1982.

calculated from the spectral data; i.e., $\Delta\sigma = 8\ M_0(f_0^3/V^3)$, and thus are critically dependent on the corner frequency f_0. The corner frequency, in turn, is dependent upon attenuation, propagation path, site response, and the seismic energy radiation pattern. The moment M_0 and velocity of propagation V are less affected by these factors and are probably reliable estimates of the true values. Therefore these stress decrease figures are probably a lower bound.

Also, we note the fault plane solutions and the distribution of foci. For the first time in the experiment, enough data have been collected to infer fault planes and principal stress directions in the zones of AE activity. Examining Fig. 12-1, it can be seen that the events are distributed along east-west planes. Although there was only marginally enough data available for reliable fault plane solutions, the events are primarily dip-slip with right lateral components on the north side of the canister drift and left lateral components in the south side of the canister drift. The dip of the planes is approximately 20 to 30°. The best data were obtained for the events near holes 14 and 15, although similar inferences were obtained for the events near the center of the drift.

12.3 WAVE PROPAGATION RESULTS

Shown in Figs. 12-3a, b, and c are the data from monitoring the P- and S-wave amplitudes over several years for various paths throughout the array. The full details of the monitoring system and procedures are described in Patrick et al., 1982. Briefly, the procedure is to monitor weekly the amplitude of the first arrival at stations 19, 12, 2, 5, 3 and 11. The source is at the bottom of hole AE13. The purpose was to observe any changes in attenuation properties with time relative to a reference station at AE15; i.e., attenuation differences for paths through the canister area vs those for paths outside the canister areas. The source is a 150 mm (6 in.) long cylindrical, 38 mm (1-1/2 in.) diameter piezoelectric transducer driven by a 1.6-kV, 3-μs rise time pulse. These transducer parameters yield seismic waves with dominant frequencies from 10 to 20 kHz. To avoid any ambiguity from such factors as source-rock coupling changes over time, the source was coupled to the rock by means of filling the bottom of the hole with water. This coupling technique has given a remarkably reproducible signal over time.

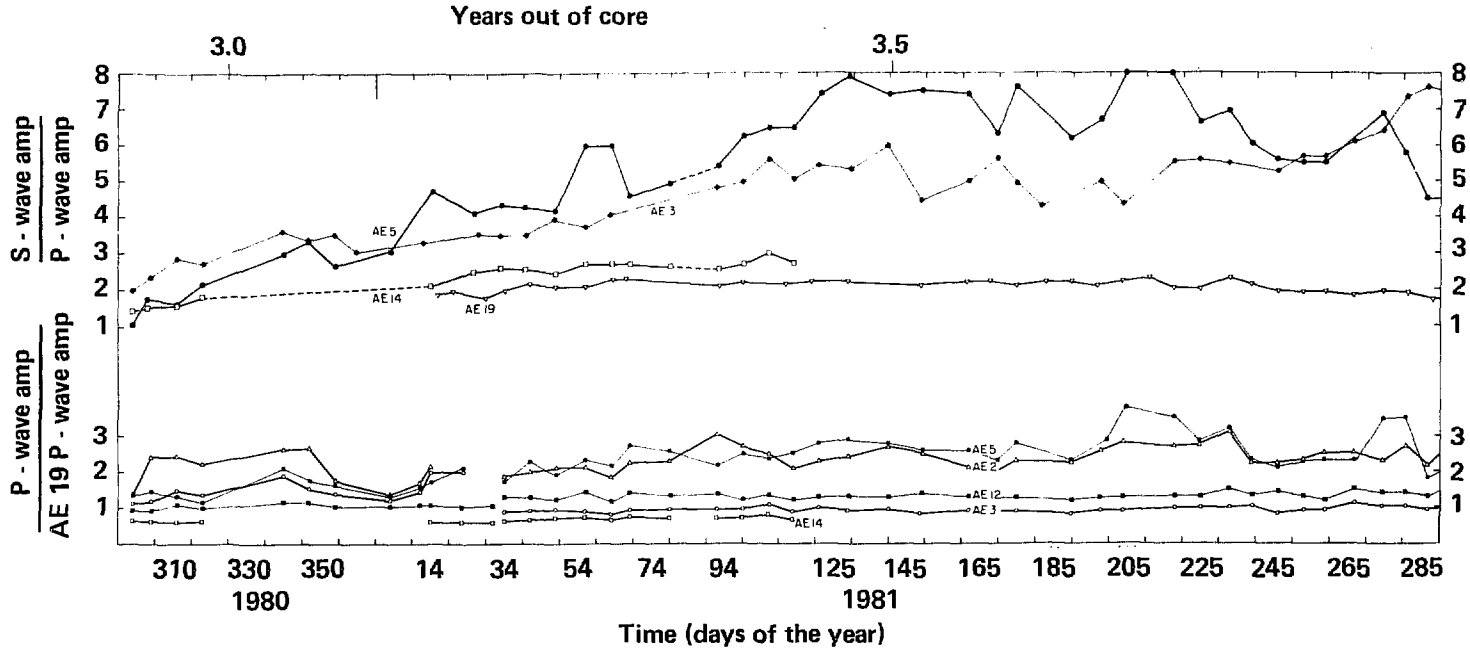

Figure 12-3a. P-wave and S-wave amplitude changes through day 285, 1981.

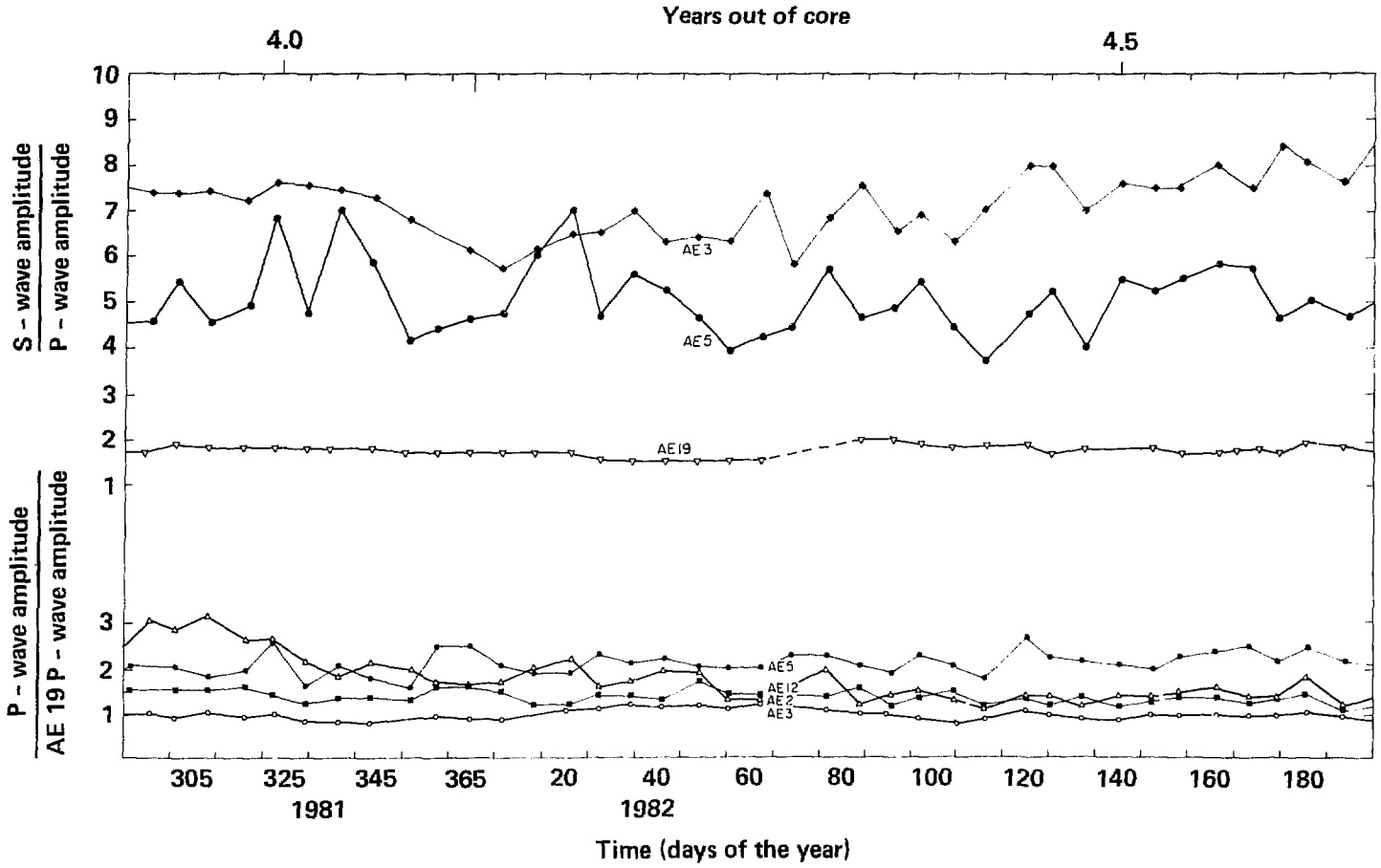

Figure 12-3b. P-wave and S-wave amplitude changes from day 285, 1981, through day 190, 1982.

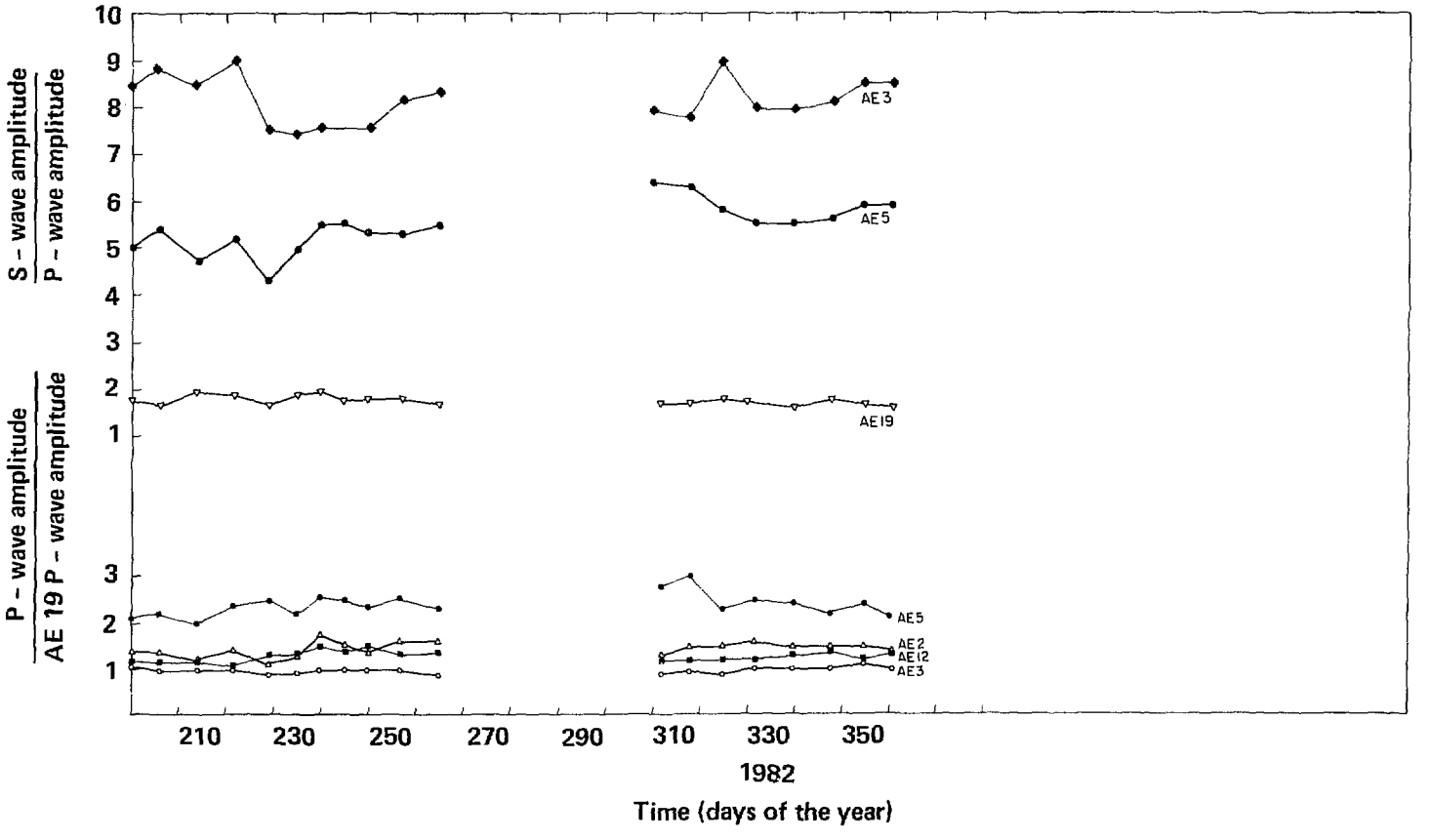

Figure 12-3c. P-wave and S-wave amplitude changes from day 190, 1982, through day 350, 1982.

As can be seen from Figs. 12-3a through 12.3c, there has been little change in P-wave amplitude relative to station 19 at stations 12 and 3. However, there has been an increase in the P-wave amplitude at station 5, and a small decrease in the amplitude at station 2, although it has been almost constant for the past year. The most significant changes have occurred in the ratio of the S-to-P amplitudes at stations 3 and 5, with little change at station 19, although it has shown some small variation in the last year. The S/P wave ratio is probably a more reliable measure of changes in the rock because it is a ratio of two waves for the same path. Assuming the path length does not change significantly, the only variation can be in the properties along the path. The constant value at AE19 indicates that the source has not changed.

Also monitored have been the arrival times at the same stations over the same time period. There has been no significant change in the arrival times within the accuracy of measurement (±10 μs): out of a propagation time of 3 ms, less than 1% change.

12.4 DISCUSSION AND INTERPRETATION

12.4.1 Acoustic Emission

The AE activity can be grouped into two categories, that associated with stress changes within the competent rock mass due to thermal loading (hereafter referred to as type 1 events) and that due to stress changes from such activities as mining, instrumentation emplacement or maintenance, or mining damage (type 2 events). At these relatively shallow depths (420 m) there is little chance of rock burst type of activity.

The tensile strength of the Climax granite is 10 to 12 MPa, and its ultimate uniaxial compressive strength is about 160 MPa (irradiated) to 200 MPa (unirradiated) (Patrick et al., 1982). The principal stresses prior to heating were 2.75, 7.13, and 11.56 MPa (Ellis and Magner, 1982). Calculated stress changes due to mining and heating are in the range of 12 to 20 MPa. Given this state of stress, noted stress changes, and the measured rock strengths, it is unlikely that significant new fracturing is occurring. Furthermore, the noted stress changes are in general agreement with the 0.1 to 5 MPa stress changes calculated from the AE data.

From the spectral data of type 1 events, the average displacements vary from 0.005 to 0.1 mm. Although much less than the observed total displacements, the cumulative AE displacement is likely contributing to the observed displacements, particularly the inelastic displacements occurring along joints (Chapter 11). Also of interest are the fault plane solutions (although there is a 90° ambiguity in any fault plane solution). If one assumes that the foci of events form the strike of the fault plane, then the fault planes are approximately orthogonal to the major geologic faults in this area (Wilder, Yow, and Thorpe, 1982a). However, what may be occurring is an echelon fracture or slip on planes parallel to the major geologic features. The data are not yet sufficient to resolve this. Whatever the case may be, the type 1 events indicate that the events result from increases in the principal stresses due to thermal loading. Other areas are also under thermal loading and there are displacements occurring but AE activity is not present. The displacements in these areas are aseismic, probably resulting from thermoelastic expansion of the rock mass.

The type 2 events seem to occur at random and are always in areas where rock has been excavated or instruments emplaced. It is thought that these events are only mildly affected by the thermal changes. Although they may be due to temperature effects on the instruments or from slips of incompetent rock, these events are difficult to analyze due to their low signal-to-noise ratio, and probably would not shed much light on the rock properties of interest. On the other hand, some of these events may be an indication that the displacement is partially aseismic; i.e., somewhere between stick slip and continuous slip. It is also worth noting that there have been several "low frequency" events with relatively impulsive beginnings. They appear to emanate from the center of the canister drift. These may be occurring on the known fault zones and may be an indication of thermally induced activity along these features.

12.4.2 Wave Propagation

As reported last year, changes in the ratio in S- to P-wave amplitudes were thought to be due to crack closure and dewatering of the rock in the canister drift area. These phenomena are still present and appear to be causing the continuing changes in S/P-wave amplitudes. It appears that these changes have stabilized over the last year. This stabilization can be seen

in the data at AE5 and AE3 in Fig. 12-3. Although AE5 appears to have stopped increasing, AE3 is still slightly increasing.

As mentioned earlier, there has been no observable change in the arrival times over the period of time monitored. The lack of even a 1% velocity change is somewhat surprising. However, if one takes into account some similar data taken at the Stripa experiment (Paulsson 1983), this lack of velocity variation can be explained. Figures 12-4a and 12-4b show the results of monitoring arrival times over similar time periods, but on a somewhat reduced scale. Paulssons' measurements were over 3- to 5-m distances vs 10 to 20 m for this experiment. However, the temperatures encountered were quite similar along the paths of propagation. As can be seen in Figs. 12-4a and 12-4b there was a dramatic increase in both P- and S-wave velocity immediately after the heater was energized. However, even though the rock continued to heat, little or no changes were observed until the heater was de-energized. Our velocity and attenuation monitoring did not start until some 200 days after emplacement. Even though the SFT-C is on a larger scale than the Stripa

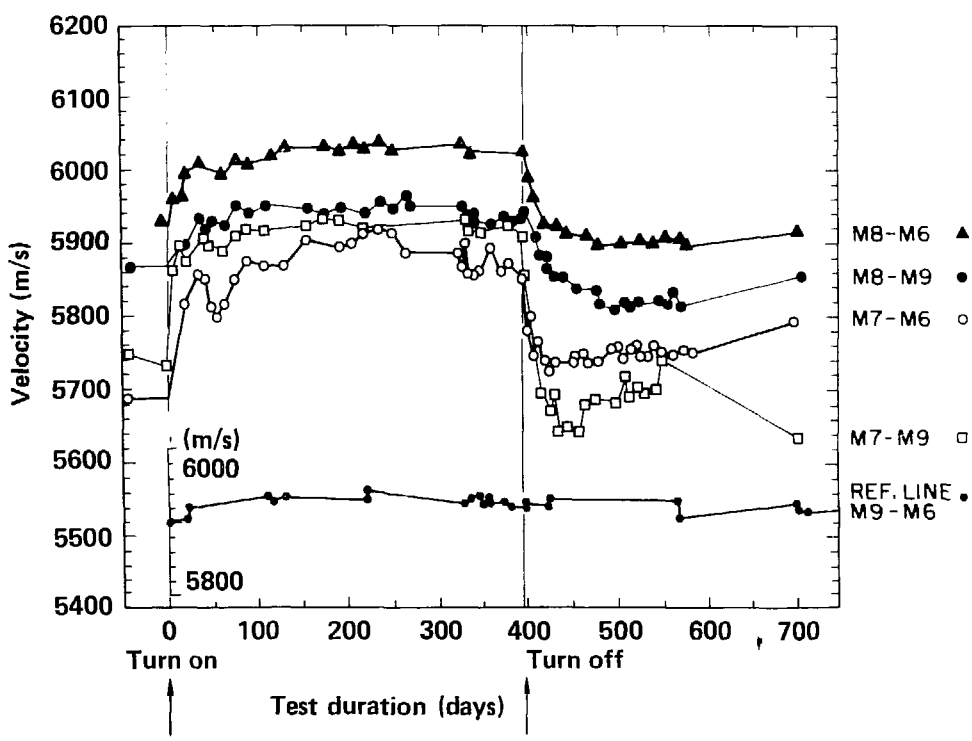

Figure 12-4a. Effects of heat on P-wave velocities recorded at Stripa (after Paulsson, 1983).

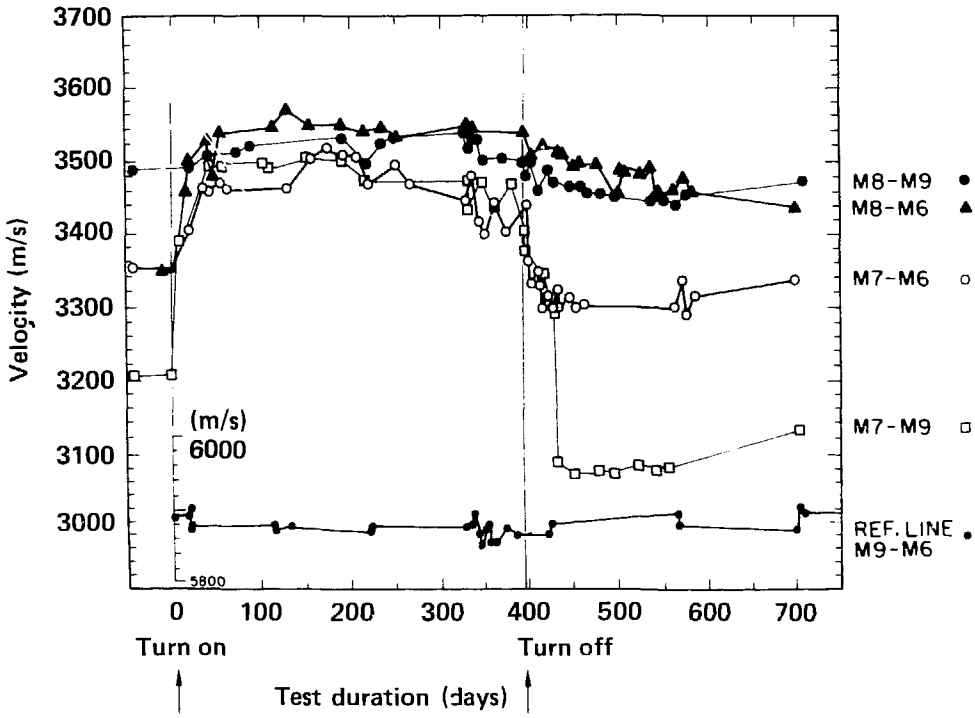

Figure 12-4b. Effects of heat on S-wave velocities recorded at Stripa (after Paulsson, 1983).

experiments, it appears we have missed the sudden increase in velocity that occurs on initial heating. It is important to realize that if we had relied upon velocity measurements alone, we would have missed the changes in rock properties observed with the other techniques. Obviously it is important to monitor amplitudes (both P- and S-) as well as travel times, over the total duration of the experiment.

12.5 CONCLUSIONS

We arrived at the following conclusions relative to AE and wave propagation monitoring:

- Two types of AE events have been identified: definite shear failure events associated with thermal loading, and events associated with stress changes from cultural (nonthermal) activities. The former type 1 events have relatively large stress decreases (0.1 to 5.0 MPa), small displacements (0.005 to 0.01 mm), and are on planes consistent with observed fracturing. The latter type 2 events have

low frequency content (thus much lower stress decreases) and commonly occur near zones of incompetent rock or instrument emplacements. These events are usually of smaller magnitude, but have larger source dimensions than the type 1 events.

- Wave propagation data reflect the position of the thermal pulse and its concomitant effects on existing fractures.
- It is important to collect AE, arrival time, and amplitude data concurrently. Relying on one technique may lead to false conclusions on rock behavior or may cause the experimenter to miss important changes.
- Attenuation properties are much more sensitive to change in rock properties than is velocity.

CHAPTER 13
DATA MANAGEMENT SYSTEM

13.1 CURRENT PROCESSING TECHNIQUE AND MODIFICATIONS

The processing of data from raw data tapes (received from NTS) through its plotting and permanent storage is shown in Figure 13-1. The system is generally unchanged from last year, but is running more smoothly and accurately. Much of the effort this year has been directed toward improvements to the data sieve, accumulation and organization of calibration data and parameters needed for temperature corrections, and improvement to the plotting and other diagnostic capabilities to make data and algorithm validation both more efficient and more complete.

The binary read (BREAD) processor has been changed in two ways since last year. Because at that time we were getting relatively few data records with bad channel numbers, these were written to the output file flagged with a "C?" for manual correction. File SF055B/A contained 65 921 such errors making manual correction impractical. The BREAD data sieve was therefore changed to handle channel number errors in the same manner as license errors. Thus if both license and channel number are bad, the data record is now deleted. If the channel is bad, but the license is one for which a proper channel number is known, the channel number is corrected automatically if the "correct channel number" switch is set on. This switch is set by the operator at the

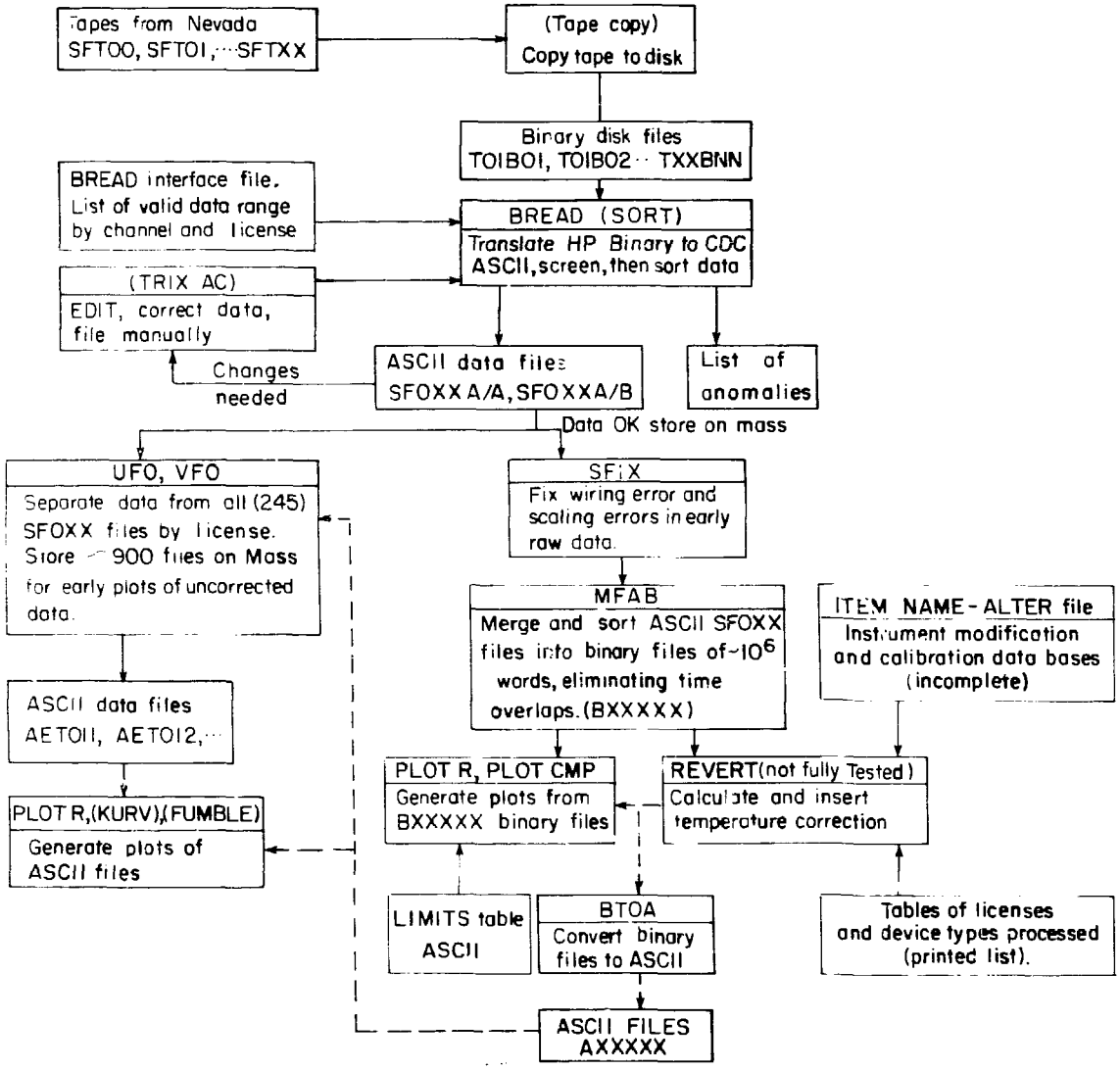

Figure 13-1. Block diagram of Data Management System.

time BREAD is started and complements the existing "replace bad license" and "discard by time range" switches.

Another change to BREAD was to improve quality assurance (Q/A) of the data transfer from NTS. BREAD now lists the first and last data record found in each file of the HP tape being processed. This list can be compared with a similar listing made at NTS which is delivered with the tape to ensure that BREAD has read all the data written by the HP data acquisition system. After these changes BREAD was documented (Hage, 1983).

SFIX, the small code used to implement systematic corrections to selected blocks of data, was supplemented by SFIX2, which was needed to correct time values on one tape, SF055A/A. The code corrected bad time words by subtracting 150.4 from time values between Julian day (JD) 45305.851 and JD 45306.776, then resorted the file by license and time. All other modifications to incoming data were done with the public utility routine TRIX.

The code used to merge data files in one million word segments and convert them from ASCII to binary (MFAB) was improved and renamed MFAB2 since last year. MFAB2 tests all input files to see whether they are sorted and if not, sorts them. Although files are normally sorted at the end of a BREAD run, that sort is optional. Also, some data editing procedures can perturb the data order, requiring a new sort.

The code used to reconvert raw data to temperature compensated form (REVERT) has seen extensive modification, with over 20 recompilations made in the last year. Previously, REVERT was described as needing a subsidiary data table containing decision-making information and calibration data for all the instrumentation. The table was called HPDATABASE and originated as a system dump of the descriptive data base serving a similar function on the HP system at NTS.

The HPDATABASE changed with time as instruments were added or deleted and calibration data became available or changed, thus complicating the conversion process. Twenty system dumps were taken over the period 30 July 1980 to 6 January 1983 and shipped to Livermore. They are stored in files with names of the form HPTPyymmdd, where yymmdd is the date the dump was taken, as written on the label of the tape (see Table 13-1). The structure of the data in the HPTP-files is space-efficient but complicated to read. Formatting the file for easier reading is one of the several capabilities of REVERT and requires a supplementary data file ITEMNAME, which lists the names of the data fields needed for the HPTP file. Not all the data in the HPTP-file are needed for data conversion, and different HPTP-files require different ITEMNAME files, named IN1 through IN10.

Besides its main task of data conversion and temperature correction, REVERT has several additional modes of operation. First, it can produce a CDC-7600 binary file, HPDBYYMMDD, which is not as space-efficient as the HPTP-file but which is more suited to the many random accesses required during the conversion process. Here the YYMMDD is not the date written on the tape

Table 13-1. List of REVERT data base files.

Base No.	HP dump file	Octopus list file	Octopus data file
1	HPTP800731	LIST800730	HPDB800730
2	HPTP800814	LIST800814	HPDB800814
3	HPTP800922	LIST800919	HPDB800919
4	HPTP800117	LIST801016	HPDB801016
5	HPTP810119	LIST780805	HPDB980805
6	HPTP810313	LIST810226	HPDB810226
7	HPTP810402	--	--
8	HPTP810409	LIST810409	HPDB810409
9	HPTP810418	--	--
10	HPT0810625	LIST810625	HPDB810625
11	HPTP811130	LIST811130	HPDB811130
12	HPTP811215	LIST811215	HPDB811215
13	HPTP811223	LIST811222	HPDB811222
14	HPTP820114	LIST820114	HPDB820114
15	HPTP820323	LIST820324	HPDB820324
16	HPTP820413	LIST820413	HPDB820413
17	HPTP820701	LIST820701	HPDB820701
18	HPTP820819	LIST820819	HPDB820819
19	HPTP821118	LIST821119	HPDB821119
20	HPTP830105	LIST830106	HPDB830106

label, but a value inserted into the tape itself at dump time. (These dates are not always the same, as shown on Table 13-1). Each logical record in a HPDB-file is a direct copy of data as it needs to appear in a 100-word common block when that license is being converted. The structure of the common block, COM00, is shown in Table 13-2 and varies with device type. The first twelve words are the same for all device types. The first two letters of the remaining item names indicate device type. REVERT can also produce a listing file, LISTYYMMDD which can be sent to a printer or viewed on a TV monitor.

A third operational mode of REVERT merges data from a HPDB-file and a HPTP-file into a new HPDB-file. This mode ignores data in the HPTP-file for

Table 13-2. Coefficient definitions in COM00.

Item name	Data type	COM00 index	Data description
LCNMBR	I1	1	Logical channel number
LCDESC	X6	2	License plate
PDTYPE	X2	3	Physical device type
LCDSTR	X30	4-6	Channel descriptor string
DATEIN	X10	7	Date device installed
DATEOU	X10	8	Date device removed
DATEMO	X10	9	Date coefficients modified
DVM	X2	10	DVM setting
NRATE	R2	11	Normal scan setting
TLAST	X6	12	Time of last scan
WTSLOP	R2	13	Slope coefficient
WTINTR	R2	14	Intercept
TCOHMS	R2	13	TC resistance
TCCOEF	I1	14	TC quartic coefficient set
TCREFC	I1	15	TC reference channel
TCOC	R2	16	TC offset constant
ESWLOC	R2	13	Excitation wire loss offset
RXESLC	I1	13	RX excitation channel
RXRODL	R2	14	Rod length, metres
RXKCP1-9	R2	15-23	Calibration position 1-9
RXKCC1-9	R2	24-32	Calibration reading 1-9
RXTLC0-6	I1	33-39	Temp ref channel 0-6
RXDTT0-6	R2	40-46	Distance to temp reading
RXTOC0-6	R2	47-53	RX calibration temperature
RXPCL1-7	R2	54-60	Physical component length 1-7
RXMTC1-7	R2	61-67	Thermal expansion value 1-7
RXOC	R2	68	RX offset constant
RTRO	R2	13	Reference resistance
RTCA	R2	14	Coefficient A
RTCB	R2	15	Coefficient B
SDOC	R2	13	SD offset constant
LDSLOP	R2	13	Linear device slope
LDINTR	R2	14	Linear device intercept
MDPRON	X6	13	Misc processor name
MDPAR1-5	I1	14-18	Misc processor param 1-5

Table 13-2. (continued)

Item name	Data type	COM00 index	Data description
VWSLOP	R2	13	IRAD gage sensitivity
VWOC	R2	14	Zero load reading
VWMM	R2	15	Gage-rock thermal modulus
VWTI	R2	16	Initial temperature
VWTIC	R2	17	Initial set gage reading
VWTLC	I1	18	Gage temperature channel
WXESLC	I1	13	WX excitation channel
WXWIRL	R2	14	WX wire length
WXSEN	R2	15	Sensitivity,
WXTEMP1-7	R2	16-22	WX calibration temperature 1-7
WXTLC1-7	I1	23-29	WX temperature ref channel 1-7
WXMTY1-7	R2	30-36	Future expansion 1-7
WXTEC1-7	R2	37-43	Thermal expansion coefficient 1-7
WXOC	R2	44	WX offset constant
PNC0-4	R2	13-17	Polynomial coefficient 0-4
SYPRON	X6	13	System processor name
SYPAR1-5	I1	14-18	System processor param 1-5

licenses which exist in the HPDB-file, and was used going backwards through all HPTP-files* to produce an HPDB-file which contains the most recent data for all licenses ever used.

In order to correct errors transmitted in the HPTP-files and to add data not contained in them, a fourth REVERT mode is needed, the ALTER mode, which received a major share of the effort this year. There are five basic commands, each of which require the beginning word or index in COM00 to modify, the number of words to modify, the data type (real, integer, or text), and a set of values to copy. The "A" command adds a new license. The "C" command overwrites the existing data positions of the given license with the given new values. A more powerful command, "CD" overwrites the defined locations of all licenses of a given device type with the given values. Another powerful command, "CM" operates like "C", but allows the license to be

* Except HPTP810402 and HPTP810418, which are identical to HPTP810313 and HPTP810409, and HPTP810119, which, except for one error, is identical to HPTP810313 and HPTP810402.

masked with an asterisk for each character of the license to be ignored in testing for a match. For example, G*E011 would operate on licenses GAE011, GBE011, GCE011, and GDE011, but not GAE012, etc. The last command, which has also proved very useful is the "CO" command, which is similar to "CM" except that another license name (with masking allowed) is given instead of data values. With this command the defined data for one license are copied from the same data positions of another license. For example, if the first license is G*E011 and the second is G*E211, data are copied from GAE211 to GAE011, from GBE211 to GBE011, from GCE211 to GCE011, and from GDE211 to GDE011. Thus the "temporary" characters substituted for the masks must be the same, and the remaining characters must match for data to be copied. Commands may be entered from the teletype or may be read from a file, which for convenience is appended to the ITEMNAME file needed for that data base. Although license masking and device selection enable one alter command to modify hundreds of coefficients in a data base, over 150 alter lines are needed to prepare a typical HPDB-file from its unmodified state. Preparation of these files would be a difficult task without a powerful ALTER capability.

Of the many other changes to REVERT, two deserve special note. The first is implementation of a data screen on the date. This feature prevents converting a data point if its time does not fall within the effective time range for that license. This time range is controlled by positions 7, 8, and 9 in COM00, which contain the date the instrument was installed, the date the coefficients in the base become valid, and the date the coefficients become invalid, for example, if the instrument was removed. Because of the real time nature of the NTS data base, COM00 positions 8 and 9 are not, in general, correct in the HPTP-file and must be reset with ALTER commands. In response to instrument failures and insights gained during operation of the test, changes have occurred in the instrumentation so that different coefficients are required at different times. An example is the addition of thermocouples to the rod extensometer heads in January 1982 (~JD 44990) coefficients after that date refer to the TCs, while before then nearby RTDs should be referenced.

Because successive data bases are contiguous in time, there are no time periods for which the coefficients are undefined. When a given B-file contains data over a time range which exceeds that of a single data base, the file must be reprocessed successively with data bases of different effective time ranges, until all the input data have been processed.

Note that with the existing system an entire new data base is needed even if only one instrument had a change. Current work is proceeding first to reference field data by license rather than channel, then to allow multiple entries of the same license, each valid for a different time range, in the same data base. Using the license will allow processing of any B-file with only one data base: the most recent.

The second distinctive change involves running speed. After REVERT had been tested on small (3-day) test files, and a normal one million-word file was tried, we found execution times were very long: on the order of 30 min. The reason had to do with the many disc accesses required to convert pass three device types. (Note: Pass 1 devices require no reference channels. Pass 2 devices require pass 1 reference devices. Pass 3 devices require pass 2 reference devices.) Since the code is fairly small, the problem could be alleviated by saving recent disc reads in a large block of memory. A subroutine, SHELF, was written to keep track of what data blocks were "on-the-shelf" in memory, and to supply that data without a disc read when possible. Implementation of SHELF resulted in a sevenfold increase in operation speed, reducing the time to process a typical file from 30 to 4 min.

REVERT appears to be essentially operational at this point. A data base applicable to the first year's data has been constructed and initial comparisons are being made between the HP and Octopus converted values. One thing is apparent in the early files: the Octopus version has the advantage of calibration coefficients which were not available during the first few months of the test. The HP system, operating in real time, was unable to convert many licenses which the Octopus system can now convert at a later date. There are some data points Octopus cannot convert which the HP system was able to convert. One surmises that this is due to data lost in transmission, but this has not yet been confirmed.

13.2 QUANTITY AND QUALITY OF DATA RECEIVED TO DATE

Table 13-3 shows the data received to date. The "Discard" column primarily accounts for data from radiation monitors and various status devices which are not analyzed and reported. These are discarded to reduce the volume of data handled. This reduction is significant (~50%) as is evident in Table 13-3. The small fraction of discarded data which could have been analyzed were it available is shown in the "NUMBER OF ERRORS" columns of

Table 13-3. Note that these erroneous data typically represent much less than 1% percent of the acquired data. The last column reflects the change in the BREAD data sieve to deal with the 65 921 channel and license errors on file SF055B/C. The multiple occurrence of exactly 46 "channel and license bad" lines is remarkable, but the reason is unknown at this time.

Table 13-3. Summary of processed data.

File Name	Time, Absolute Julian Day		Number of data points			Number of errors			
						Range			
	Start	Stop	Copied	Discard	Total	TOR[a]	VOR[b]	License	License and Channel
000A/B	44331.437	44569.498	30191	0	30191	--	--	--	--
002A/E	44342.196	44354.011	25393	11407	36800	0	144	39	0
003A/C	44344.790	44345.250	1692	2245	3937	0	0	0	143
004A/C	44345.389	44346.967	11181	6548	17729	32	90	32	149
005A/C	44346.960	44351.929	26491	13114	39605	18	21	0	0
006A/C	44351.914	44351.917	37567	7027	44594	0	81	0	0
007A/D	44357.845	44358.507	7145	1636	8781	0	4	0	0
008A/D	44358.485	44360.566	8883	2427	17310	0	231	0	0
009A/D	44359.926	44361.134	17281	5971	23252	0	1451	0	0
010A/C	44361.143	44370.452	119807	45263	175070	0	54	0	0
011A/D	44370.452	44375.167	50161	18770	68931	0	44	0	0
012A/C	44375.161	44388.456	150312	57590	207902	0	141	0	0
013A/C	44388.196	44409.271	159424	58090	217514	0	300	33	0
014A/D	44409.266	44416.590	91569	28941	120510	0	73	196	0
015A/C	44416.590	44421.242	45953	14735	60688	0	28	67	0
016A/C	44421.246	44438.653	182950	68700	251650	0	108	409	0
016B/C	44438.648	44451.121	138409	52772	191181	0	79	320	0
017A/C	44451.107	44467.378	178992	68629	247621	0	50	0	0
017B/C	44467.161	44474.286	72545	23302	95847	3	10	0	0
018A/F	44474.278	44490.198	154345	56843	211188	6	35	220	205

Table 13-3. (continued)

File Name	Time, Absolute Julian Day		Number of data points			Number of errors			
						Range			
	Start	Stop	Copied	Discard	Total	TOR[a]	VOR[b]	License	License and Channel
019A/C	44490.193	44501.576	118107	40305	158412	0	58	24	0
020A/B	44501.563	44513.328	97757	48058	145815	0	7	21	0
021A/B	44513.321	44526.480	156160	69170	225330	0	2	0	0
022A/B	44526.478	44541.537	172533	64458	236991	0	5	0	1
022B/A	44541.532	44550.332	115831	73133	188964	0	4	0	0
023A/B	44550.252	44562.241	113601	50159	163760	0	24	161	0
024A/B	44557.484	44576.247	72353	31718	102071	0	38	2	0
025A/C	44529.807	44590.272	104444	31095	135539	0	60	39	0
026A/C	44577.327	44610.263	84131	117970	202101	0	13	8	0
027A/C	44610.564	44618.247	40686	203970	244650	12	8	84	229
028A/C	44618.247	44632.397	84205	165522	249727	2	16	204	0
029A/C	44632.368	44651.453	88284	164419	252703	0	11	12	0
029B/C	44650.669	44661.224	30935	53536	84471	0	266	3	0
030A/C	44656.339	44686.187	90861	157447	248308	1	7	3	47
030B/B	44686.067	44695.245	45207	95148	140355	0	4	3	0
031A/C	44695.350	44705.889	48884	43058	91942	14	186	19	606
032A/C	44703.304	44722.290	78070	80297	158367	3	8	102	23
033A/C	44722.617	44781.117	124320	123839	248159	1	37	1	160
034A/B	44723.271	44772.087	141038	108318	249356	0	79	11	0
034B/B	44772.087	44781.122	22451	20664	43115	0	2	1	0

Table 13-3. (continued)

File Name	Time, Absolute Julian Day		Number of data points			Number of errors			
						Range			
	Start	Stop	Copied	Discard	Total	TOR[a]	VOR[b]	License	License and Channel
035A/C	44781.126	44801.610	72433	56439	128872	0	22	1	245
036A/C	44781.122	44802.173	45460	54589	100049	0	286	3	678
037A/B	44802.184	44826.246	125763	122361	248124	0	6	3	0
037B/B	44826.180	44842.202	60618	60467	121085	0	5	184	0
038A/C	44837.205	44852.215	59890	51625	111515	1	2	1	0
039A/B	44852.223	44873.582	106996	129470	236466	0	12	206	0
039B/B	44873.582	44890.343	139520	72851	212371	1	28	28	0
040A/A	44890.566	44905.159	65577	89464	155041	0	10	20	0
041A/A	44905.151	44932.186	137485	114641	252126	0	31	6	0
041B/B	44932.184	44939.266	30576	27134	57710	0	2	1	0
042A/B	44939.300	44965.522	119826	124187	244013	2	102	80	0
042B/A	44965.484	44984.225	78904	82118	161022	0	5	75	0
043A/E	44990.234	45005.301	101456	119178	220634	1	117	1869	12
044A/B	45005.305	45053.225	132236	114582	246818	2	6	109	166
045A/A	45005.260	45030.390	87612	48097	135709	0	44	333	0
045B/A	45030.397	45053.204	81367	47567	128934	0	72	0	0
046A/D	45053.229	45077.681	186845	59844	246689	1	111	59	46
046B/B	45077.681	45080.213	137590	112400	149990	0	14	0	0
047A/D	45053.207	45080.231	116475	79060	195535	1	562	3	46
048A/A	45080.271	45084.987	115728	12690	28418	0	13	319	0

Table 13-3. (continued)

File Name	Time, Absolute Julian Day		Number of data points			Number of errors			
						Range			
	Start	Stop	Copied	Discard	Total	TOR[a]	VOR[b]	License	License and Channel
049A/B	45080.683	45106.363	84845	166315	251160	1	154	16	493
049B/A	45106.361	45109.549	21836	16270	38106	0	15	1	0
050A/B	45085.646	45103.386	44184	34166	78350	1	49	16	217
051A/A	45110.252	45133.155	187505	67807	255311	0	260	66	0
051B/B	45133.153	45152.179	149434	58448	207882	0	82	104	0
052A/A	--	--	0	125108	125108	8738	20	8775	112568
053A/B	45129.603	45148.636	177163	55377	232540	1	51	1	46
054A/A	45152.319	45177.430	28130	23752	51882	0	2	0	0
055A/C	45152.182	45169.359	161569	91101	252670	433	24	576	5035
055B/C	45169.354	45177.468	38772	93132	131904	1731	22	1769	65921
056A/A	45177.431	45201.199	77471	68863	146334	0	65	773	0
057A/A	45177.411	45201.192	70506	61908	132414	0	97	168	0
058A/A	45201.192	45221.369	36943	62424	119367	0	39	162	0
059A/A	45201.199	45218.443	50135	204568	254703	0	5	189	0
060A/A	45226.448	45256.339	76218	88038	164256	0	4	21	0
061A/A	45221.416	45256.336	99734	92536	192270	0	49	0	0
062A/A	45256.339	45288.544	141186	106148	247334	1	12	245	46
062B/A	45288.533	45292.298	19574	199242	39498	0	5	167	0
063A/A	45256.339	45285.208	62320	55826	118146	0	30	109	0
064A/A	45292.298	45331.300	115960	125014	240774	1	1191	29	46

Table 13-3. (continued)

File Name	Time, Absolute Julian Day		Number of data points			Number of errors			
						Range			
	Start	Stop	Copied	Discard	Total	TOR[a]	VOR[b]	License	License and Channel
065A/A	45292.219	45339.403	127878	127829	255707	1	83	7	46
065B/A	45339.406	45340.228	1297	481	1784	0	0	0	0
Totals									
00-45	44331.437	45053.255	4785868	3601064	8386932	99	4599	4933	2663
46-65	45053.229	45340.228	2249098	2009035	4258133	10910	3056	14075	184510
overall	44331.437	45340.228	7034966	5610099	12645065	11009	7655	19008	187173

[a] TOR, Time out of range.
[b] VOR, Value out of range.

ACKNOWLEDGMENTS

Overall technical guidance for this and other NNWSI projects at LLNL is provided by L. Ramspott. We also acknowledge the contributions of several other colleagues at LLNL--R. Stager in data acquisition system support; N. Cotter, M. Higuera, W. Richardson, and L. Rogers in data processing; J. Button as Operations Coordinator; K. Raschke and T. Roy in LLNL-N Health and Safety; and J. Beiriger, P. Burklund, R. Neurath, D. Peifer, J. Scarafiotti, F. Schumacher, B. Sellick for technical support. We would furthermore like to thank A. Duba, H. Heard, L. Ramspott, S. Spataro, and R. Terhune for their careful reviews of this manuscript.

R. Noyes and J. Pelles of EG&G-LV provide laboratory calibration of instrumentation, while B. Bailey, R. Sievert, and W. Webb provide field support for instrument installation and calibration.

G. Adair, L. Cheney, D. Daffer, G. Frye, and C. Halstead of REECo maintain and provide access to the surface and subsurface facilities.

This manuscript was typed by D. Verrett.

REFERENCES

Ballou, L. B., Patrick, W. C., Montan, D. N., and T. R. Butkovich (1982), Test Completion Plan for Spent Fuel Test--Climax, Nevada Test Site, Lawrence Livermore National Laboratory, Livermore, CA, UCRL-53367.

Bathe, K. J. (1977), ADINAT, A Finite Element Program for Automatic Dynatic Analysis of Temperature, Massachusetts Institute of Technology, Cambridge, MA, 82448-5.

Bathe, K. J. (1978), ADINA, A Finite Element Program for Automatic Dynamic Incremental Non-linear Analysis, Massachusetts Institute of Technology, Cambridge, MA, 82448-1.

Blake, W. F., Leighton, F., and W. I. Duvall (1974), Techniques for Monitoring the Behavior of Rock Structures, USBM Bulletin # 665.

Brough, W. G., and W. C. Patrick (1982), Instrumentation Report #1: Specification, Design, Calibration, and Installation of Instrumentation for an Experimental, High Level, Nuclear Waste Storage Facility, Lawrence Livermore National Laboratory, Livermore, CA, UCRL-53248.

Butkovich, T. R. (1982), The Effects of Boundary Conditions on Thermomechanical Calculations: Spent Fuel Test--Climax, Lawrence Livermore National Laboratory, Livermore, CA, UCRL-53338.

Butkovich, T. R., Yow, Jr., J. L., and D. N. Montan (1982), Influence of Heat Flow on Drift Closure During Climax Granite Spent Fuel Test: Measurements and Calculations, Lawrence Livermore National Laboratory, Livermore, CA, UCRL-87248.

Carlson, R., Patrick, W. C., Wilder, D., Brough, W., Montan, D. N., Harben, P., Ballou, L., and H. Heard (1982), SFT-C Technical Measurement Interim Report Fiscal 1980, Lawrence Livermore National Laboratory, Livermore, CA, UCRL-53064.

Carr, W. J. (1974), Summary of Tectonic and Structural Evidence for Stress Orientation at the Nevada Test Site, USGS Open File Report 74-176, Denver, CO.

Durham, W. B. (1982), The effect of gamma irradiation on the strength of Climax stock quartz monzonite, Lawrence Livermore National Laboratory, Livermore, CA, UCRL-87475.

Ellis, W. L., and J. Magner (1982), Determination of the In Situ State of Stress at the Spent Fuel Test--Climax Site, Climax Stock, Nevada Test Site, USGS Open-File Report 82-458.

Hage, G. L. (1983), BREAD - A CDC 7600 Program That Processes Spent Fuel Test-Climax Data, SFT 82-156, Lawrence Livermore National Laboratory, Livermore, CA, UCID-19814.

Heuze, F., Butkovich, T. R., and J. Peterson (1981b), An Analysis of the "Mine-By" Experiment in Climax Granite, Nevada Test Site, Lawrence Livermore National Laboratory, Livermore, CA, UCRL-53133.

Heuze, F., Patrick, W. C., De la Cruz, R. V., and C. F. Voss (1981a), In-Situ Geomechanics Climax Granite, NTS, Lawrence Livermore National Laboratory, Livermore, CA, UCRL-53076.

Jacobs, S. F. (1982), Letter report on thermal expansion measurements of 1/4 in. diameter superinvar rods, University of Arizona, LLNL purchase order 6687501.

Majer, E. L., McEvilly, T. V., and M. S. King (1981), "Monitoring an Underground Repository with Modern Seismological Methods," Int. J. Rock Mech. and Mining Eng., 18, 517-527.

Mirkovich, V. V., Durham, W. B., and H. C. Heard (1982), Measurement of Thermal Diffusivity of Rocks at High Pressure, Lawrence Livermore National Laboratory, Livermore, CA, UCRL-87217.

Montan, D. N., and W. C. Patrick (1981), Thermal Calculations for the Design, Construction, Operation, and Evaluation of the Spent Fuel Test--Climax, Nevada Test Site, Lawrence Livermore National Laboratory, Livermore, CA, UCRL-53238.

Nyholm, R., Brough, W., and N. Rector (1982), Spent Fuel Test-Climax Data Acquisition System Integration Report, Lawrence Livermore National Laboratory, Livermore, CA, UCRL-53304.

Nyholm, R. (1982), Spent Fuel Test-Climax Data Acquisition System Operations Manual, Lawrence Livermore National Laboratory, Livermore, CA (in preparation).

Patrick, W. C., Ballou, L. B., Butkovich, T. R., Carlson, R. C., Durham, W. B., Hage, G. L., Majer, E. L., Montan, D. N., Nyholm, R. A., Rector, N. L., Wilder, D. G., and J. L. Yow, Jr. (1982), Spent Fuel Test--Climax: Technical Measurements Interim Report, Fiscal Year 1981, Lawrence Livermore National Laboratory, Livermore, CA, UCRL-53294.

Patrick, W. C., Carlson, R. C., and N. L. Rector (1981), Instrumentation Report #2: Identification, Evaluation, and Remedial Actions Related to Transducer Failures at the Spent Fuel Test--Climax, Lawrence Livermore National Laboratory, Livermore, CA, UCRL-53251.

Paulsson, B. N. P., and M. S. King (1980), A Cross-Hole Investigation of a Rock Mass Subjected to Heating, Lawrence Berkeley Laboratory, Berkeley, CA, Report 10849.

Paulsson, B. N. P. (1983), Seismic Velocities and Attenuation in a Heated Undesignated Granite Repository, Ph.D. Thesis, University of California, Berkeley, CA, 322 pp.

Ramspott, L. D., Ballou, L. B., Carlson, R. C., Montan, D. N., Butkovich, T. R., Duncan, J. E., Patrick, W. C., Wilder, D. G., Brough, W. G., and M. C. Mayr (1979), Technical Concept for a Test of Geologic Storage of Spent Reactor Fuel in the Climax Granite, Nevada Test Site, Lawrence Livermore National Laboratory, Livermore, CA, UCRL-52796.

Smith, N., and R. Belles (1981). XPORT Reference Manual, Lawrence Livermore National Laboratory, Livermore, CA, LCSD-1196.

Quam, W., and T. Devore (1982), Climax Spent Fuel Dosimetry Progress Report, September 1981-September 1982, Lawrence Livermore National Laboratory, Livermore, CA, UCRL-15419 (EGG 1183-2455).

Quam, W., Devore, T., and D. Sever (1982), letter report entitled, Short-Term TLD Measurements at the Climax Spent Fuel Test Facility, EG&G Santa Barbara Operations, Santa Barbara, CA.

Schmittroth, F., Neely, G. J., and J. C. Krogness (1981), A Comparison of Measured and Calculated Decay Heat for Spent Fuel Near 2.5 Years Cooling Time, Hanford Engineering Development Laboratory, Richland, WA, HEDL-TC-1759.

Van Konynenburg, R. (1982), Comparison of Measured and Calculated Radiation Doses in Granite Around Emplacement Holes in the Spent Fuel Test--Climax Nevada Test Site, Lawrence Livermore National Laboratory, Livermore, CA, UCRL-53341.

Weed, H. C., and W. B. Durham (1983), Drilling-Induced Borehole-Wall Damage at Spent Fuel Test--Climax, Lawrence Livermore National Laboratory, Livermore, CA, UCID-19672.

Wilcox, T., and R. Van Konynenburg (1981), Radiation Dose Calculations for Geologic Media Around Spent Fuel Emplacement Holes in the Climax Granite, Nevada Test Site, Lawrence Livermore National Laboratory, Livermore, CA, UCRL-53159.

Wilder, D., and W. C. Patrick (1981), Geotechnical Status Report for Test Storage of Spent Reactor Fuel in Climax Granite, Nevada Test Site, Lawrence Livermore National Laboratory, Livermore, CA, UCRL-85096.

Wilder, D., Yow, Jr., J. L., and R. Thorpe (1983b), Structural Geology Report--Spent Fuel Test--Climax, (in preparation).

Wilder, D., Yow, Jr., J. L., and R. Thorpe (1983a), Core Logging for Site Investigation and Instrumentation, Spent Fuel Test--Climax, Lawrence Livermore National Laboratory, Livermore, CA, UCID-19646.

Yow, Jr., J. L., and T. R. Butkovich (1982), Calculated and Measured Drift Closure During The Spent Fuel Test in Climax Granite, Lawrence Livermore National Laboratory, Livermore, CA, UCRL-87179.

BRS/dab

U. S. Government Printing Office: 1983/10-687-002/A4003